ECMWF COPERNICUS REPORT

Copernicus Atmosphere Monitoring Service

Validation of the CAMS regional services: concentrations above the surface

Status update for the period March - May 2021

Issued by: KNMI

Date: 30 September 2021

Ref: CAMS84_2018SC3_D4.1.1-MAM2021.pdf

European Commission

Copernicus
Europe's eyes on Earth

IMPLEMENTED BY
ECMWF

Validation of the CAMS regional services: concentrations above the surface

Status update for the period March - May 2021

AUTHORS:
D. Akritidis (AUTH), T. Antonakaki (AA), Y. Bennouna (CNRS-LA), A.-M. Blechschmidt (IUP-UB), T. Bösch (IUP-UB), H. Clark (CNRS-LA), P. Frietzsche (DWD), C. Gielen (BIRA-IASB), F. Hendrick (BIRA-IASB), J. Kapsomenakis (AA), S. Kartsios (AUTH), E. Katragkou (AUTH), D. Melas (AUTH), A. Mortier (MetNo), E. Peters (IUP-UB), K. Petersen (MPI), A. Piters (KNMI), A. Richter (IUP-UB), M. van Roozendael (BIRA-IASB), M. Schulz (MetNo), N. Sudarchikova (MPI), A. Wagner (MPI), P. Zanis (AUTH), C. Zerefos (AA)

EDITORS:
J. Douros (KNMI), H.J. Eskes (KNMI)

REPORT OF THE COPERNICUS ATMOSPHERE MONITORING SERVICE, VALIDATION SUBPROJECT (CAMS-84).

CITATION:
Douros, J., H.J. Eskes, D. Akritidis, T. Antonakaki, Y. Bennouna, A.-M. Blechschmidt, T. Bösch, H. Clark, P. Frietzsche, C. Gielen, F. Hendrick, J. Kapsomenakis, S. Kartsios, E. Katragkou, D. Melas, A. Mortier, E. Peters, K. Petersen, A. Piters, A. Richter, M. van Roozendael, M. Schulz, N. Sudarchikova, A. Wagner, P. Zanis, C. Zerefos, Validation of CAMS regional services: concentrations above the surface, Status update for March - May 2021, Copernicus Atmosphere Monitoring Service (CAMS) report, CAMS84_2018SC3_D4.1.1-MAM2021, September 2021, doi:10.24380/d7g4-sy07.

STATUS:
Version 1.0

DATE:
30 September 2021

REF:
CAMS84_2018SC3_D4.1.1-MAM2021

Executive Summary

The Copernicus Atmosphere Monitoring Service (CAMS, http://atmosphere.copernicus.eu) is a component of the European Earth Observation programme Copernicus. The CAMS service consists of two major forecast and analysis systems. First, the CAMS global near-real time (NRT) service provides daily analyses and forecasts of reactive trace gases, greenhouse gases and aerosol concentrations, and is based on the ECMWF Integrated Forecast System (called CAMS-global in this document). Secondly, nine models in Europe, perform air quality forecasts and analyses on a daily basis, nested within CAMS-global. Based on these individual forecasts and analyses, an ensemble forecast of air quality over Europe is produced and disseminated by Météo-France (called ENSEMBLE or CAMS-regional below). The regional members use the global forecasting results as boundary conditions at the sides and top of the domain.

This document reports on two validation activities, namely

- an evaluation of the consistency between the global and regional modelling components of CAMS, focussing on the boundaries of the regional domain, and
- an evaluation of the regional ENSEMBLE and the nine individual models contributing to the ensemble with independent observations, focusing on the concentrations above the surface.

The current analysis includes ozone (O_3), nitrogen dioxide (NO_2), aerosol (PM10/PM2.5/AOD) and carbon monoxide (CO) forecasts covering the period up to May 2021.

The forecasts from the regional models were compared with the following set of observations:

- aerosol lidar observations from the EARLINET network;
- aerosol AOD observations from the AERONET network;
- IAGOS routine aircraft measurements of ozone and CO;
- ozone sonde profiles;
- MAX-DOAS NO_2 tropospheric columns;
- GOME-2/MetOp-A NO_2 satellite tropospheric column retrievals (IUP-UB v1.0 product);
- high-altitude ozone surface stations;
- CO and O_3 from GAW mountain stations; and
- CO observations from the MOPITT satellite instrument.

These observations are available to CAMS within one month after the observations were made.

This report is based on regional model data available for the months May 2016 to May 2021, with a focus on March – May 2021 (MAM2021). The report is updated every 3 months. The main results are summarised below, focusing on the performance of the regional ensemble. Detailed results, also for the individual models, are presented in sections 3 to 11, and each of these sections starts with a summary of the main results. Model specific findings are summarised in section 12. The last upgrade implemented in CAMS-global was on 6 October 2020, while the last upgrade for the CAMS regional models happened on 25 November 2020, implementing new anthropogenic emissions and making available an additional pollen species.

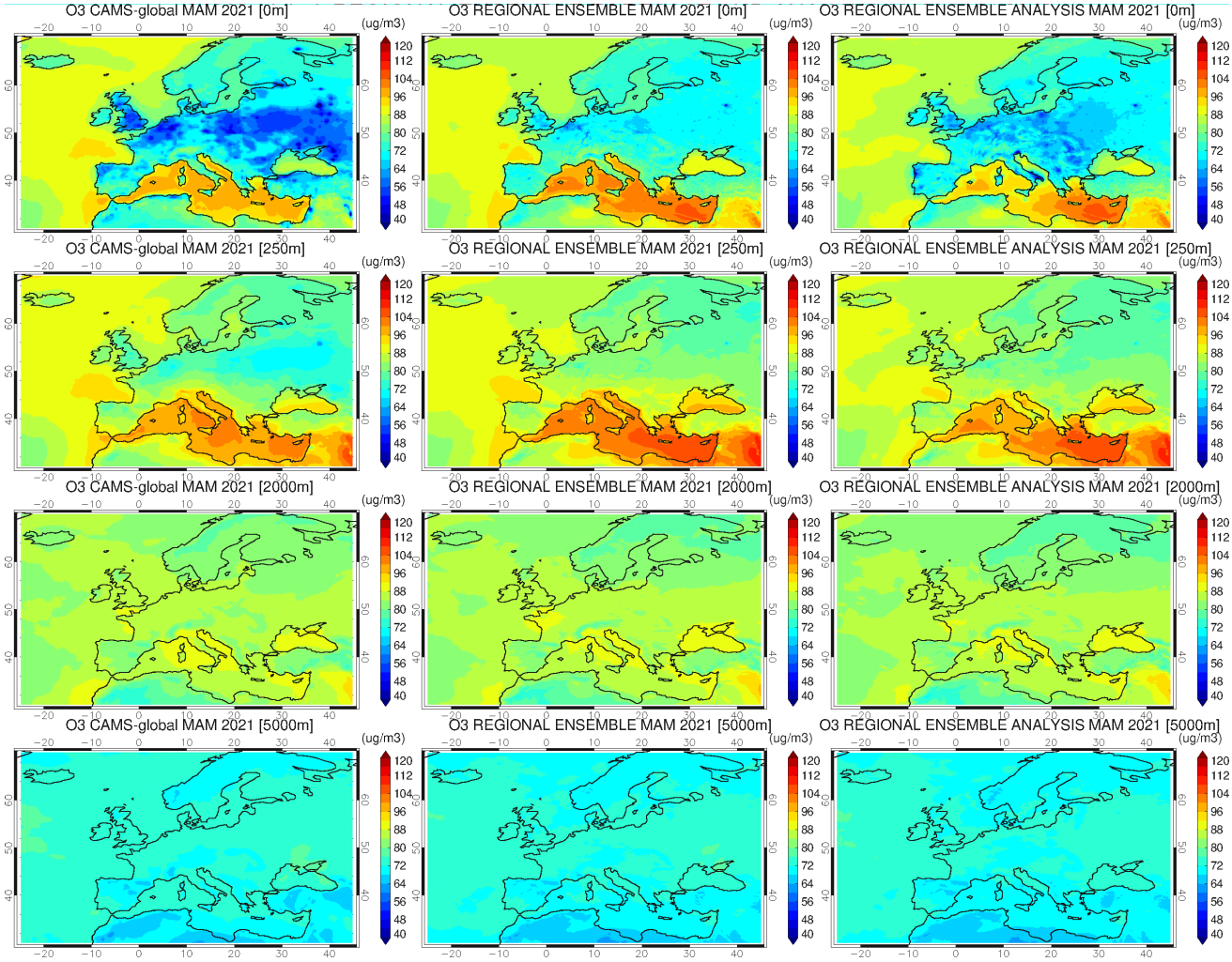

Figure S.1. A comparison of the CAMS global ozone forecast for day 1 (left), CAMS regional ENSEMBLE ozone forecast for day 1 (middle), and CAMS regional ozone analysis (right). From top to bottom: 0, 250, 2000, 5000m altitude level. The results are averaged over the March to May 2021 period.

General conclusions for the regional ENSEMBLE

The comparison of the European regional CAMS ENSEMBLE air quality forecasts and analyses against above-surface observations of O_3, NO_2, CO for the period up to the 1st of June 2021 demonstrates that overall, the biases observed are small, often within the uncertainty of the validation approach while temporal correlations for ozone and CO are reasonable. Performance of the ENSEMBLE analysis product is found to be generally superior to that of the ENSEMBLE forecasts. The ENSEMBLE performs generally better than any of the individual models for ozone, NO_2 and CO, showing the strength of the ensemble approach adopted in CAMS.

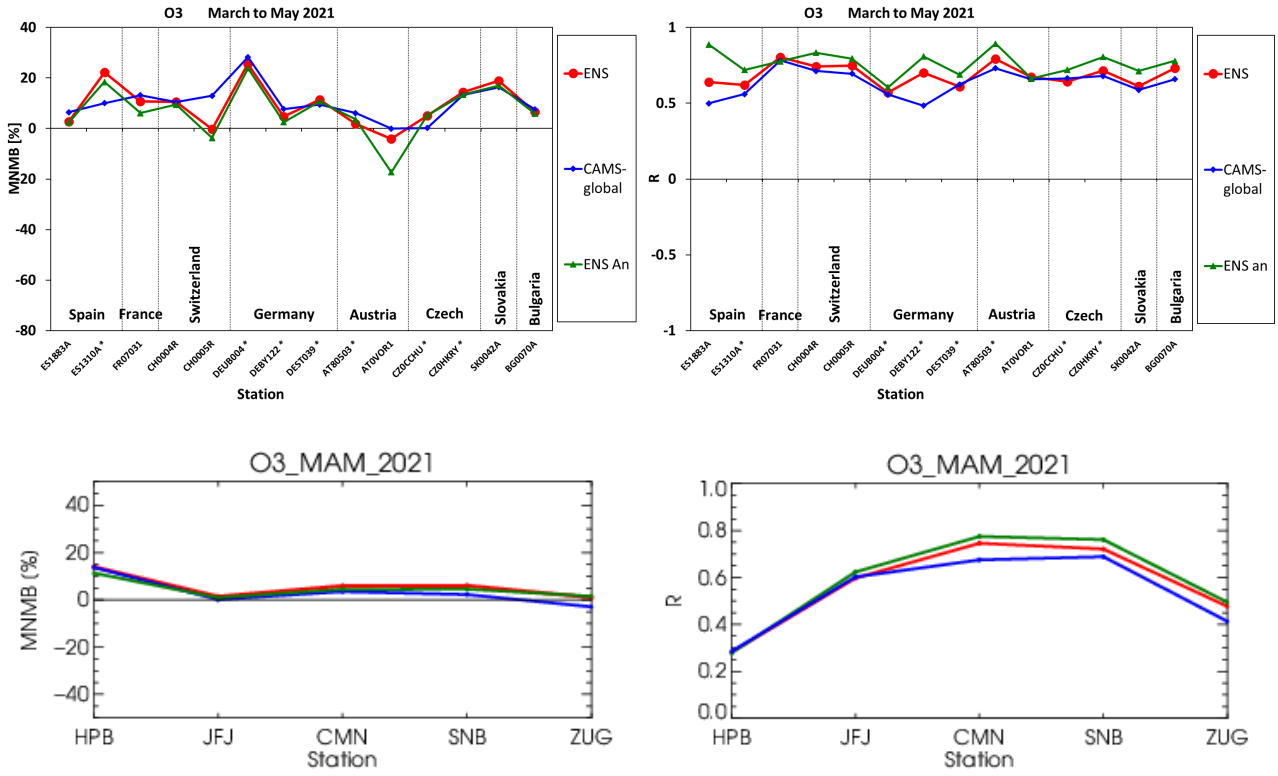

Figure S.2. Normalised bias (left) and correlation coefficient (right) for ozone for the high-altitude (above 1 km) EEA Air Quality e-reporting stations (top) and the 5 high-altitude European GAW stations (bottom). Lines represent ENSEMBLE forecast (solid red), ENSEMBLE analysis (solid green) and CAMS-global system (blue) for March - May 2021. The horizontal axis is the station identifier referring to Hohenpeissenberg (HPB), Jungfraujoch (JFJ), Monte Cimone (CMN), Sonnblick (SNB) and Zugspitze (ZUG).

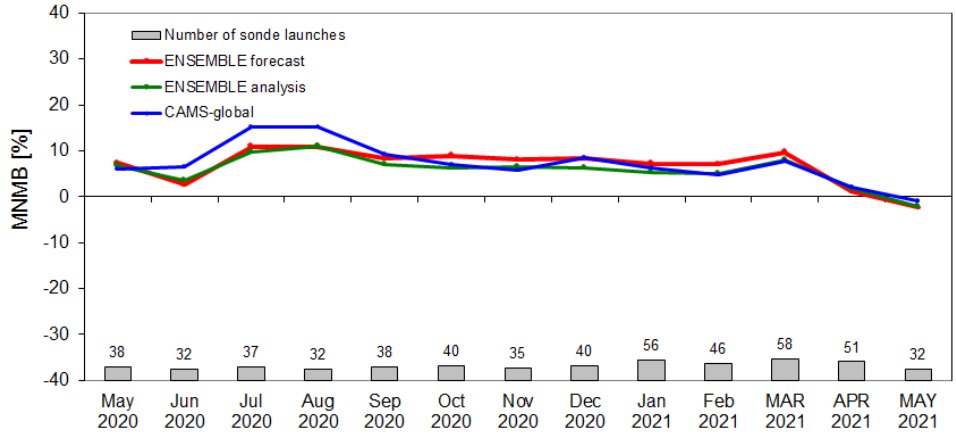

Figure S.3 Modified normalised mean bias (MNMB) against ozone sondes for the regional ENSEMBLE forecasts (red) and analyses (green) from May 2020 to May 2021 (horizontal axis). Ozone was averaged over the lower-middle free troposphere region, 500 hPa < p < 850 hPa.

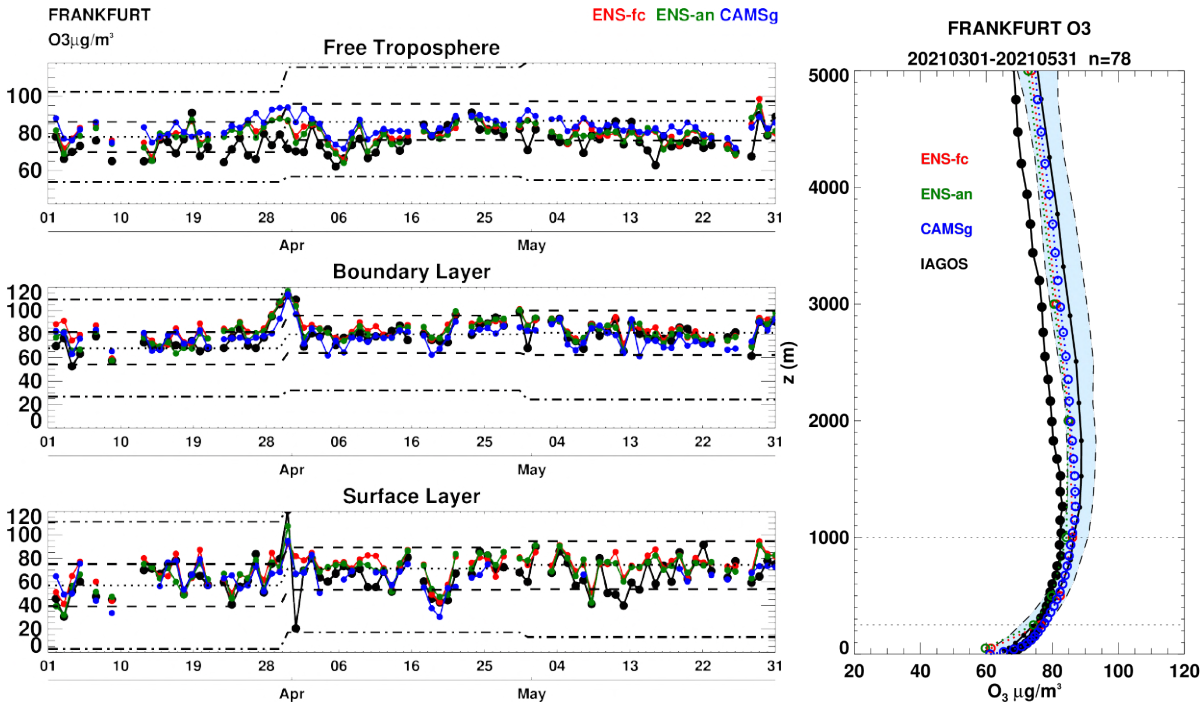

Figure S.4 Daily time series of ozone at Frankfurt for March to May 2021. The black dotted line is the monthly mean of the observations over the period 2003-2016 (IAGOS/MOZAIC, Level 2 data), the black dashed line shows 1 standard deviation from the monthly mean and the black doted-dashed line shows 3 standard deviations from the monthly mean. Right: Mean profile of ozone at Frankfurt for the period March - May 2021. The shaded area indicates the range of the mean climatology of the observations plus/minus one standard deviation during the same period for all years between 2003 and 2016 (IAGOS/MOZAIC, level 2 data). In both panels, IAGOS observations are shown in black, the regional ENSEMBLE and associated analysis are shown in red and green respectively, and the global o-suite is shown in blue.

Ozone

At the boundaries of the regional domain, the ENSEMBLE agrees well with CAMS-global, indicating that the implementation of the boundary conditions is done properly. Over the full domain there is a good match between the global and regional CAMS analyses and forecasts between 1 and 5 km altitude. These results are similar to previous quarters.

The differences between the global and regional systems reveal themselves in the boundary layer and at the surface over land, as expected. A comparison of the regional analysis product with the regional day 1 forecast (Fig. S.1) shows some differences between the regional ENSEMBLE forecast and analysis, with the analysis generally having lower concentrations near the surface.

For high altitude stations, Fig. S.2, the observed ozone levels are reproduced to within -5% to 30% by the ENSEMBLE first day forecast, while comparison against ozone sondes shows a milder overestimation in the -3% to 15% range (Fig. S.3). Time correlations at high-altitude and GAW stations range between 0.3 and 0.8 during this period, with improved figures for the ENSEMBLE analyses as compared to the ENSEMBLE forecast at the GAW stations.

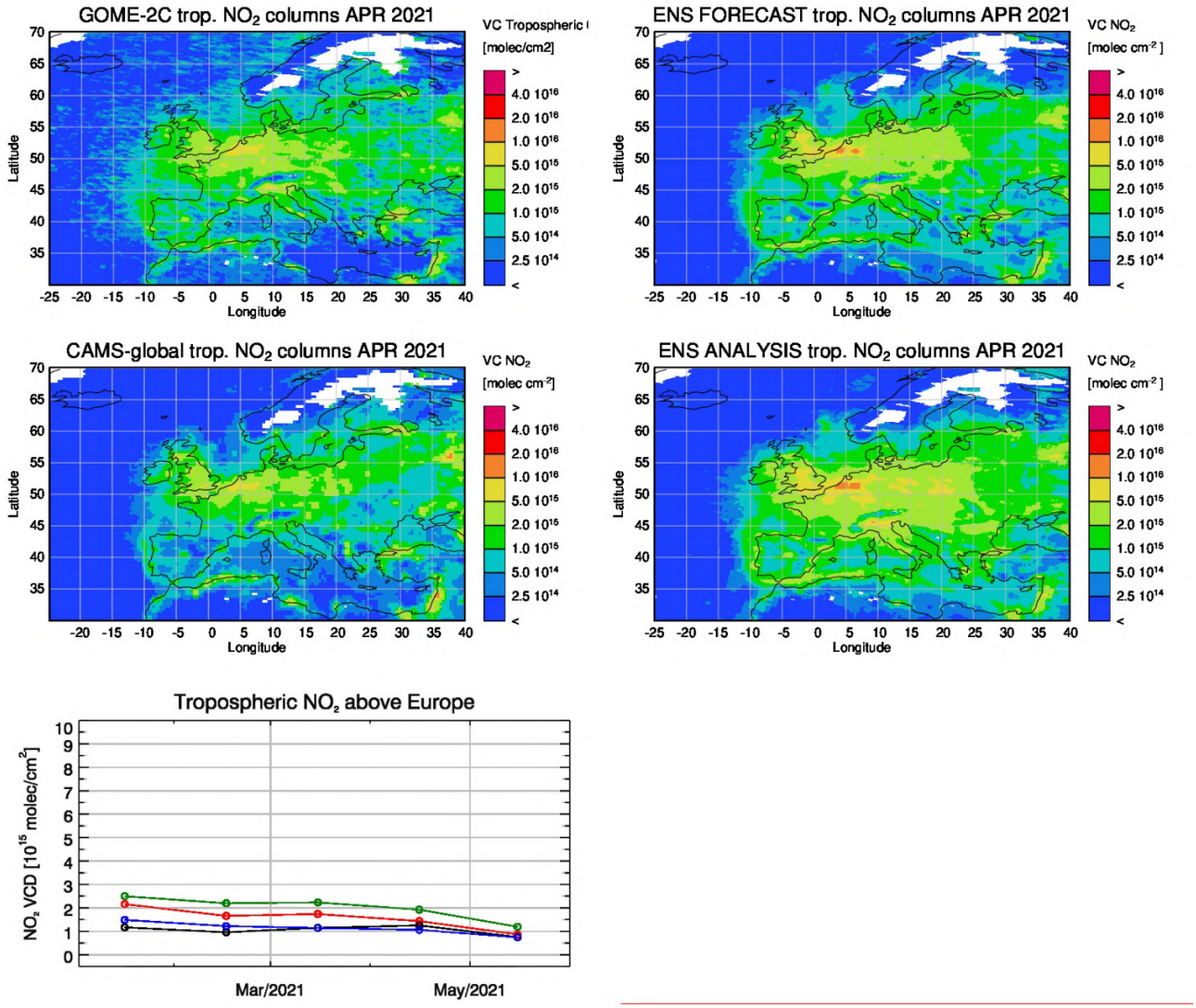

Figure S.5: Maps of satellite-retrieved and model-simulated tropospheric NO_2 columns [molecules cm^{-2}] for April 2021 for GOME-2C (top left), regional ENSEMBLE forecasts (top right) CAMS-global forecasts (middle left) and regional ENSEMBLE analyses (middle right). The panel at the bottom shows corresponding time series of average tropospheric NO_2 columns [10^{15} molecules cm^{-2}] from GOME-2C (black), regional ENSEMBLE forecasts (red), CAMS-global forecasts (blue) and regional ENSEMBLE analyses (green). GOME-2 data were gridded to regional model resolution (i.e., 0.1° x 0.1°). Model data were treated with the same reference sector (25°W - 20°E) subtraction approach as the satellite data and linearly interpolated to the satellite overpass time (9:30 LT).

Comparisons with IAGOS aircraft observations at Frankfurt, see Fig. S.4, reveals that ozone is mostly well reproduced by both the regional ensemble and CAMS-global in the low troposphere while larger overestimations are obtained in the free troposphere for all models.

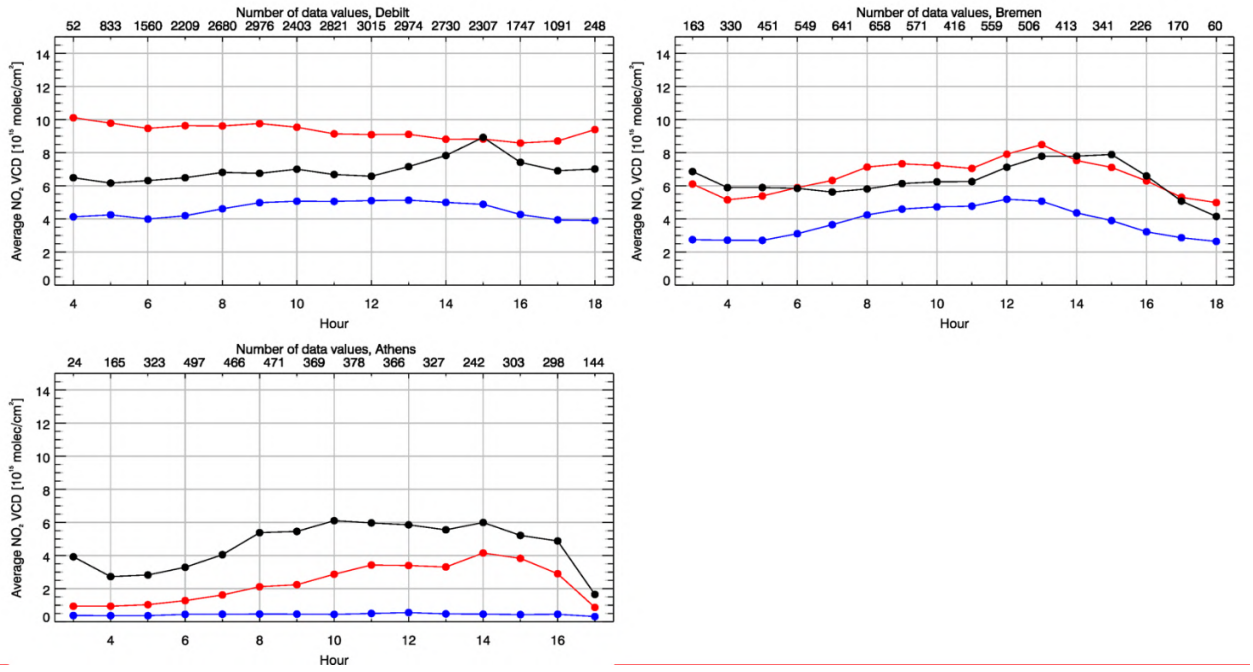

Figure S.6: Diurnal cycles (averages over hourly bins) of tropospheric NO_2 VCDs [10^{15} molec. cm^{-2}] from MAX-DOAS and models for De Bilt (the Netherlands) (top left), Bremen (Germany) top right and Athens (Greece) (bottom). The coloured lines show (black) MAX-DOAS retrievals, (red) regional ENSEMBLE forecasts and (blue) CAMS-global. Period: June 2020 – May 2021.

Nitrogen dioxide (NO_2)

The overall spatial distribution of tropospheric NO_2 as observed from space by GOME-2C is reproduced by the ensemble during MAM2021 (see Fig. S.5). Values over central European emission hotspots are overestimated by most of the models, which results in a positive bias of ~1-2 x 10^{15} molec/cm^2 for the regional ensemble analysis for values averaged over the region of Europe, while the also positive bias for CAMS-global is < 0.5 x 10^{15} molec/cm^2.

Systematic uncertainties in the retrievals (on average on the order of 20% – 30% over polluted regions) depend on the season, with winter values in mid and high latitudes normally associated with larger error margins. Conclusions may differ for comparisons to other satellite NO_2 products (e.g. TEMIS GOME-2A, http://www.temis.nl). We note that since 05 May 2020 GOME-2C observations are assimilated by the CAMS global system. This is, however, a different retrieval product than what is used in the validation reported here (University of Bremen retrieval).

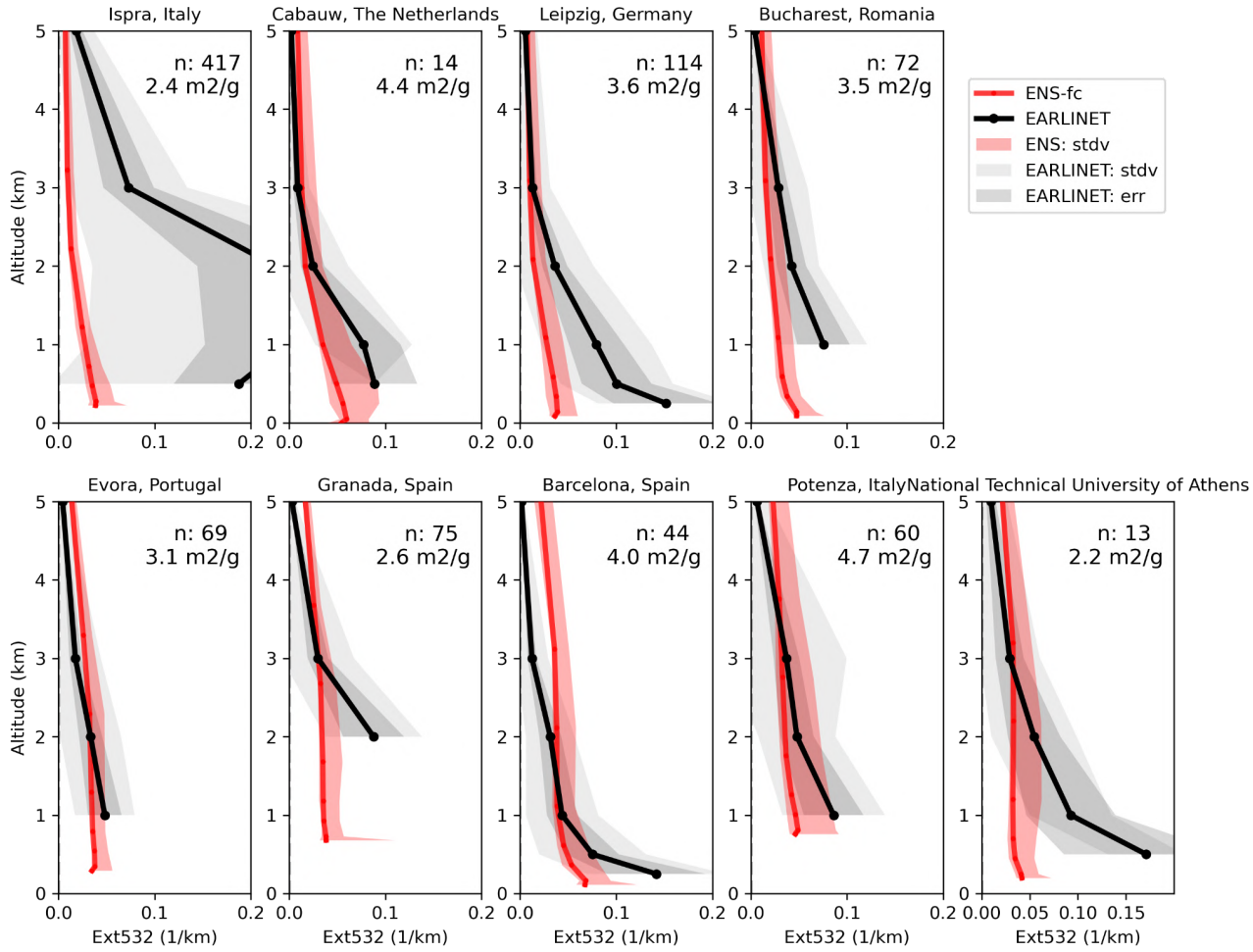

Figure S.7. Extinction profiles March - May 2021 derived from the ENSEMBLE forecast mass concentration profiles (red envelope) and from EARLINET (climatology) backscatter profiles (grey envelope: lidar ratio uncertainty, light grey: including sampling error). "n: XX means number of individual EARLINET profiles assembled (March-May 2006-2018). The EMC used for the calculation of the extinction from the concentration profiles is indicated for each station below the number of EARLINET profiles "n" used for the calculation of the climatology.

Comparisons to ground-based remote-sensing MAX-DOAS retrievals at three different European stations (see Figure S.6) for the period of June 2020 – May 2021 show that regional ENSEMBLE forecasts are closer to the urban station observations of Bremen and Athens than CAMS-global, mainly attributed to the difference in spatial resolution. The performance of simulations for diurnal cycles of tropospheric NO_2 columns depends on the location, but generally shows a moderate performance for the ENSEMBLE products.

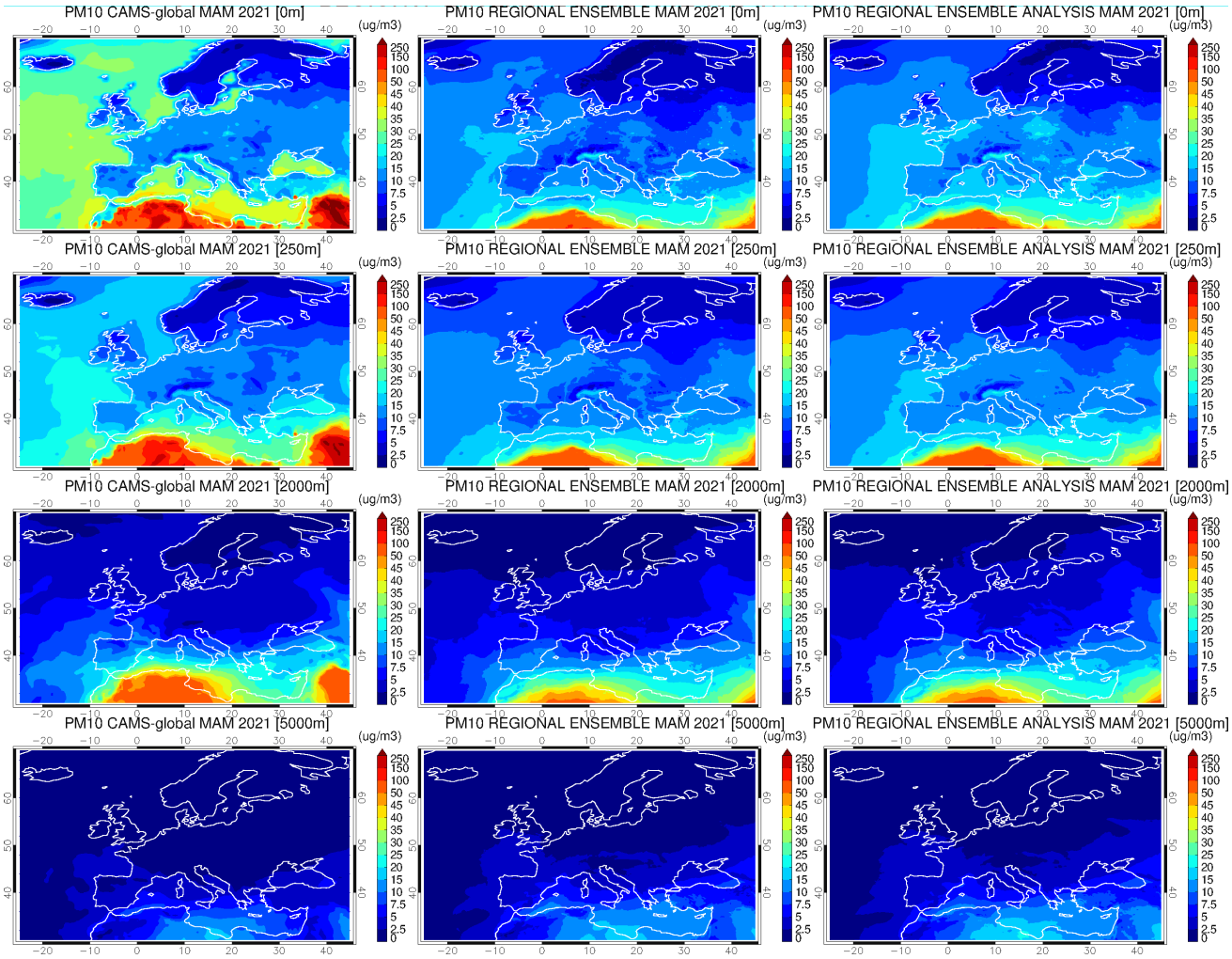

Figure S.8. CAMS global PM10 forecast for day 1 (left), CAMS regional ENSEMBLE PM10 forecast for day 1 (middle), CAMS regional PM10 analysis (right). From top to bottom: 0, 250, 2000, 5000m altitude level. Period: March to May 2021.

Aerosol / PM

The regional models are compared with EARLINET climatological lidar profiles for the same season (data from 2006-2020), Fig. S.7. The standard dissemination of CAMS-regional forecasts does not include information on composition, size, and humidity growth of the aerosol in the models. This introduces considerable uncertainty to the PM derived extinction, which conservatively spans a factor 10 for absolute extinction values. Relative differences among nearby stations and the form of extinction profiles are more certain. The order of magnitude in extinction is similar between the ENSEMBLE and the lidar profiles, with Ispra, Italy, close to the Alps, Granada, Spain and Athens, Greece being the most notable exceptions. The decrease in extinction with height seems to be generally steeper in the observations.

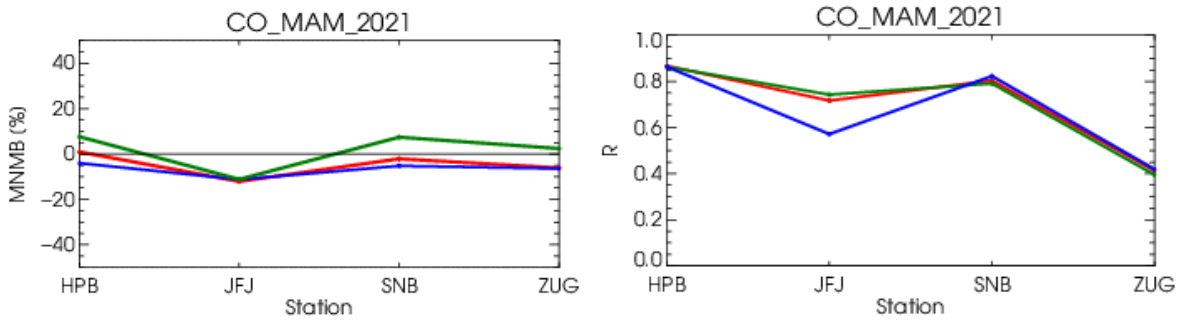

Figure S.9. MNMBs [%] (top) and correlation coefficients (bottom) for CO regional ENSEMBLE forecasts (red), analyses (green) and CAMS-global (blue) compared to observations at GAW stations. Period: March - May 2021.

The PM10 concentrations in the regional ENSEMBLE forecasts and analyses are similar, but larger PM values are observed for the analysis over areas of Central and Western Europe at the surface level, see Figure S.8. CAMS-global shows higher PM10 values over the Atlantic and the Mediterranean, especially at the lower levels. The agreement between CAMS-global and the ENSEMBLE products is better for PM10 and PM2.5 in the upper layers compared to the lower layers, as expected.

Carbon monoxide (CO)

Comparison at the GAW stations reveal biases between -15% and 15% for the forecast and between -5% and ~25% for the forecast, while temporal correlations coefficients are between 0.3 and 0.85 for both the forecast ana analysis (Fig. S.9).

Comparisons with MOPITT CO satellite observations (version 8, Fig. S.10) data also reveal good agreement with the observations, exhibiting a slight negative bias within 20% (with some regional and temporal exceptions). The modelling data captured well both, relatively high CO values over the northern and middle parts of domain and relatively low values over the southern part. Analysis data are similar to the forecast data, showing slightly smaller negative bias.

General conclusions for the individual regional models

Regional models in general appear to have efficiently implemented the use of global CAMS boundary conditions and provide 3D fields that are comparable to those of the global model.

For ozone, bias and correlation at GAW and EEA e-reporting high altitude surface stations show a small spread among most of the models and an improved performance of the analysis compared to the forecast. The comparisons with ozone sondes in the lower free troposphere show similar results.

For NO_2, the validation with MAX-DOAS shows a sizeable spread between individual models, especially when considering the diurnal cycles. However, most of the simulated values probably fall within the uncertainty range of MAX-DOAS retrievals. The overall spatial distribution of tropospheric NO_2 as seen by GOME-2A/MetOp-C is reproduced by the regional models, but values over central European emission hotspots are underestimated by most models.

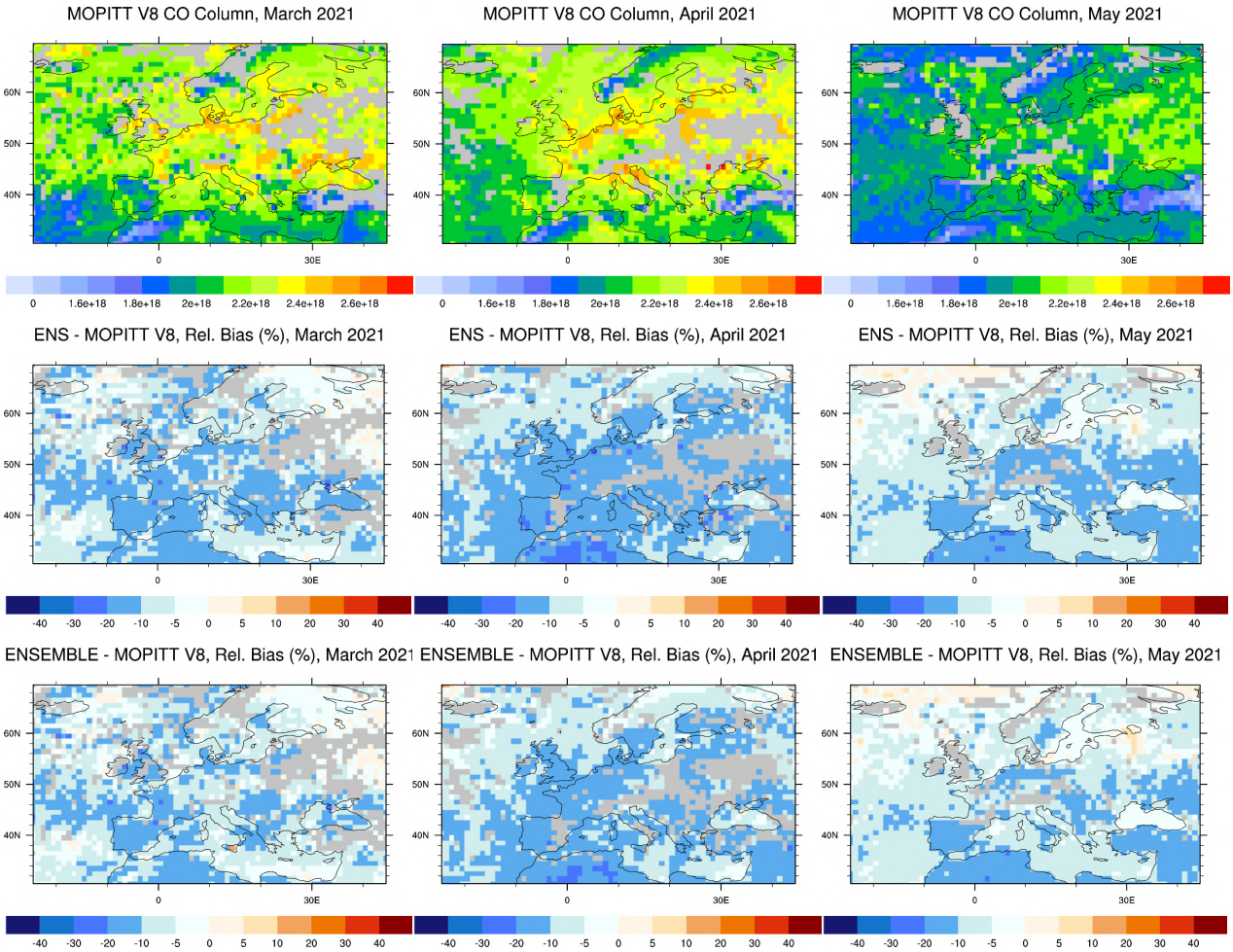

Figure S.10. CO total column for MOPITT v8 satellite retrievals (top row, in molecules/cm^2), relative difference between the regional ENSEMBLE forecasts and MOPITT (middle row) and regional ENSEMBLE analyses and MOPITT (bottom row) for March (left column), April (middle column) and May 2021 (right column). Grey colour indicates missing values.

For CO, comparisons at GAW mountain stations show a slightly negative bias and small model spread for the forecasts. For the analyses, the bias is positive for some models and the spread is higher. The latter is especially true for the correlation coefficient. Comparisons with MOPITT retrievals reveal a small underestimation over the whole domain for most of the models.

For PM, observations from the EARLINET and AERONET networks reveal that the order of magnitude in extinction is similar between the models and the lidar profiles at most locations, while the decrease in extinction with height seems to be generally steeper in the observations.

Table of Contents

1 Introduction

The Copernicus Atmosphere Monitoring Service (CAMS, https://atmosphere.copernicus.eu) is a component of the European Earth Observation programme Copernicus. The CAMS near-real time services consist of daily analysis and forecasts with the IFS system with data assimilation of trace gas concentrations and aerosol properties. The global modelling system is also used to provide the boundary conditions for an ensemble of more detailed regional air quality models that are used to zoom in on the European domain and produce 4-day forecasts of air quality. The regional forecasting service provides daily 4-days forecasts of the main air quality species and analyses of the day before, based on the results from 9 state-of-the-art atmospheric chemistry models. The ensemble represents the median of these 9 model forecasts.

Routine validation of the regional models against surface observations from the European member states (EEA Air Quality e-reporting) is provided for each model individually as well as the ENSEMBLE in separate quarterly validation reports. Validation reports of the CAMS regional products are available in the following portal:
https://atmosphere.copernicus.eu/regional-air-quality-production-systems.
This web page provides access to the quarterly reports on the daily analyses and forecast activities and verification of the regional ENSEMBLE. An overview of the regional air quality forecasting system is provided by Marécal et al (2015).

Validation reports (e.g. Wagner et al., 2020) for the CAMS global products are available at https://atmosphere.copernicus.eu/node/325, including the evaluation on Earth's troposphere, stratosphere, aerosols and greenhouse gases, with state-of-the art observational datasets (GAW, IAGOS, MOPPIT, EMEP, GOME-2A, OMPS-LP, BASCOE, AERONET etc.). A published overview on the validation of reactive gases and aerosols in the global analysis and forecast system can be found in Eskes et al (2015). A validation study of the global surface ozone reanalysis for Europe is provided by Katragkou et al (2015).

Details of the various observational datasets can be found in Eskes et al. (2021), "Observations characterisation and validation methods document", also available at:
https://atmosphere.copernicus.eu/eqa-reports-global-services.

This document presents an evaluation of the concentrations above the surface as modelled by the set of the 9 individual regional models and the ensemble median derived from those 9 individual forecasts and analyses, as well as the consistency between the global and regional modelling systems of CAMS.

2 Regional and global CAMS forecasting systems

2.1 Regional models

The European Air Quality products are provided from the Copernicus Atmosphere Monitoring Service (http://atmosphere.copernicus.eu/). These data are available in NetCDF or Grib-Edition2 format. The files are available each day through ftp protocol from the Météo-France server (ftp.cnrm-game-meteo.fr). Since the beginning of February 2020, the data are also available through the Atmosphere Data store (https://ads.atmosphere.copernicus.eu), although the reliability of data retrievals from was relatively low during this quarter. The products are available in Near Real Time (NRT) for four forecast days, following the protocol below:

- Each day 96h model forecasts and 24h analyses for the previous day are provided with hourly resolution.
- Products are available at eight vertical height levels: surface, 50, 250, 500, 1000, 2000, 3000, 5000 meters.
- The pollutants are O_3, CO, NO_2, SO_2, PM2.5, PM10, NO, NH_3, NMVOC, PANs, dust aerosols (fraction below 10µm), secondary inorganic aerosols (fraction below 2.5µm), birch, grass, olive, ragweed and alder pollen. Since the upgrade of February 4th, 2020 three new aerosol species (PM from wildfires, EC from fossil fuels and EC from wood burning) are also available.
- The regional datasets cover the longitudes 335.05°E to 44.95°E every 0.1°, and latitudes 71.95°N – 30.05°N also at 0.1° resolution (~10km).
- The forecasts until the 48th hour are available before 7:30 UTC
- The forecasts for the 49-96th hour are available before 9:30 UTC
- The analyses are provided before 12:00 UTC
- Since the November 2020 upgrade, the regional models make use of the CAMS-REG-AP_v4_2 emissions dataset (reference year: 2017).

The NRT forecast and analysis regional air quality data are available for the nine air quality models and their ensemble median (CAMS-regional or ENSEMBLE):

- MOCAGE model (MFM)
- LOTOS-EUROS model (KNM)
- EMEP MSC-W model (EMP)
- MATCH model (SMH)
- EURAD-IM model (RIU)
- CHIMERE model (CHI)
- SILAM model (FMI)
- DEHM model (DEM)
- GEM-AQ model (GEM)

Before October 16th, 2019 the regional ensemble was calculated based on 7 regional models (except for DEHM and GEM-AQ). This is the third quarterly report which explicitly includes results and analysis from those two new models.

Every evening, a full download of the 96h forecasts and 24h analyses fields to KNMI at full resolution is performed. These fields are co-located to the set of surface stations used, and this largely reduced datasets is shared with all validation partners.

Documentation about the regional models may be found at the address https://atmosphere.copernicus.eu/regional-air-quality-production-systems. For the purposes of this report however, it's useful to indicate what kinds of observations are actively assimilated in each model (Table 2.1).

Table 2.1: Surface and other observations that are actively assimilated in regional models.

Model	**Method**	**Surface**	**Other**
CHIMERE	Kriging	O_3, NO_2, PM10, PM2.5	
EMEP	Intermittent 3D-var	O_3, SO_2, NO_2, CO, PM10, PM2.5	OMI NO_2
EURAD	Intermittent 3D-var	O_3, SO_2, NO_2, PM10, PM2.5	OMI and MetOp/GOME-2 NO_2 and SO_2, MOPITT and IASI CO
LOTOS-EUROS	Ensemble Kalman filter	O_3, NO_2, PM10, PM2.5	OMI NO_2
MATCH	Intermittent 3D-var	O_3, NO_2, CO, PM10, PM2.5	
MOCAGE	3D-var	O_3, NO_2, PM10	
SILAM	Intermittent 3D-var	O_3, NO_2, CO, PM10, PM2.5	
DEHM	Sequential intermittent 3D-var	O_3, NO_2, SO_2, CO, PM10, PM2.5	
GEM-AQ	Optimal interpolation	O_3, NO_2, CO, SO_2, PM10, PM2.5	

Validation reports of the CAMS regional products are available in the following portal: https://atmosphere.copernicus.eu/regional-services.

Whenever possible, in this report, models follow the naming and colour scheme of Table 2.2.

Table 2.2: Naming and colour scheme followed throughout this report.

Model	***Short model name***	***Colour name***	***Colour***
CAMS-global	CAMSg	Blue	
ENSEMBLE forecast	ENS-fc	Red	
ENSEMBLE analysis	ENS-an	Green	
CHIMERE	CHIM	Yellow	
EMEP	EMEP	Brown	
EURAD	EURAD	Cyan	
LOTOS-EUROS	LOTOS	Purple	
MATCH	MATCH	Grey	
MOCAGE	MOCA	Pink	
SILAM	SILAM	Orange	
DEHM	DEHM	Fuchsia	
GEM-AQ	GEMAQ	Light Green	

2.2 Global CAMS system based on the ECMWF IFS model

The CAMS-global operational assimilation/forecast system consists of the IFS-CB05 chemistry combined with the MACC aerosol model. The chemistry is described in Flemming et al. (2015); aerosol is described by the bulk aerosol scheme (Morcrette et al., 2009). Dissemination of CAMS-global forecasts is twice a day, at about 10:00 and 22:00UTC. The forecast length is 120 h. Users can get access at https://ads.atmosphere.copernicus.eu. Table 2.3 provides information on the satellite data used in CAMS-global.

The most recent upgrade relevant to this report, was the upgrade to cycle 47R2 which took place on 18 May 2021 and involved a number of small changes related to emissions and to the numerical treatment of aerosol and chemistry schemes. A detailed changelog and the corresponding validation reports for this last upgrade can be found in Eskes et al., 2021.

Upgrade and version information is available here:
https://atmosphere.copernicus.eu/changes-cams-global-production-system.

Documentation on the global system can be found here:
https://atmosphere.copernicus.eu/global-production-system.

Table 2.3: Satellite retrievals of reactive gases and aerosol optical depth that are actively assimilated in CAMS-global.

Instrument	Satellite	Provider	Version	Type	Status
MLS	AURA	NASA	V4	O3 profiles	20130107 -
OMI	AURA	NASA	V883	O3 total column	20090901 -
GOME-2	Metop-A	EUMETSAT	GDP 4.8	O3 total column	20131007 - 20181231
GOME-2	Metop-B	EUMETSAT	GDP 4.8	O3 total column	20140512 -
GOME-2	Metop-C	EUMETSAT	GDP 4.9	O3 total column	20200505 -
SBUV-2	NOAA-19	NOAA	V8	O3 21 layer profiles	20121007 - 20201005
OMPS	Suomi-NPP	NOAA / EUMETSAT		O3 13-layer profiles	20170124 - 20190409 20201006 -
OMPS	NOAA-20	NOAA / EUMETSAT		O3 13 layer profiles	20201006 - 20201215
TROPOMI	Sentinel-5P	ESA		O3 column	20181204 -
IASI	MetOp-A	LATMOS/ ULB EUMETSAT		CO total column	20090901 - 20180621 20180622 - 20191118
IASI	MetOp-B	LATMOS/ ULB EUMETSAT		CO total column	20140918 - 20180621 20180622 -
IASI	MetOp-C	EUMETSAT		CO total column	20191119 -
MOPITT	TERRA	NCAR	V5-TIR V7-TIR V7-TIR Lance V8-TIR	CO total column	20130129 - 20160124 - 20180626 20180626 - 20190702 -
OMI	AURA	KNMI	DOMINO V2.0	NO2 tropospheric column	20120705 - 20210331
GOME-2	MetOp-A	EUMETSAT	GDP 4.8	NO2 tropospheric column	20180626 - 20200504
GOME-2	MetOp-B	EUMETSAT	GDP 4.8	NO2 tropospheric column	20180626 -
GOME-2	MetOp-C	EUMETSAT	GDP 4.9	NO2 tropospheric column	20200505 -
GOME-2	MetOp-A	EUMETSAT	GDP 4.8	SO2 total column	20150902 - 20191210
GOME-2	MetOp-B	EUMETSAT	GDP 4.8	SO2 total column	20150902 -
GOME-2	MetOp-C	EUMETSAT	GDP 4.9	SO2 total column	20200505 -
MODIS	AQUA / TERRA	NASA	Col. 5 Deep Blue Col. 6, 6.1	Aerosol total optical depth, fire radiative power	20090901 - 20150902 - 20170124 -
PMAp	METOP-A METOP-B METOP-C	EUMETSAT		AOD	20170124 - 20210719 20170926 - 20210719 -

3 Consistency between the global and regional modelling components of CAMS

3.1 Summary

This chapter reports on the consistency between the global and regional modelling components of CAMS, and the impact of global CAMS boundary conditions on regional forecasts. The current evaluation includes ozone (O_3) Carbon Monoxide (CO), Nitrogen Dioxide (NO_2) and aerosol (PM_{10}/$PM_{2.5}$) forecasts covering the period from March to May 2021.

Global and regional ensemble forecasts: Overall, the two forecast products compare well, except for ozone near the surface over continental Europe where CAMS-global exhibits lower concentrations. Some differences are also seen in aerosol (PM_{10}), which is higher in CAMS-global over the southern boundary and over the Atlantic in altitudes < 2Km.

Regional forecast variability: The regional ensemble members exhibit the expected regional variability for O_3, CO, NO_2 and particulate matter. Minor deviations (compared to CAMS-global and the majority of the regional models) are generally found, with MOCAGE having the most distinct PM_{10} behaviour over western (sea salt) and southern (dust) Europe. CHIMERE has a problematic O_3/CO boundary condition implementation.

Daily time series. There is a good temporal agreement for all species between the regional ensemble members and CAMS-global, with SILAM, EMEP, and GEMAQ only exhibiting occasionally higher PM peaks than CAMS-global.

Regional forecast and analysis: The comparison of regional analyses and forecasts shows strong model and species dependence.

3.2 Methodology for the comparisons of CAMS-global and CAMS-regional

Operational download

The daily regional CAMS forecasts are retrieved on a daily basis by the AUTH-server. This includes the 3-hourly (0,3,6,9 etc.) regional forecast data (ensemble members and regional ENSEMBLE) for all provided species at all vertical layers for the 5 forecast days extracted from the Météo-France ftp server, and the 3-hourly (0, 3, 6, 9 etc.) global forecast data for 5 forecast days extracted from the ECMWF CAMS ftp server

Methodology of global-regional comparison

The following methodology is used to a) convert CAMS-global species from mass mixing ratio (kg/kg) to concentration (µg/m^3) and, b) extract CAMS-global species concentrations from the vertical levels that lie closest to the regional height levels.

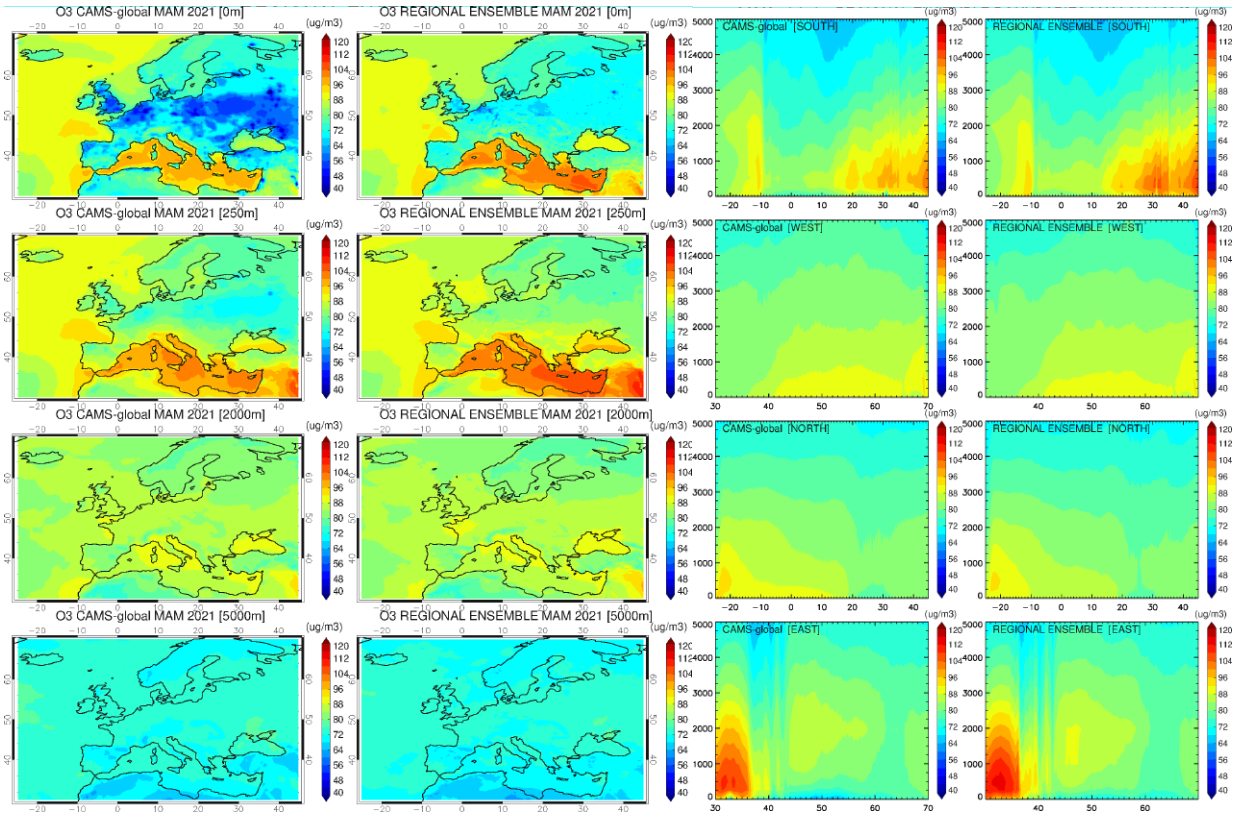

Figure 3.1. Left: Mean global and regional ENSEMBLE forecast ozone fields for four different vertical layers (0, 250, 2000, 5000 m) for MAM2021. Right: Cross sections for the same period of the global and regional ENSEMBLE ozone boundaries (south, west, north, east).

The following parameters are used from the CAMS-global model: hybrid layer coefficients; temperature, surface pressure; "GEMS" ozone; carbon monoxide; "aermr01-11" and "aermr16-18" (aerosol species, kg/kg). Data from the first 78 vertical layers (from the surface) are used.

The thickness of each vertical layer Δz (m) is calculated:

$$\Delta z_k = \frac{R * T_k}{M_{air} * g} * \ln\left(\frac{p_{i_{k+1}}}{p_{i_k}}\right) \qquad (E.1)$$

where R=8.314 J/mol·K the gas constant, T the temperature at vertical layer midpoint, M_{air}=28.97·10^{-3} kg/mol the molecular weight of air and g=9.8 m/s^2 the gravity acceleration.

The mass-mixing ratio (kg/kg) for ozone (go3) and carbon monoxide (CO) is initially provided. Conversion from mass mixing ratio (kg/kg) to concentration (μg/m^3) is performed using the following approach:

$$\rho_{O3} = mmr_{O3} * \left(\frac{p_m * M_{air}}{R * T}\right) \qquad (E.2)$$

where ρ_{O3} is the ozone concentration (kg/m^3) and mmr_{O3} the ozone mass mixing ratio (kg/kg). The expression inside the parentheses in E.2 corresponds to the air concentration (kg/m^3). The same approach is also used for the CO unit conversion from kg/kg to μg/m^3.

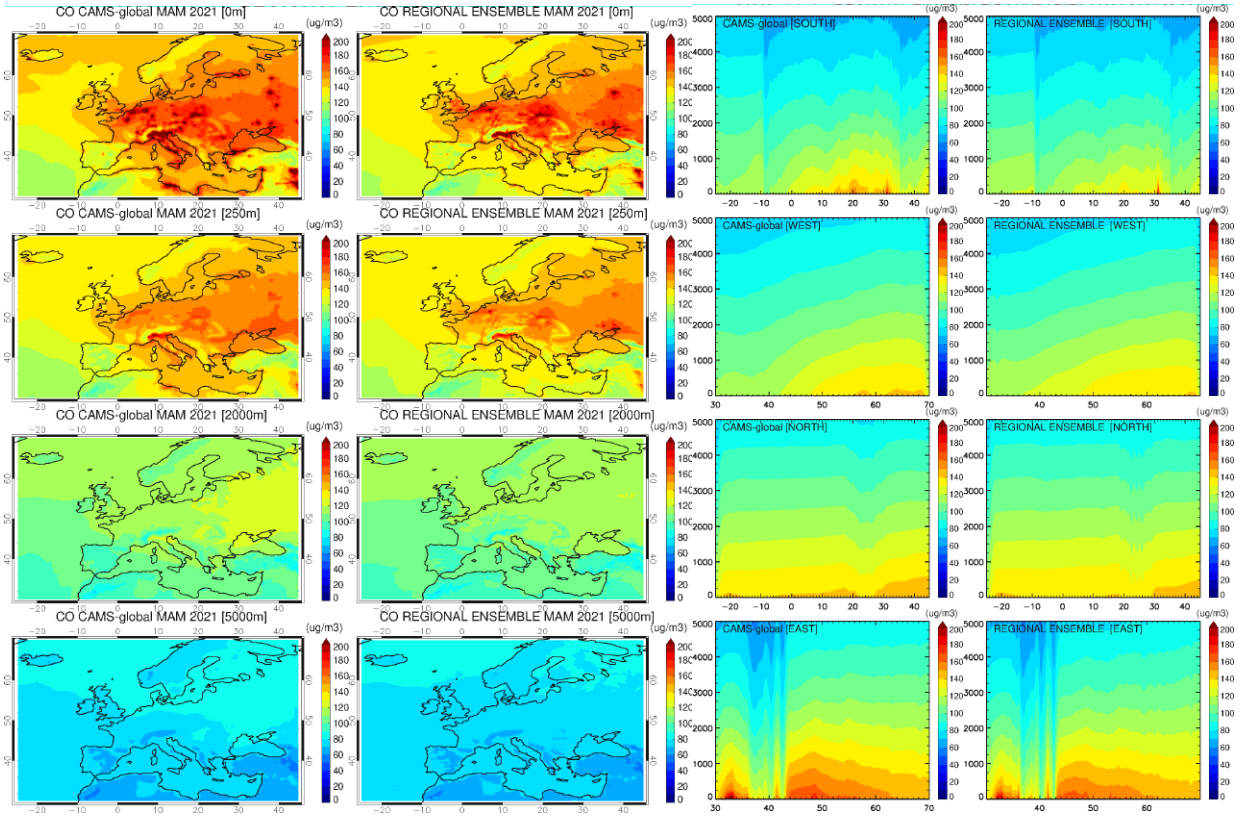

Figure 3.2. Left: Mean global and regional ENSEMBLE forecast CO fields for four different vertical layers (0, 250, 2000, 5000 m) for MAM2021. Right: Cross sections for the same period of the global and regional ENSEMBLE CO boundaries (south, west, north, east).

The mass mixing ratio for all aerosol species (see Table 3.1) is initially provided. The PM10 and PM2P5 species are converted to μg/m^3 as follows:

$$\rho_{PM10} = \left[\frac{aermr01}{4.3} + \frac{aermr02}{4.3} + aermr04 + aermr05 + 0.4 * aermr06 + aermr07 + aemr08 + aermr11 + aerm09 + aermr10 + aermr16 + aemr17 + aermr18\right] * \left(\frac{p_m}{R_{spec} * T}\right) \quad (E.3)$$

$$\rho_{PM2P5} = \left[\frac{aermr01}{4.3} + \frac{aermr02 * 0.5}{4.3} + aermr04 + aermr05 + 0.7 * aermr07 + 0.7 * aermr08 + 0.7 * aermr11 + aermr09 + aermr10 + 0.7 * aermr16 + 0.25 * aermr17 + 0.7 * aermr18\right] * \left(\frac{p_m}{R_{spec} * T}\right) \quad (E.4)$$

where R_{spec}=287.058 J/(kg·K) is the specific gas constant for dry air. The expression inside the parentheses in E.3 and E.4 corresponds to the dry air concentration (kg/m^3).

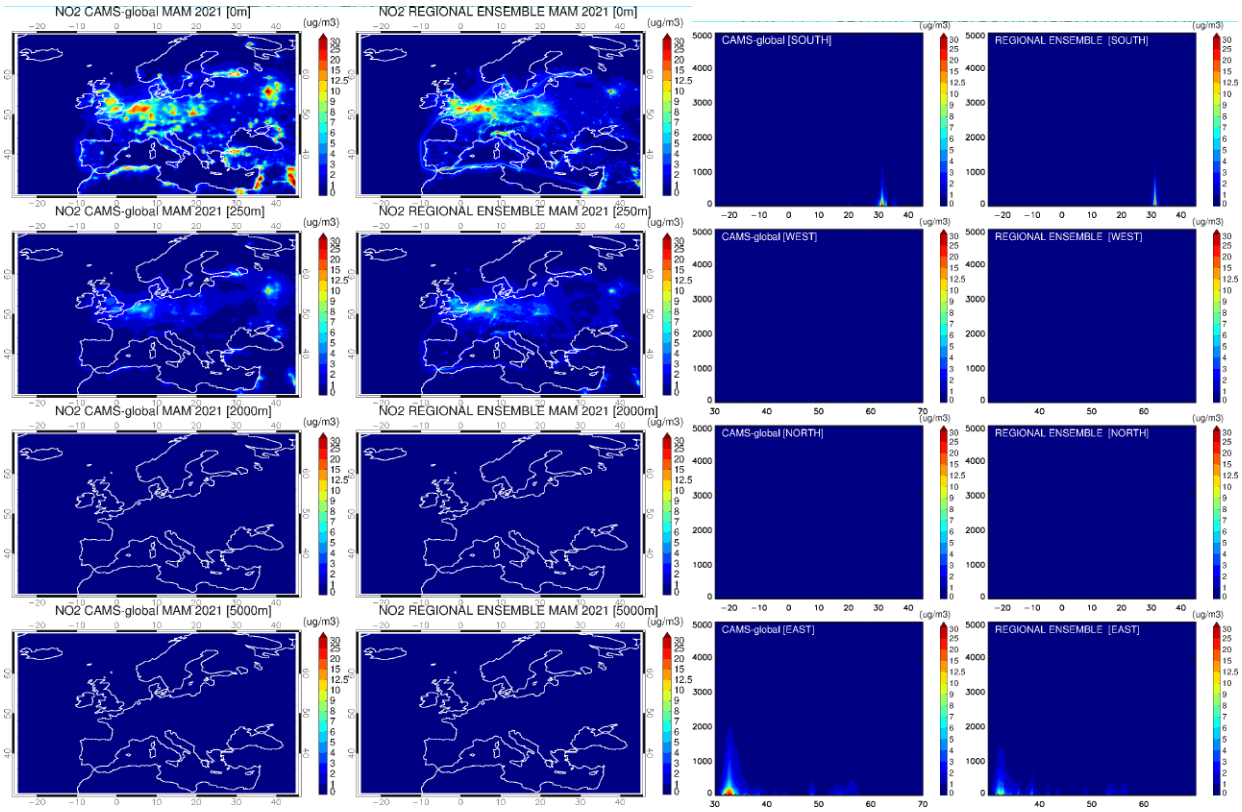

Figure 3.3. Left: Mean global and regional ENSEMBLE forecast NO_2 fields for four different vertical layers (0, 250, 2000, 5000 m) for MAM2021. Right: Cross sections for the same period of the global and regional ENSEMBLE NO_2 boundaries (south, west, north, east).

Regional model products are provided at the height levels of 0, 50, 250, 500, 1000, 2000, 3000 and 5000m. For every grid point and time step of the CAMS-global model, the differences between the height of each vertical layer midpoint z_m and the regional model height (e.g., 5000m) is calculated. The layer midpoint that exhibits the minimum height difference is the one that lies closest to the regional height level and is therefore selected for extraction of both chemical and aerosol species concentrations. The above procedure is performed for every regional height level. The final global product contains the O_3, CO, PM10 and PM2.5 concentrations in eight height levels that correspond to the CAMS-global vertical levels that lie closest to the regional height levels.

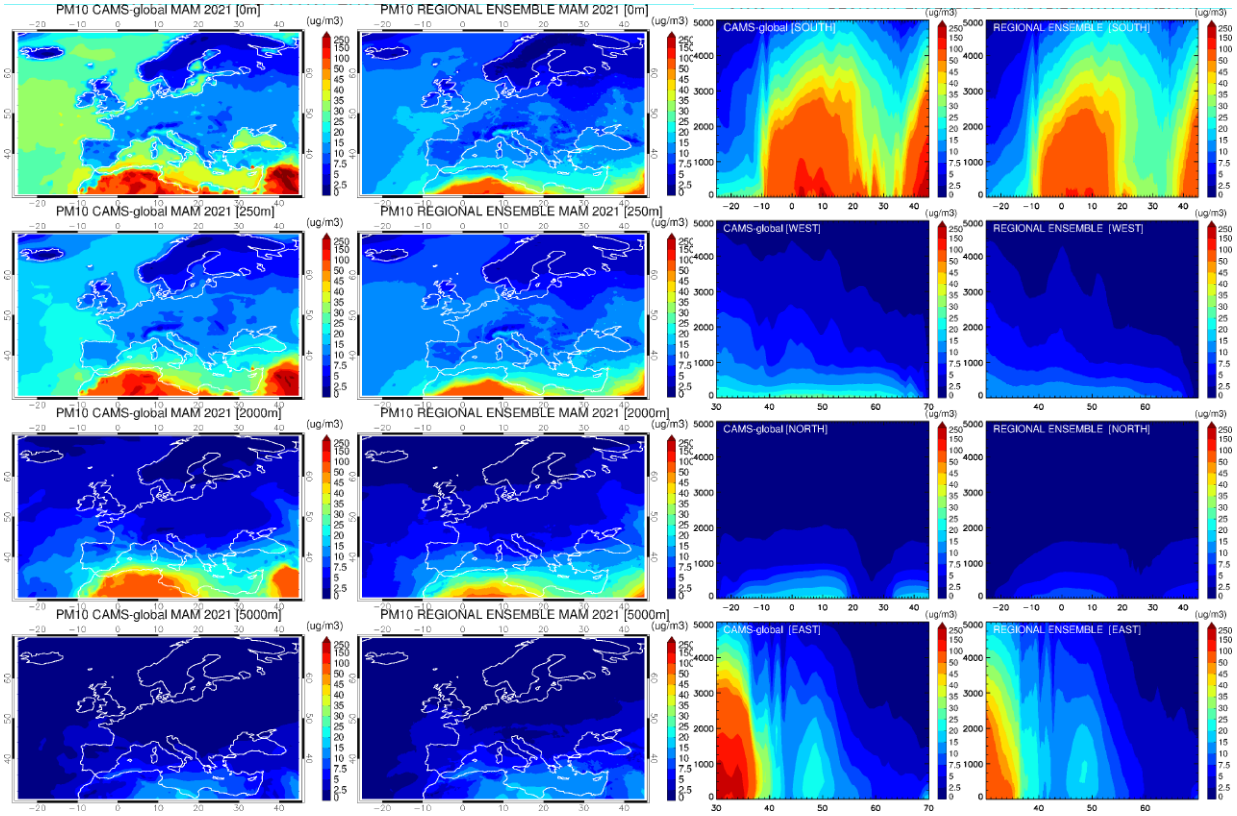

Figure 3.4 Left: Mean global and regional ensemble forecast PM10 fields for four different vertical layers (0, 250, 2000, 5000 m) for MAM2021. Right: Cross sections for the same period of the global and regional ensemble PM10 boundaries (south, west, north, east).

Table 3.1: Aerosol species description.

Label		**Name**	**Size (µm)**
aermr01	SS1	Sea Salt Aerosol	0.03-0.5
aermr02	SS2	Sea Salt Aerosol	0.5-5
aermr03	SS3	Sea Salt Aerosol	5-20
aermr04	DD1	Dust Aerosol	0.03-0.55
aermr05	DD2	Dust Aerosol	0.55-0.9
aermr06	DD3	Dust Aerosol	0.9-20
aermr07	OM1	Hydrophobic Organic Matter Aerosol	
aermr08	OM2	Hydrophilic Organic Matter Aerosol	
aermr09	BC1	Hydrophobic Black Carbon Aerosol	
aermr10	BC2	Hydrophilic Black Carbon Aerosol	
aermr11	SU1	Sulphate Aerosol	
aermr16	NI1	Nitrate fine mode aerosol	
aermr17	NI2	Nitrate coarse mode aerosol	
aermr18	NH3	Ammonium aerosol	

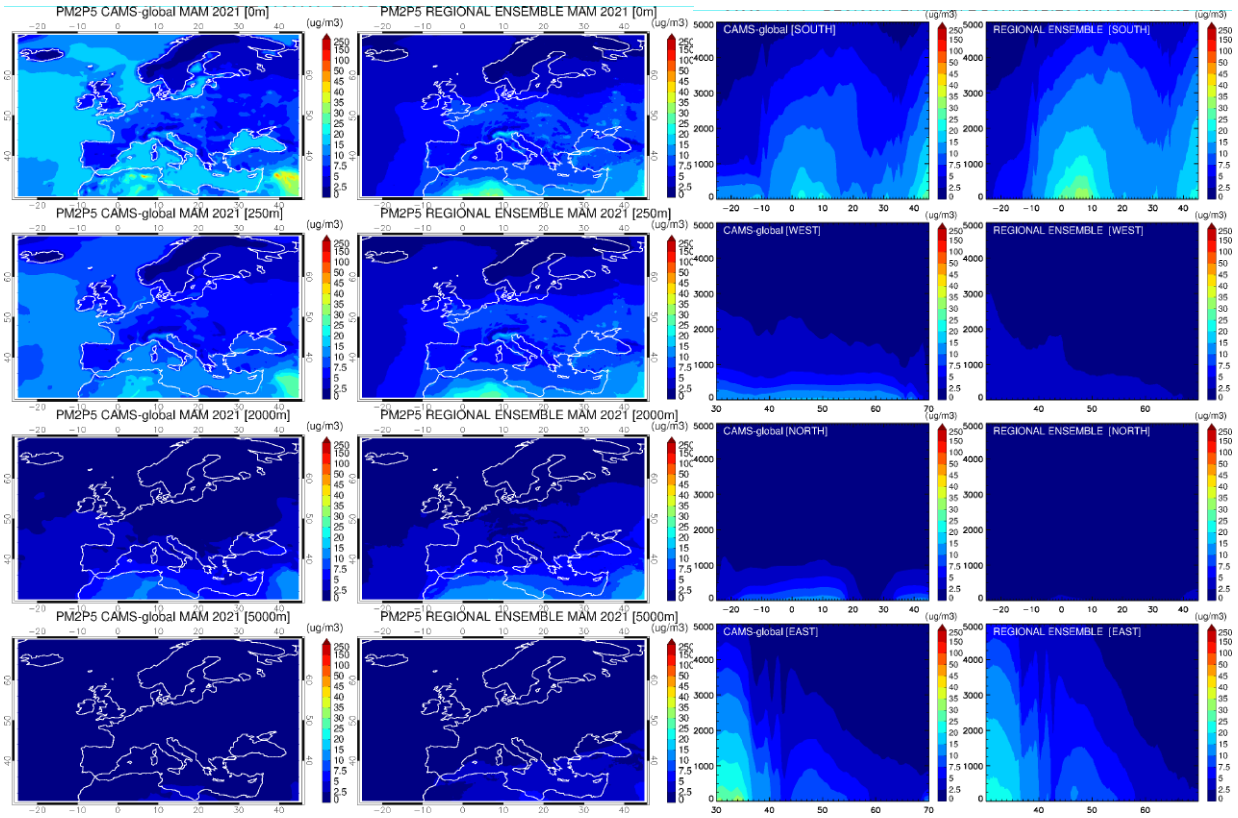

Figure 3.5 Left: Mean global and regional ENSEMBLE forecast $PM_{2.5}$ fields for four different vertical layers (0, 250, 2000, 5000 m) for MAM2021. Right: Cross sections for the same period of the global and regional ENSEMBLE ozone boundaries (south, west, north, east).

3.3 Consistency between the global and regional forecasts

This section reports on the consistency between the CAMS-global and regional ENSEMBLE forecast. The analysis is performed for O_3, CO, NO_2, PM_{10}, and $PM_{2.5}$ at four levels (0, 250, 2000 and 5000 m) for the time period from March to May 2021 (MAM2021).

Ozone (O_3)

Figure 3.1 presents the average MAM2021 spatial distribution of O_3 for several vertical layers (left) and the cross sections of the lateral boundaries (right) for the CAMS-global forecast and the regional ENSEMBLE. Overall, CAMS-global and ENSEMBLE agree well for O3, yet CAMS-global exhibits lower ozone concentrations near the surface over continental Europe and coastal North Africa. The agreement in the four boundaries is very good.

Carbon monoxide (CO)

Figure 3.2 depicts the seasonal mean fields of CO and the cross sections of lateral boundaries (right) for ENSEMBLE and CAMS-global. More local surface CO maxima are present in the CAMS-global forecast product, over eastern Europe, Italy, and the coast of North Africa. Likely, this arises from the different emissions in the two products. The comparison in the boundaries is quite good.

Nitrogen dioxide (NO_2)

Figure 3.3 shows the seasonal mean fields of NO_2 and the cross sections of lateral boundaries (right) for ENSEMBLE and CAMS-global. Overall, there are higher surface NO_2 concentrations in CAMS-global compared to ENSEMBLE over Europe, Middle-East, and North Africa. On the contrary, the ship emissions over the Mediterranean are mostly seen in the ENSEMBLE. From 2000m and above, both CAMS-global and ENSEMBLE exhibit very low concentrations (<1μg/m^3). The comparison in the boundaries is good.

Aerosols (PM_{10} and $PM_{2.5}$)

Figures 3.4 and 3.5 present the CAMS-global and ENSEMBLE spatial distributions (left) and lateral boundary cross sections (right) of PM_{10} and $PM_{2.5}$ mean fields, respectively. The main inconsistencies for particulate matter are summarized below:

- Higher PM_{10} and $PM_{2.5}$ in CAMS-global compared to ENSEMBLE in the boundary layer (mostly seen at the surface) over the Atlantic, probably associated with the latest CAMS-global upgrade (CY47R1) and the new sea-salt emissions scheme implementation.
- Higher PM_{10} in CAMS-global compared to ENSEMBLE over the southern and south-eastern boundaries of the domain up to 2000 m altitude.
- High PM_{10}/$PM_{2.5}$ surface concentrations over Middle East seen in CAMS-global are not found in ENSEMBLE.
- Higher PM_{10}/$PM_{2.5}$ at the west and north boundaries probably related to the abovementioned CAMS-global upgrade.

3.4 Regional variability

Ozone (O_3)

Figure 3.6 presents ozone mean fields for MAM2021 of the individual regional ensemble members and CAMS-global (bottom panel) for selected altitudes (0, 250, 2000, 5000 m). All regional models (to a lesser extend SILAM and LOTOS-EUROS) exhibit higher surface ozone concentrations over central Europe compared to CAMS-global. GEMAQ, LOTOS-EUROS, and EURAD models have lower O_3 values over the Atlantic, while all models, except GEMAQ and EURAD, exhibit higher concentrations over the Mediterranean near the surface. CHIMERE and MOCAGE exhibit higher O_3 concentrations up to 5000m compared to CAMS-global.

Carbon monoxide (CO)

The MAM2021 mean fields of carbon monoxide for the regional ensemble members as well as for CAMS-global are presented in Figure 3.7 for several vertical layers. No particular outliers are seen, with CO in the regional models being within the expect variability. EMEP and CHIMERE exhibit higher CO than all other regional models and CAMS-global within and above the boundary layer, respectively.

Nitrogen Dioxide (NO_2)

The MAM2021 mean fields of nitrogen dioxide for the regional ensemble members as well as for CAMS-global are shown in Figure 3.8 for different vertical layers. The two CAMS products compare generally good, and no obvious outliers are seen. EMEP and MATCH exhibit the less extended NO_2 concentrations near the surface among the regional models. The NO_2 hot spots over the coast of north western Africa in CAMS-global are mostly seen in LOTOS-EUROS. Low NO_2 concentrations (< 1µg/m^3) above 2000m are found in all regional models and the CAMS-global.

Aerosols (PM10 and PM2.5)

The mean PM_{10} and $PM_{2.5}$ fields for MAM2021 are depicted in Figures 3.9 and 3.10, respectively. Major features are noted below:

- MOCAGE and DEHM have higher surface PM_{10} over the Atlantic compared to the other regional models, with MOCAGE exhibiting higher PM_{10} even at 250 m altitude which is not consistent with the respective fields of CAMS-global .
- MOCAGE, MATCH and DEHM exhibit relatively less extended PM_{10} levels at the south boundary.
- CHIMERE has high PM_{10} near the south boundary at 5000m in contrast to the rest of regional models and CAMS-global.
- EMEP has quite higher $PM_{2.5}$ levels in the boundary layer near the south and south east boundaries compared to CAMS-global. CHIMERE, SILAM, EURAD, and GEMAG exhibit higher $PM_{2.5}$ near the south boundary, while LOTOS-EUROS, MOCAGE, MATCH, and DEHM have lower.

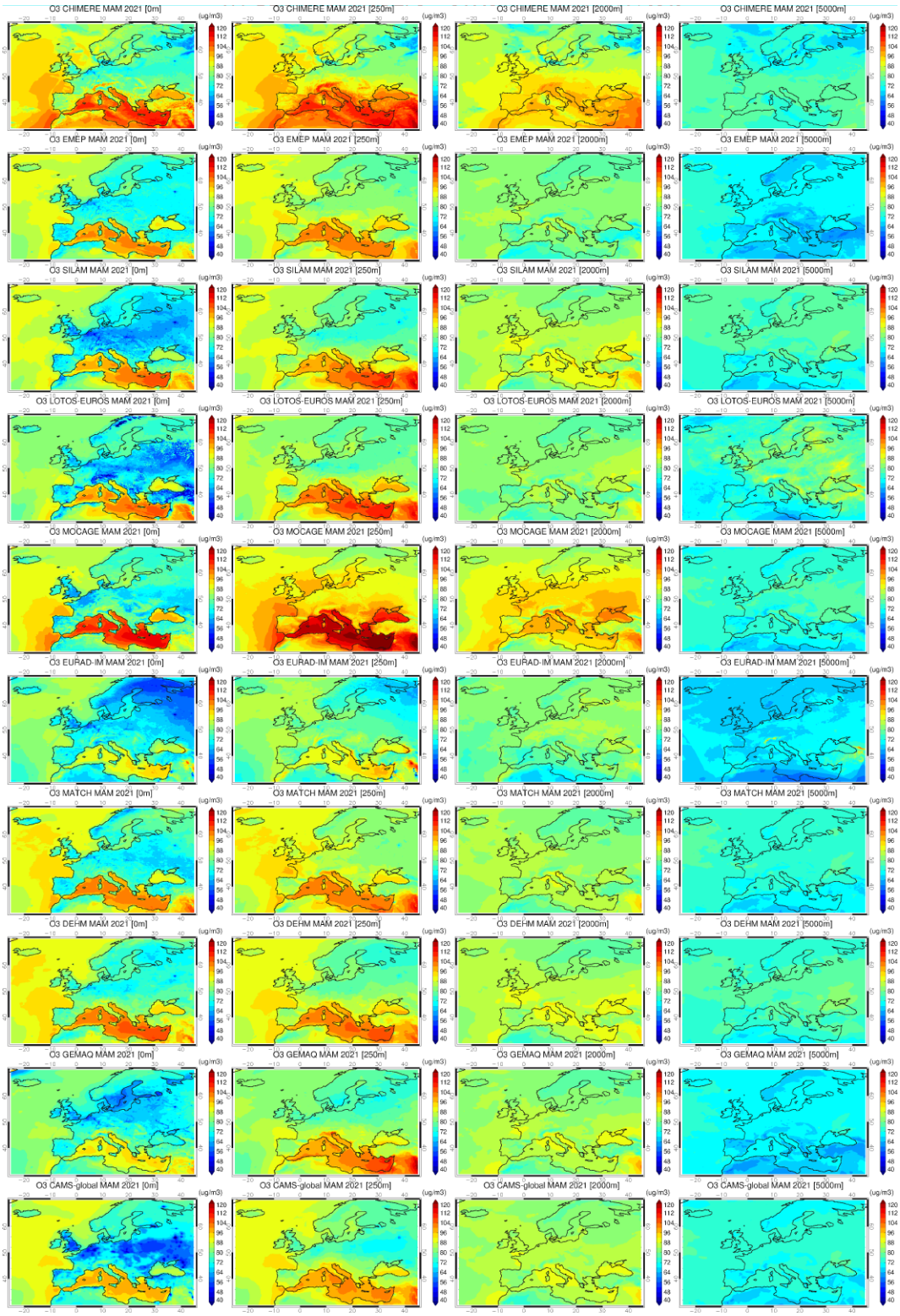

Figure 3.6 Mean regional ozone forecasts for MAM2021 for four different vertical layers (0, 250, 2000, 5000 m) from the nine ensemble members and CAMS-global (top to bottom: CHIMERE, EMEP, SILAM, LOTOS-EUROS, MOCAGE, EURAD-IM, MATCH, DEHM, GEM-AQ and CAMS-global).

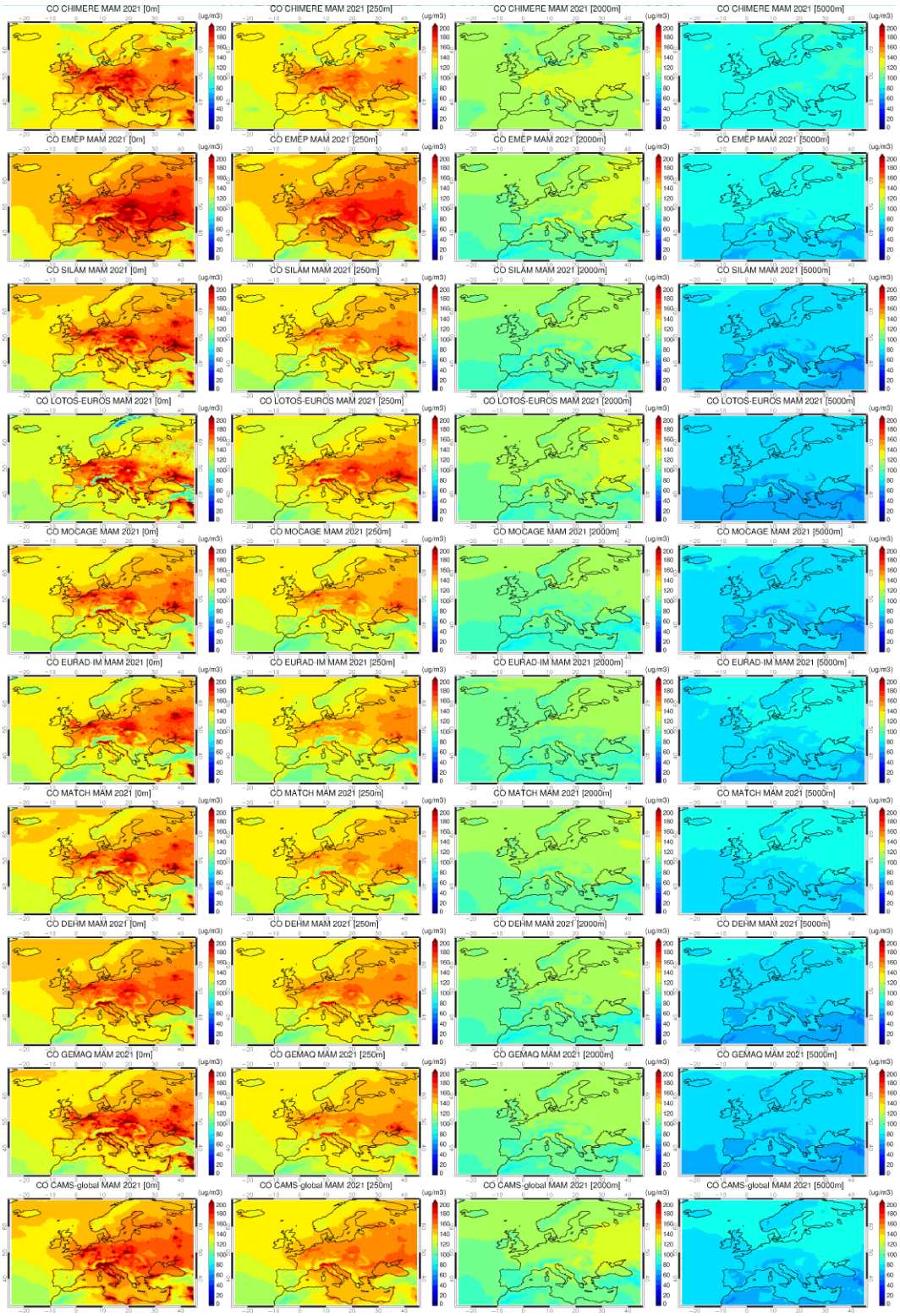

Figure 3.7. Mean regional CO forecasts for MAM2021 for four different vertical layers (0, 250, 2000, 5000 m) from the nine ensemble members and CAMS-global (top to bottom: CHIMERE, EMEP, SILAM, LOTOS-EUROS, MOCAGE, EURAD-IM, MATCH, DEHM, GEM-AQ and CAMS-global).

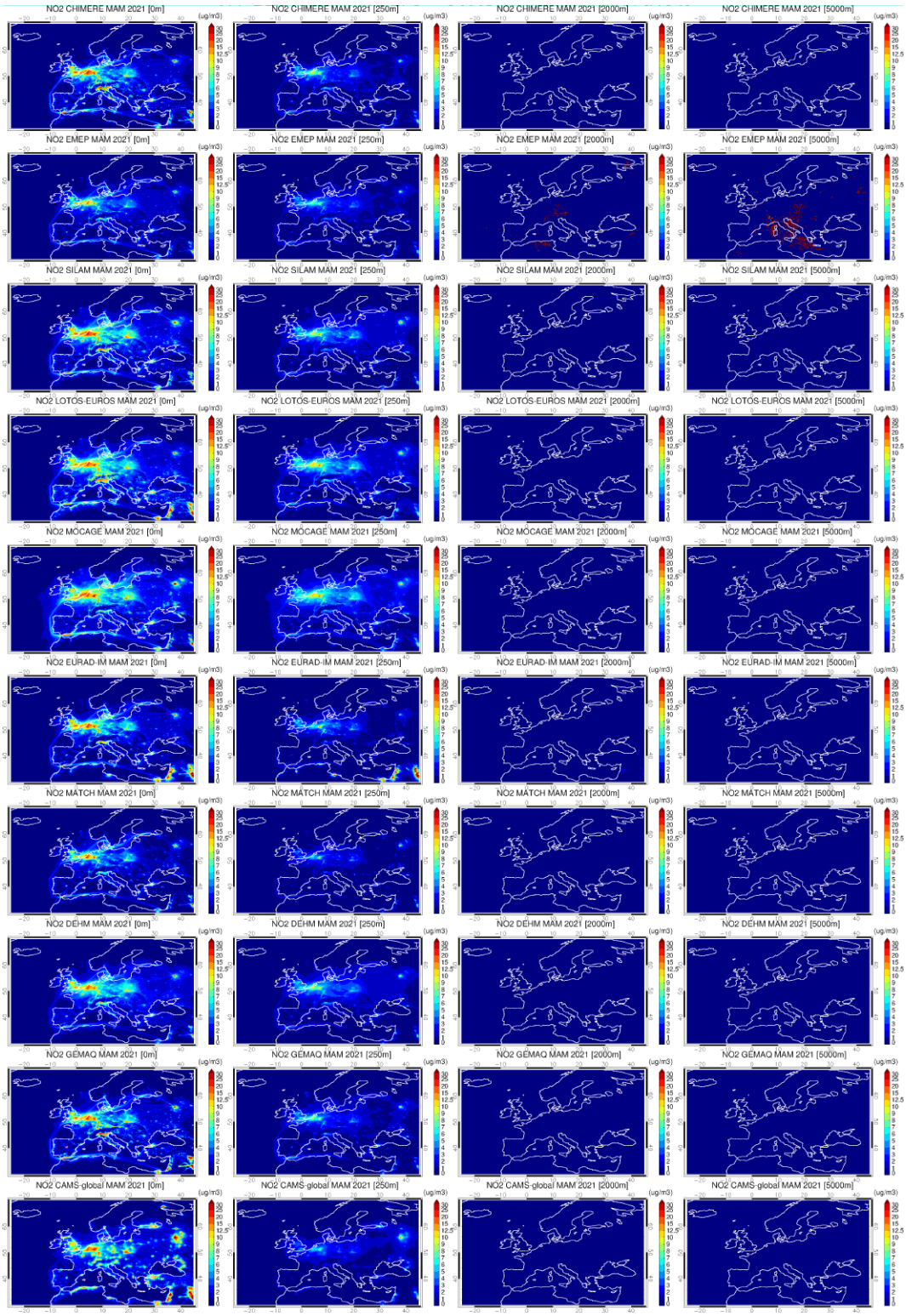

Figure 3.8. Mean regional NO_2 forecasts for MAM2021 for four different vertical layers (0, 250, 2000, 5000 m) from the nine ensemble members and CAMS-global (top to bottom: CHIMERE, EMEP, SILAM, LOTOS-EUROS, MOCAGE, EURAD-IM, MATCH, DEHM, GEM-AQ and CAMS-global).

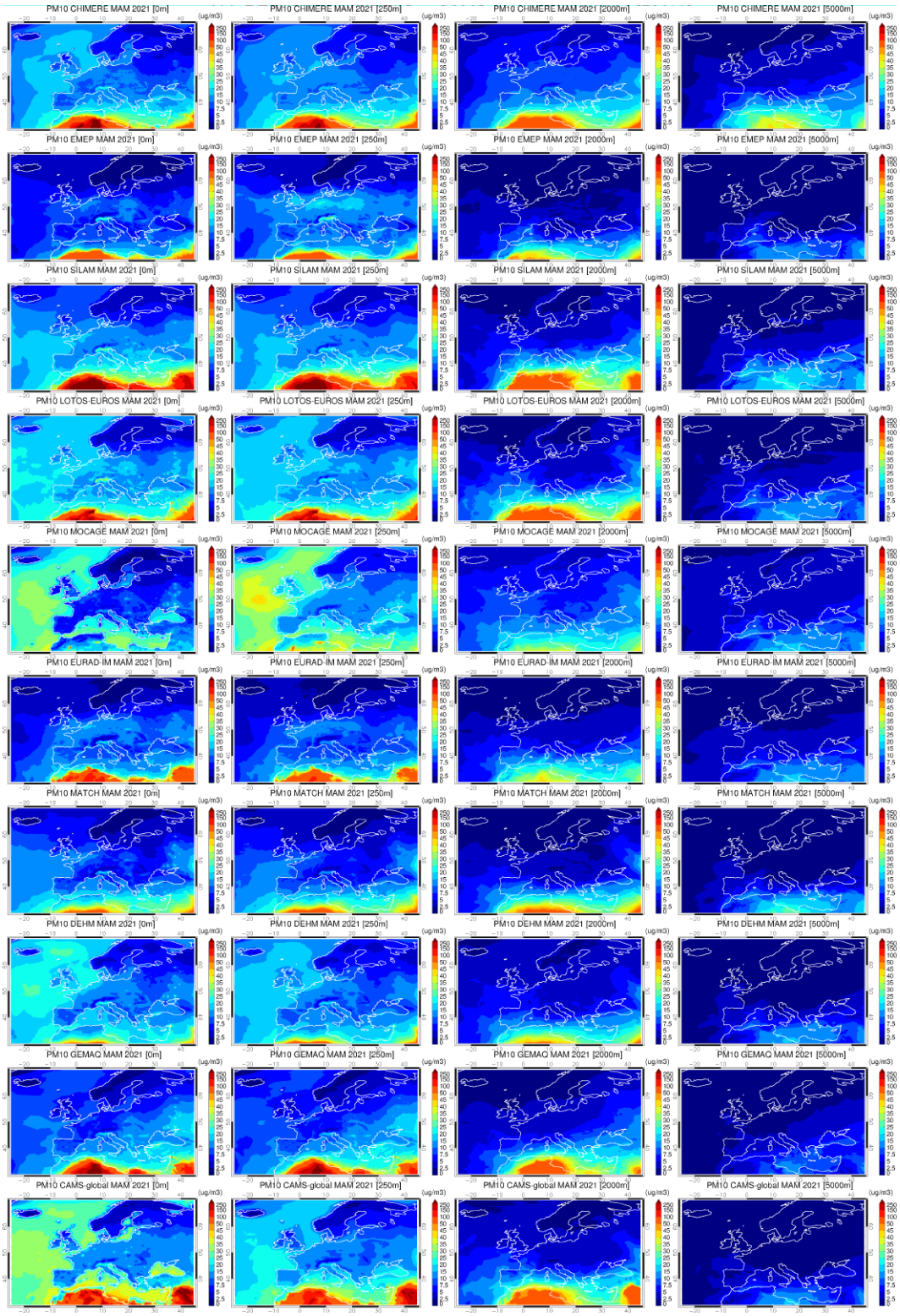

Figure 3.9. Mean regional PM_{10} forecasts for MAM2021 for four different vertical layers (0, 250, 2000, 5000 m) from the nine ensemble members and CAMS-global (top to bottom: CHIMERE, EMEP, SILAM, LOTOS-EUROS, MOCAGE, EURAD-IM, MATCH, DEHM, GEM-AQ and CAMS-global).

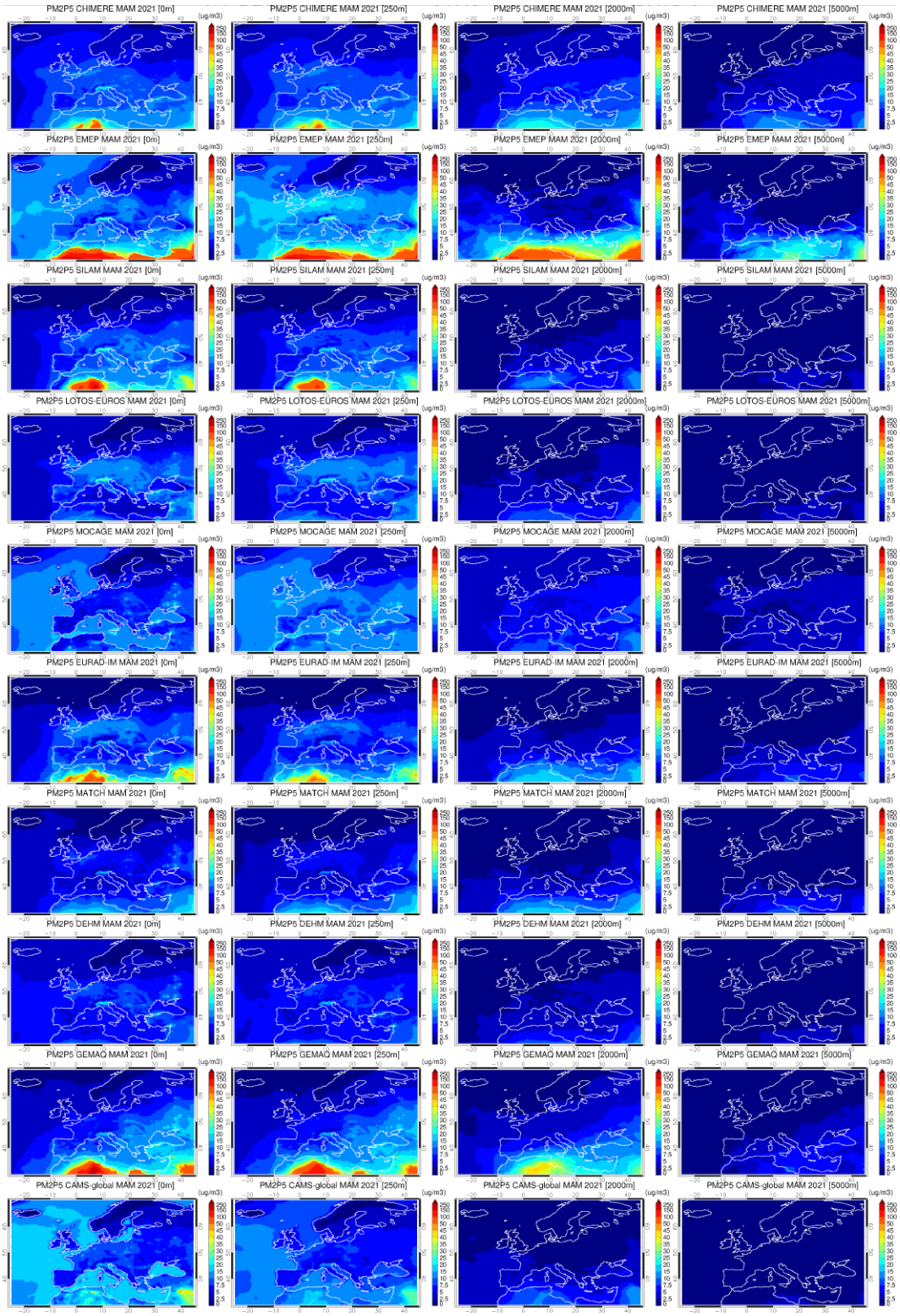

Figure 3.10. Mean regional $PM_{2.5}$ forecasts for MAM2021 for four different vertical layers (0, 250, 2000, 5000 m) from the nine ensemble members and CAMS-global (top to bottom: CHIMERE, EMEP, SILAM, LOTOS-EUROS, MOCAGE, EURAD-IM, MATCH, DEHM, GEM-AQ and CAMS-global).

3.5 Time series

Figure 3.11 shows the mean daily time series for MAM2021 for the five species, namely O_3, CO, NO_2, PM_{10}, and $PM_{2.5}$ (from left to right) for different European sub-regions (from top to bottom): Alps (AL), British Isles (BI), East Europe (EA), France (FR), Iberian Peninsula (IP), Mediterranean (MD), Mid-Europe (ME), Scandinavia (SC).

Each subregion is defined with the following latitude/longitude boundaries:

Name = (BI, IP, FR, ME, SC, AL, MD, EA)

West = (-10, -10, -5, 2, 5, 5, 3, 16)

East = (2, 3, 5, 16, 30, 15, 25, 30)

South = (50, 36, 44, 48, 55, 44, 36, 44)

North = (59, 44, 50, 55, 70, 48, 44, 55)

The letter R denotes the temporal correlation between the two products. Only concentrations over land are used.

For O_3 the temporal variability between CAMS-global and ENSEMBLE is in very good agreement (R values of 0.85 to 0.93) for all regions, but MD (0.58). CAMS-global exhibits lower O_3 for BI, EA, FR, and ME.

The temporal correlation for CO is also very good (0.87 to 0.97), with CAMS-global exhibiting higher levels mostly for the Alps.

For NO_2 the temporal variability between CAMS-global and ENSEMBLE is very good (R values of 0.83 to 0.96).

The agreement in the PM_{10} daily timeseries between the global and regional forecasts ranges is very good (R values of 0.78 to 091) for all regions, with the exception of SC (0.54).

The magnitude of PM_{10} in CAMS-global is close to the regional ensemble.

GEMAQ (light green) and to a lesser extend SILAM (orange) exhibit higher PM_{10} compared to CAMS-global during some CAMS-global peaks

The temporal agreement in surface PM2.5 is quite good (0.62 to 0.91).

EMEP (brown) and GEMAC (light green) exhibit some $PM_{2.5}$ peaks that are not seen in CAMS-global.

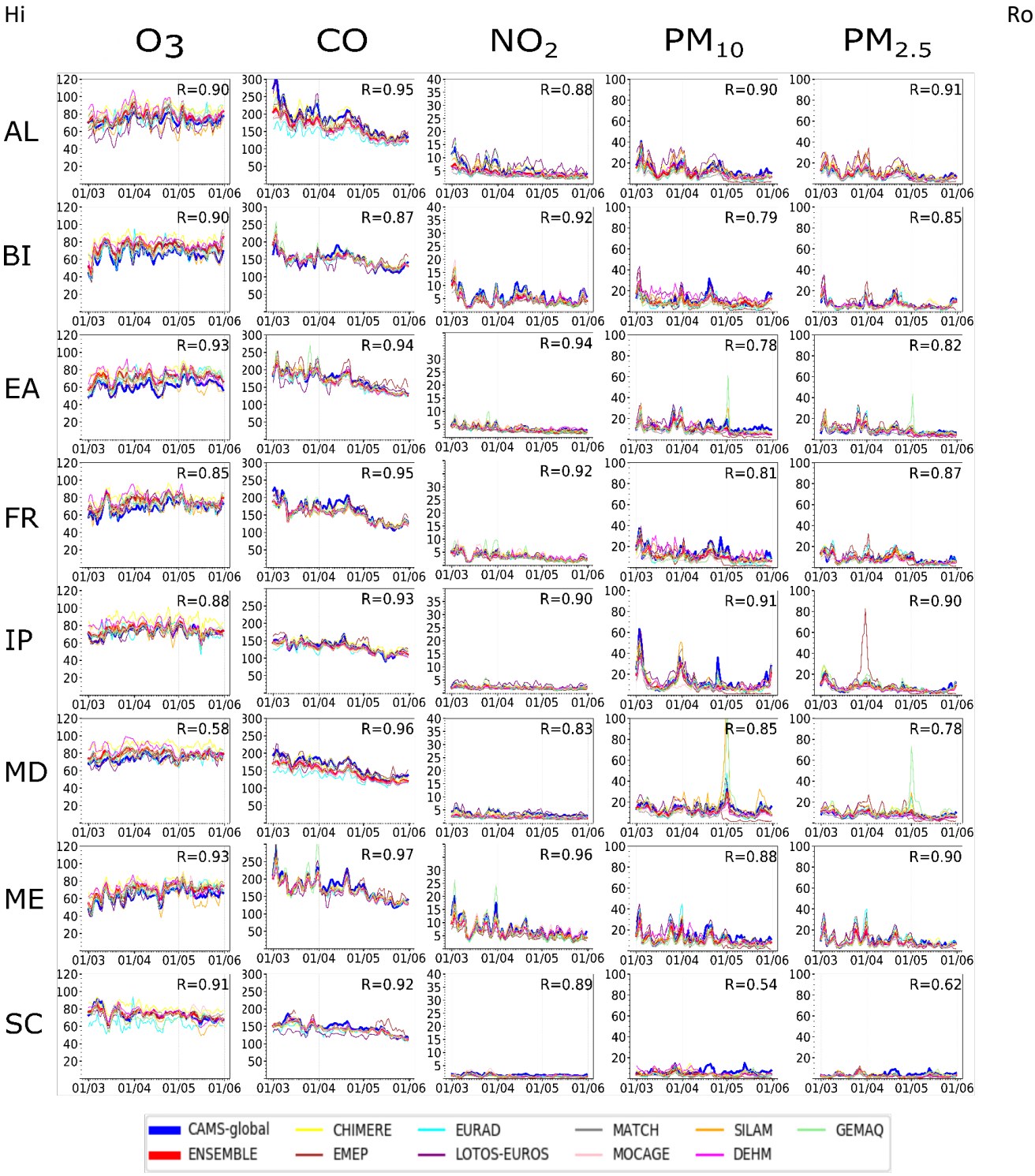

Figure 3.11. Mean daily time series for surface O_3, CO, NO_2, PM_{10}, and $PM_{2.5}$ for MAM2021 (unit µg/m^3). The blue line is CAMS-global and the red line the ENSEMBLE forecasts. Each line in the composite plot denotes a different European subregion.

3.6 Diurnal cycles

Figure 3.12 presents the diurnal cycles for surface O_3, CO, NO_2, PM_{10}, and $PM_{2.5}$ averaged over the period MAM2021 for different European sub-regions (from top to bottom): Alps (AL), British Isles (BI), East Europe (EA), France (FR), Iberian Peninsula (IP), Mediterranean (MD), Mid-Europe (ME), Scandinavia (SC). The red colour is used for the regional ensemble and the blue for CAMS-global.

There is a good agreement for between the CAMS-global and the regional diurnal cycles, both in timing and amplitude of the diurnal cycle.

The diurnal range for surface CO is less pronounced for the regional products over AL, FR, and MD.

The diurnal cycle of NO_2 at the surface indicates that the regional product and the CAMS-global forecasts agree on the shape, yet the diurnal range is higher in CAMS-global mostly over AL, BI, MD, and ME.

There is a mediocre and good agreement of the PM_{10} and $PM_{2.5}$ diurnal cycles, respectively, between the global and the regional product.

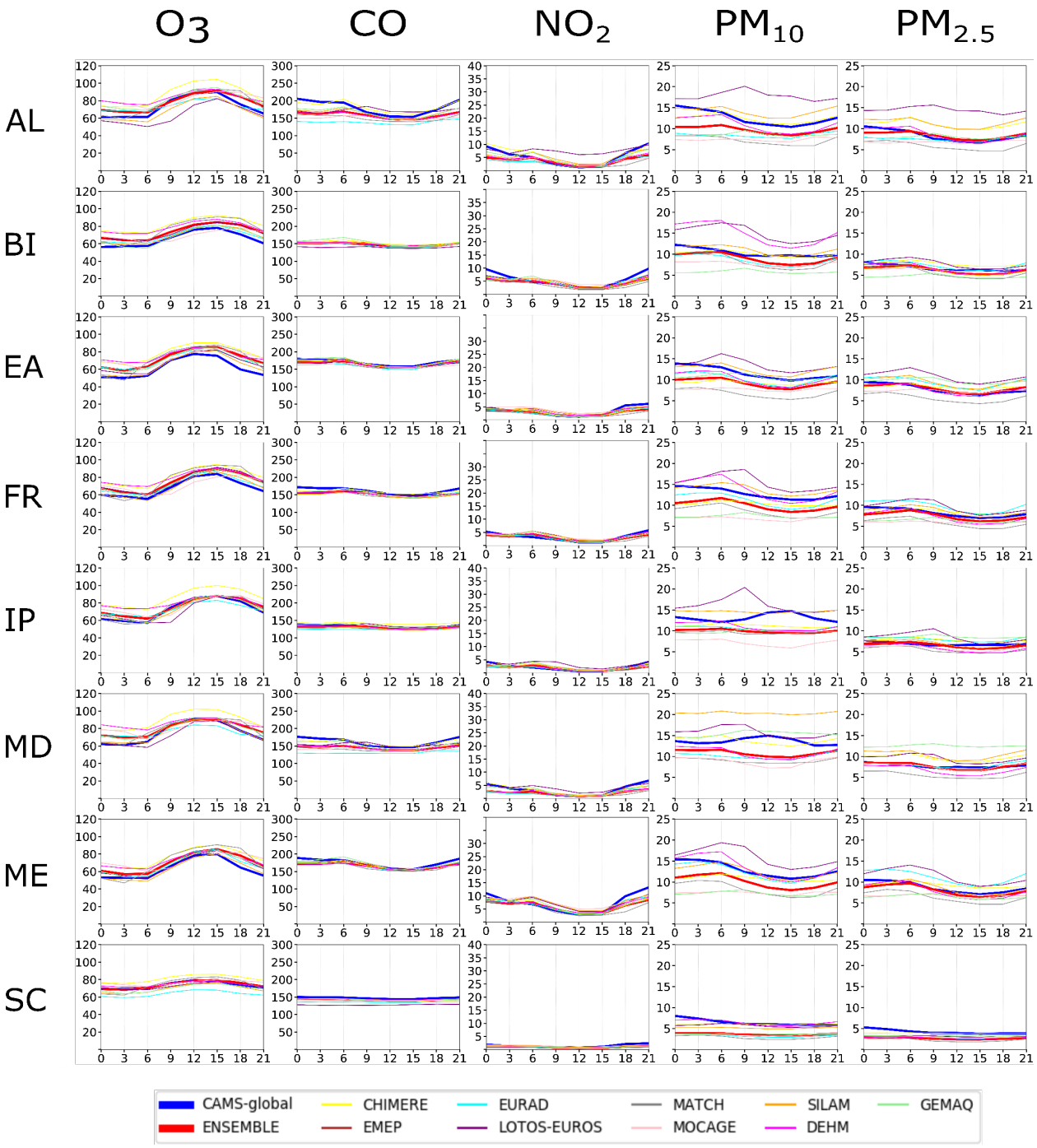

Figure 3.12. Diurnal cycles for surface O_3, CO, NO_2, PM_{10}, and $PM_{2.5}$ for the period MAM2021 (unit: µg/m^3). The blue line is CAMS-global and the red line the ENSEMBLE forecast. Each line in the composite plot denotes a different European sub-region.

3.7 Regional domain boundary cross sections

Ozone (O_3)

Figure 3.13 shows the regional variability in the lateral domain boundary cross sections of O_3 (from left to right): south, west, north, east and the different ensemble members and CAMS-global (from top to bottom) averaged over the period MAM2021. CHIMERE in all four boundaries has spurious implementation of O_3 boundaries, while EURAD at all four boundaries differs slightly from the rest of the regional models.

Carbon monoxide (CO)

Figure 3.14 presents the regional variability in the lateral cross sections of CO (from left to right): south, west, north, east and the different ensemble members and CAMS-global (from top to bottom) averaged over the period MAM2021. CHIMERE appears to have the same issue with the boundaries implementation as with ozone.

Nitrogen dioxide (NO_2)

Figure 3.15 shows the regional variability in the lateral cross sections of NO_2 (from left to right): south, west, north, east and the different ensemble members and CAMS-global (from top to bottom) averaged over the period MAM2021. Overall, there is no particular outlier for NO_2 boundaries. MOCAGE shows the most extended NO_2 concentrations at the east boundaries of the domain, with EURAD exhibiting the higher NO_2 at the east boundary from 30^o to 40^o N.

Aerosols (PM_{10} and $PM_{2.5}$)

Figure 3.16/3.17 presents the regional variability in the lateral cross sections of PM_{10}/$PM_{2.5}$ respectively (left to right) during MAM2021: south, west, north, east and the different ensemble members and CAMS-global (top to bottom). We note the following inconsistencies:

- MOCAGE and EURAD have lower PM_{10} concentrations over the south boundaries compared to CAMS-global.
- CHIMERE has the most vertically extended PM_{10} at the south boundaries.
- MOCAGE, EURAD, and to a lesser extend DEHM and GEMAQ have lower PM_{10} at the east boundaries compared to CAMS-global.
- All regional models, except MOCAGE, SILAM and LOTOS-EUROS, exhibit lower PM_{10} at the west and north boundaries, possibly related with the latest CAMS-global upgrade (sea salt emissions scheme).
- EMEP has quite higher $PM_{2.5}$ at south and east boundaries compared to the rest of regional models and the CAMS-global.
- All models except LOTOS-EUROS, MOCAGE, and DEHM have higher southern $PM_{2.5}$ boundaries than CAMS-global.
- EURAD and GEMAQ, have higher eastern $PM_{2.5}$ boundaries than CAMS-global.

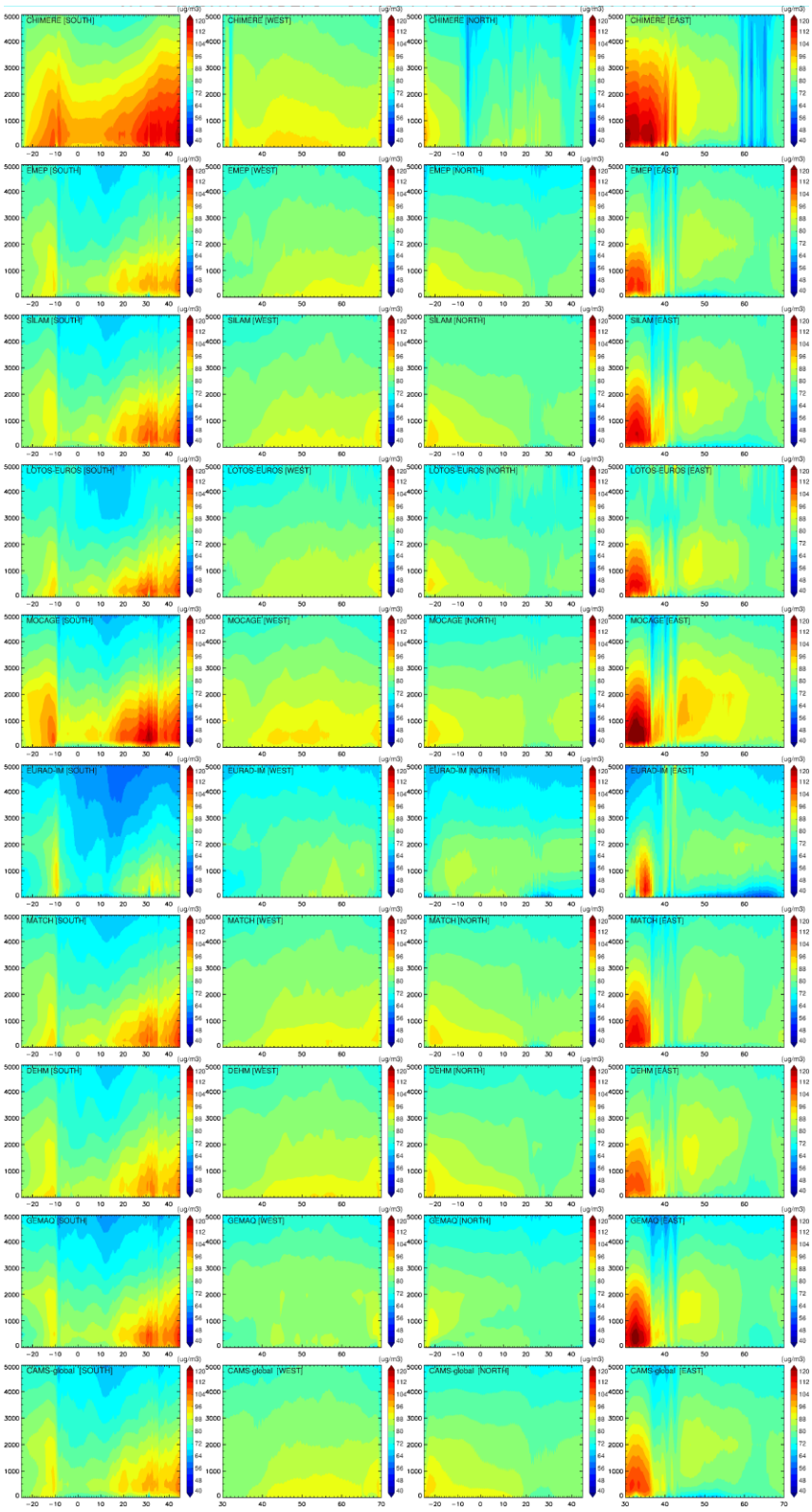

Figure 3.13. Ozone cross sections for MAM2021 for the nine ensemble members and CAMS-global (top to bottom: CHIMERE, EMEP, SILAM, LOTOS-EUROS, MOCAGE, EURAD-IM, MATCH, DEHM, GEM-AQ and CAMS-global) and the lateral boundaries (left to right: south, west, north, east).

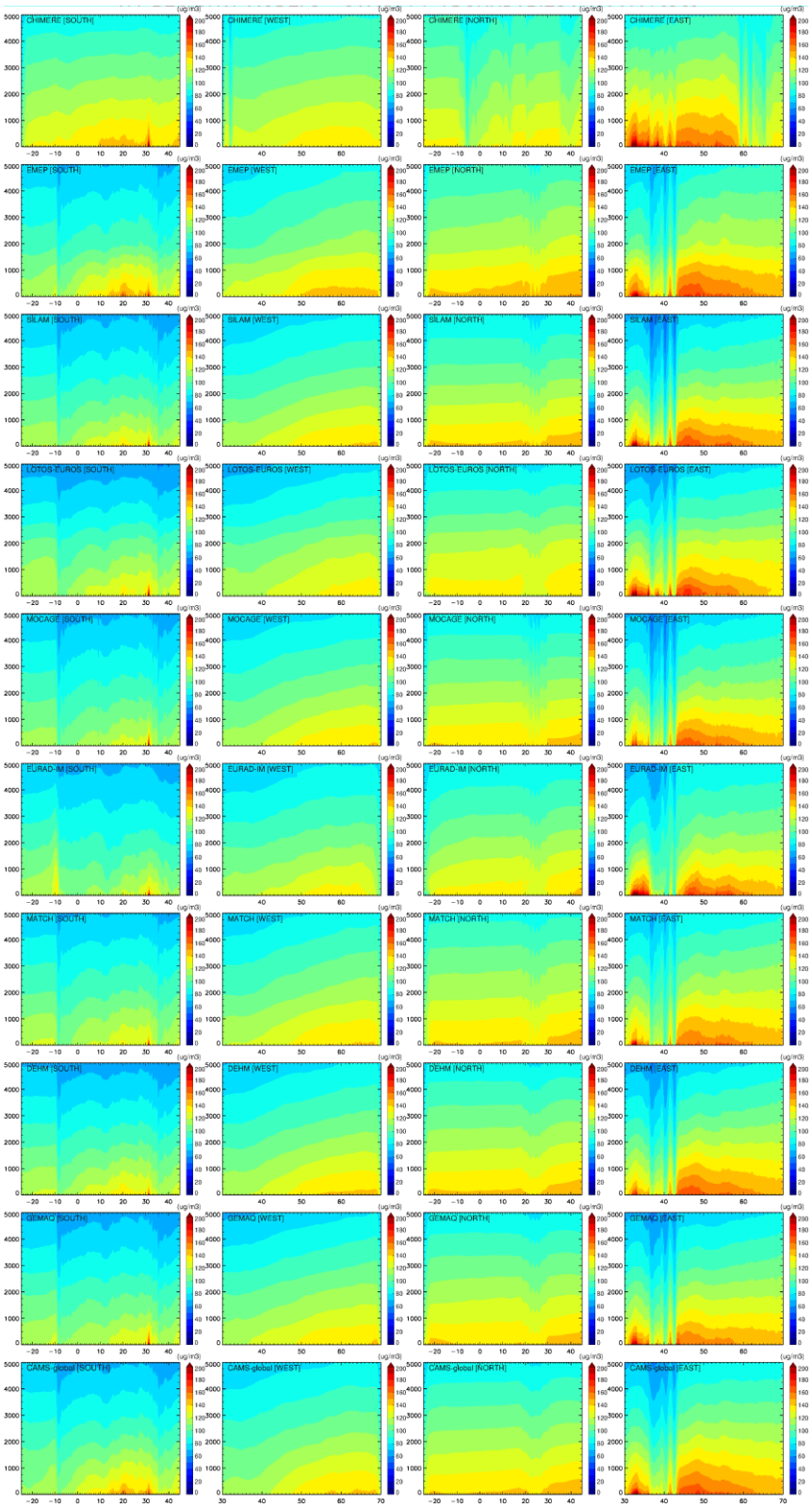

Figure 3.14. Carbon Monoxide cross sections for MAM2021 for the nine ensemble members and CAMS-global (top to bottom: CHIMERE, EMEP, SILAM, LOTOS-EUROS, MOCAGE, EURAD-IM, MATCH, DEHM, GEM-AQ and CAMS-global) and the lateral boundaries (left to right: south, west, north, east).

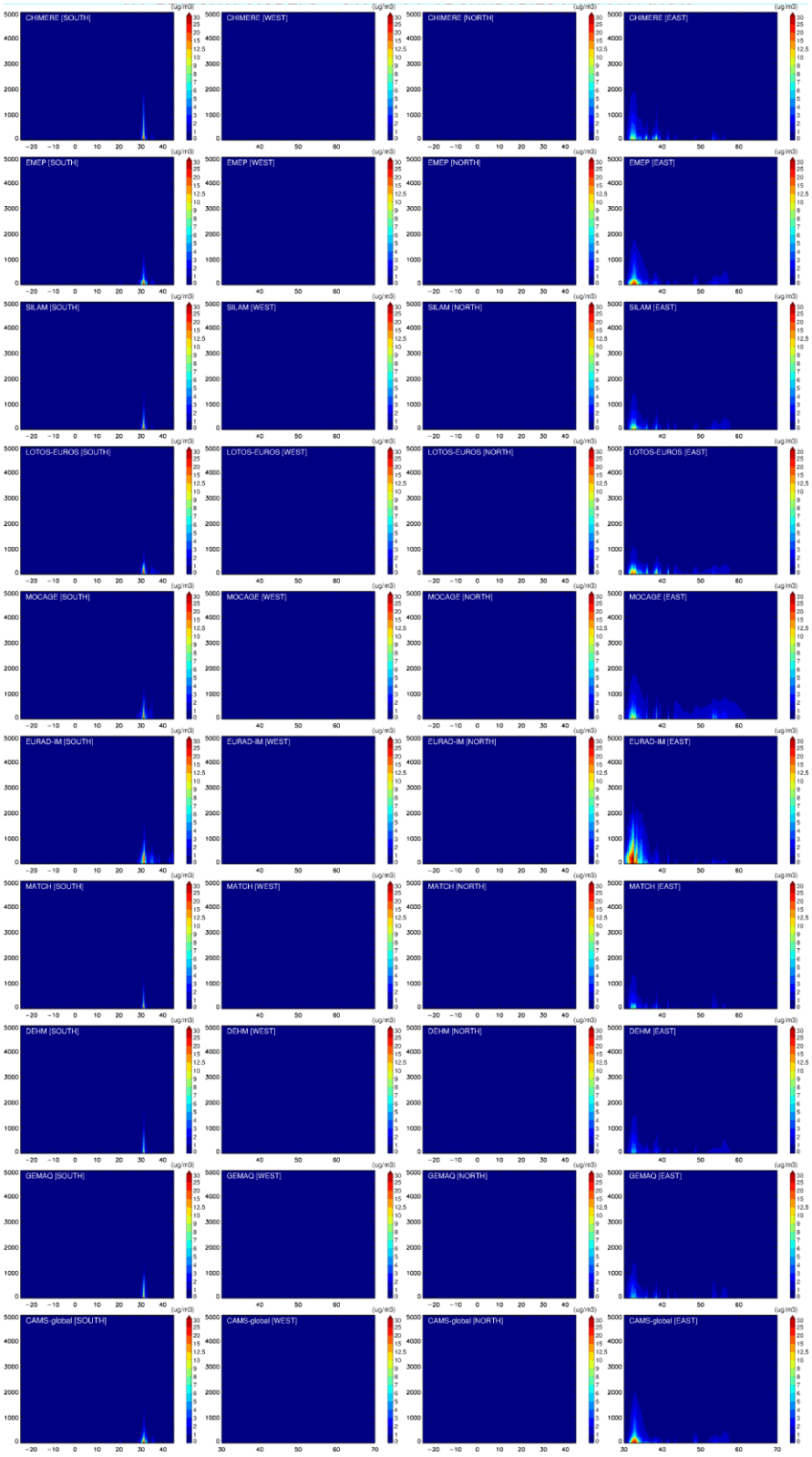

Figure 3.15. Nitrogen dioxide cross sections for MAM2021 for the nine ensemble members and CAMS-global (top to bottom: CHIMERE, EMEP, SILAM, LOTOS-EUROS, MOCAGE, EURAD-IM, MATCH, DEHM, GEM-AQ and CAMS-global) and the lateral boundaries (left to right: south, west, north, east).

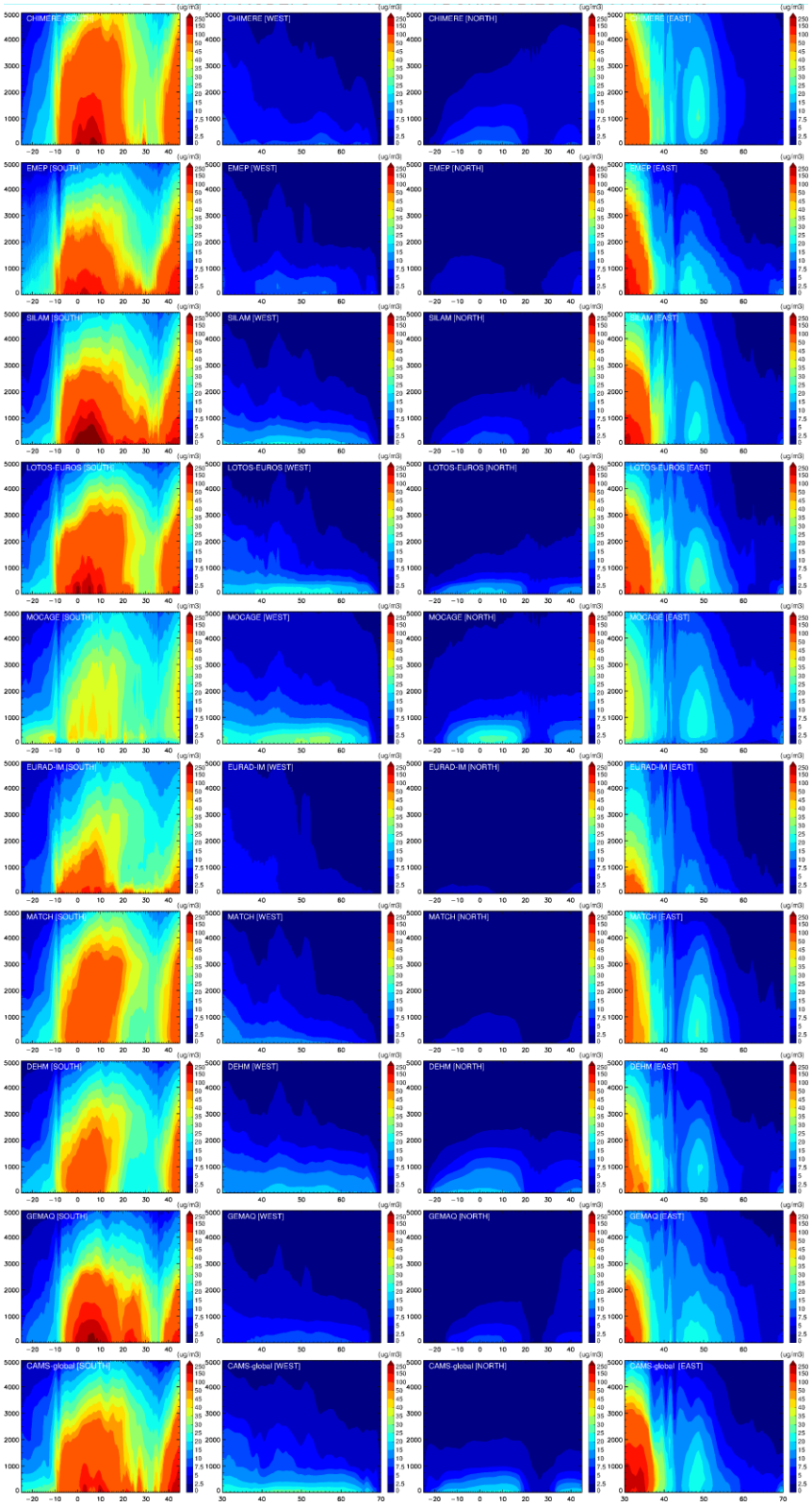

Figure 3.16. Aerosol PM_{10} cross sections for MAM2021for the nine ensemble members and CAMS-global (top to bottom: CHIMERE, EMEP, SILAM, LOTOS-EUROS, MOCAGE, EURAD-IM, MATCH, DEHM, GEM-AQ and CAMS-global) and the lateral boundaries (left to right: south, west, north, east).

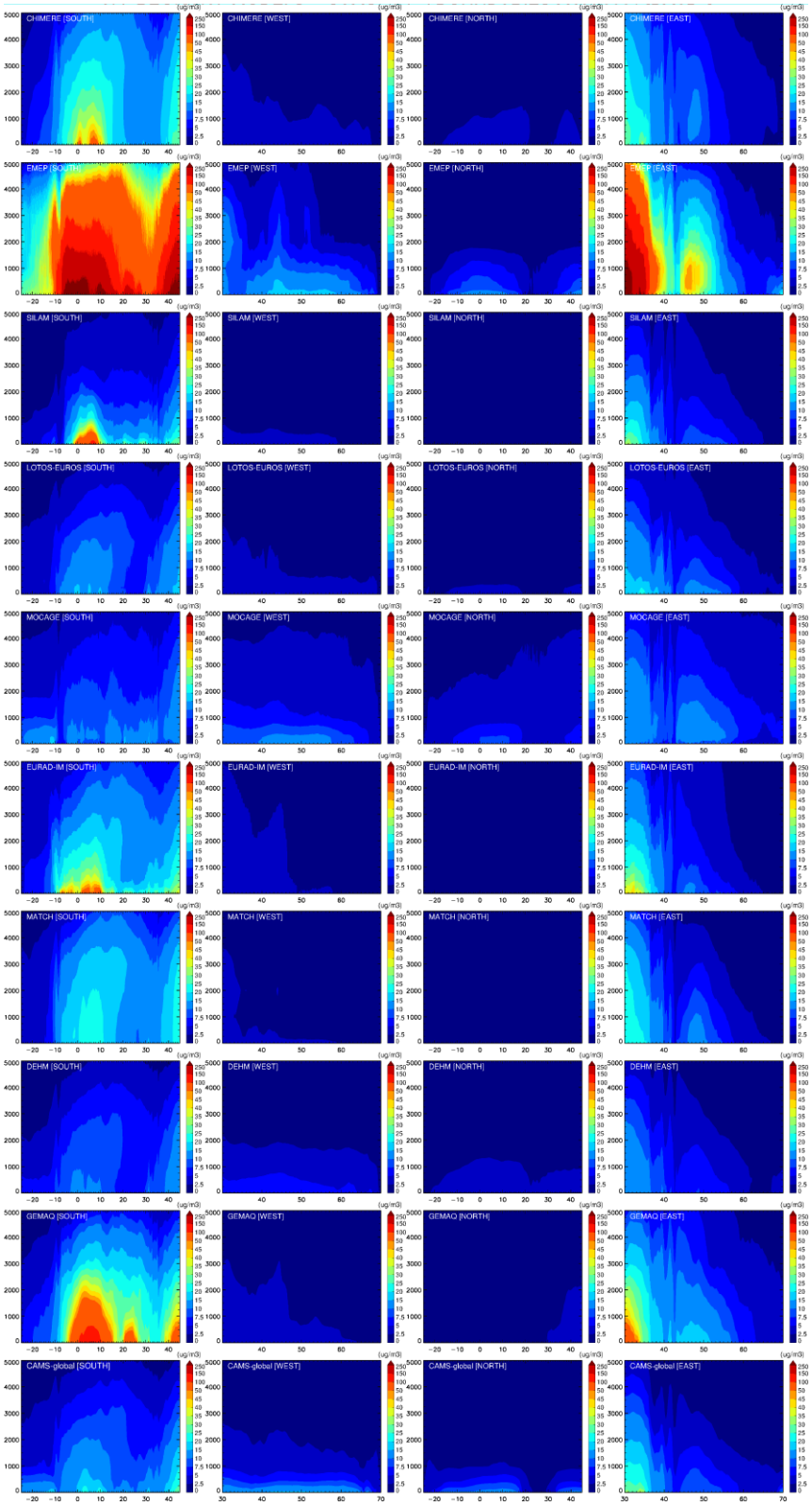

Figure 3.17 Aerosol $PM_{2.5}$ cross sections for MAM2021 for the nine ensemble members and CAMS-global (top to bottom: CHIMERE, EMEP, SILAM, LOTOS-EUROS, MOCAGE, EURAD-IM, MATCH, DEHM, GEM-AQ and CAMS-global) and the lateral boundaries (left to right: south, west, north, east).

3.8 Regional analysis vs. regional forecasts

Here we compare the regional analysis products with the regional forecasts (Day1). The four following figures (3.18-3.22) show the mean regional differences between analysis and forecasts for the time period MAM2021 at four different vertical layers (0, 250, 2000, 5000 m, left to right) including O_3, CO, NO_2, PM_{10}, and $PM_{2.5}$, respectively.

Regional models with the largest differences between the analyses and the 1st day forecasts are for:

Ozone

- CHIMERE and SILAM near the surface.
- EMEP and DEHM mostly within the boundary layer.
- MATCH, MOCAGE, and LOTOS-EUROS in all levels. For LOTOS-EUROS, this difference can be attributed to the difference in vertical resolution between the forecast and analysis suites.

Carbon monoxide

Differences are seen in:

- MATCH and SILAM up to 2000m, and EMEP and DEHM within the boundary layer, exhibit much lower CO levels compared to analysis.
- CHIMERE and GEMAQ at the surface.

Nitrogen dioxide

- Lower NO_2 forecast compared to analysis at the surface for CHIMERE and SILAM, and in the boundary layer for EMEP.

PM_{10} and $PM_{2.5}$

- Minor differences in some models. Most pronounced are in MATCH for PM_{10} and $PM_{2.5}$ with lower forecast compared to analysis, and LOTOS-EUROS and EMEP for PM_{10} and $PM_{2.5}$, respectively, at the south boundary.

It is important to note that the differences observed between the forecast and the analysis do not only reflect the impact of the assimilation but may also result from differences in the model setup between the analysis systems and the forecast systems.

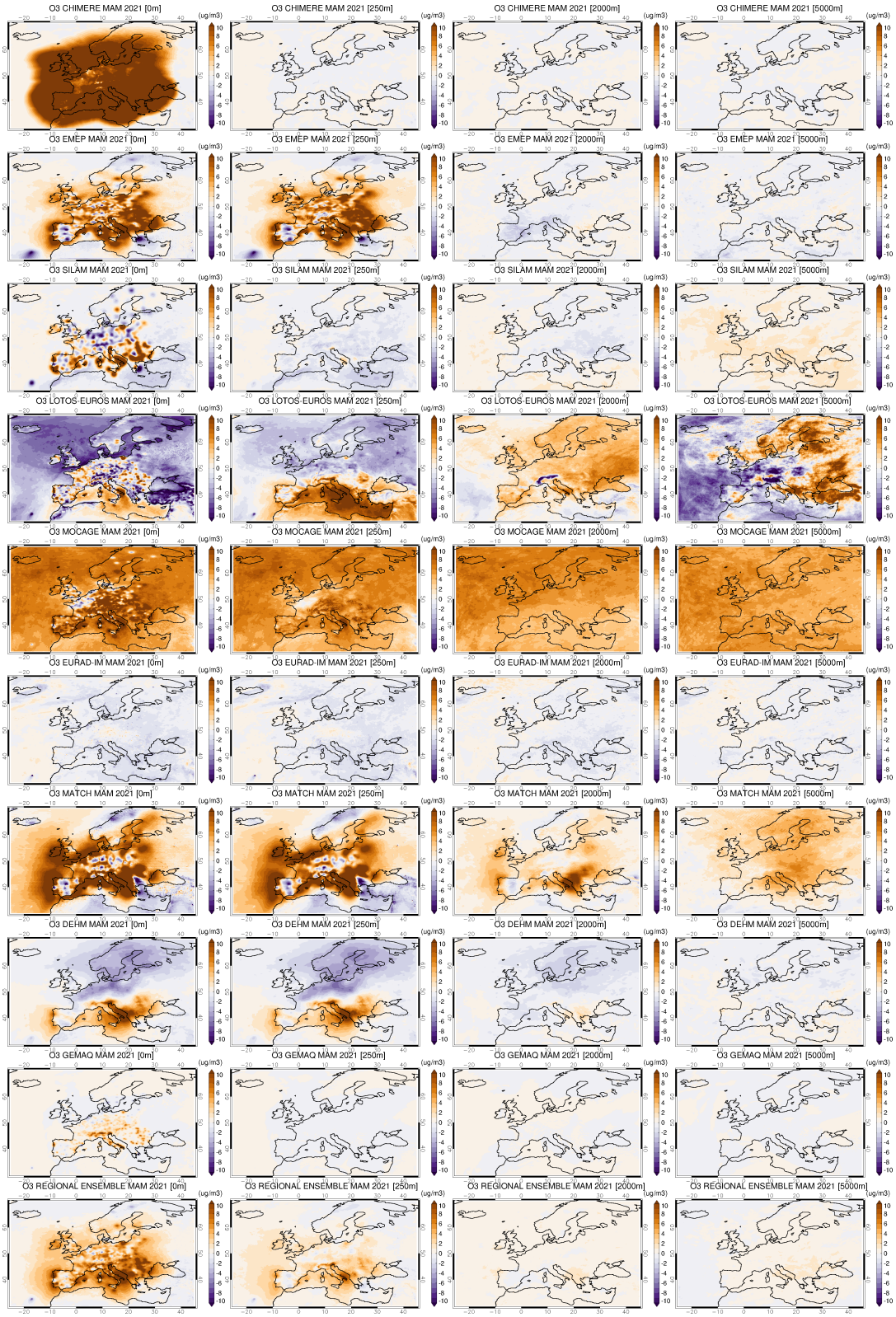

Figure 3.18. Mean regional O_3 differences between analysis and forecast for MAM2021 for four different vertical layers (0, 250, 2000, 5000 m) from regional ENSEMBLE and individual ensemble members (top to bottom: CHIMERE, EMEP, SILAM, LOTOS-EUROS, MOCAGE, EURAD-IM, MATCH, DEHM, GEM-AQ and ENSEMBLE).

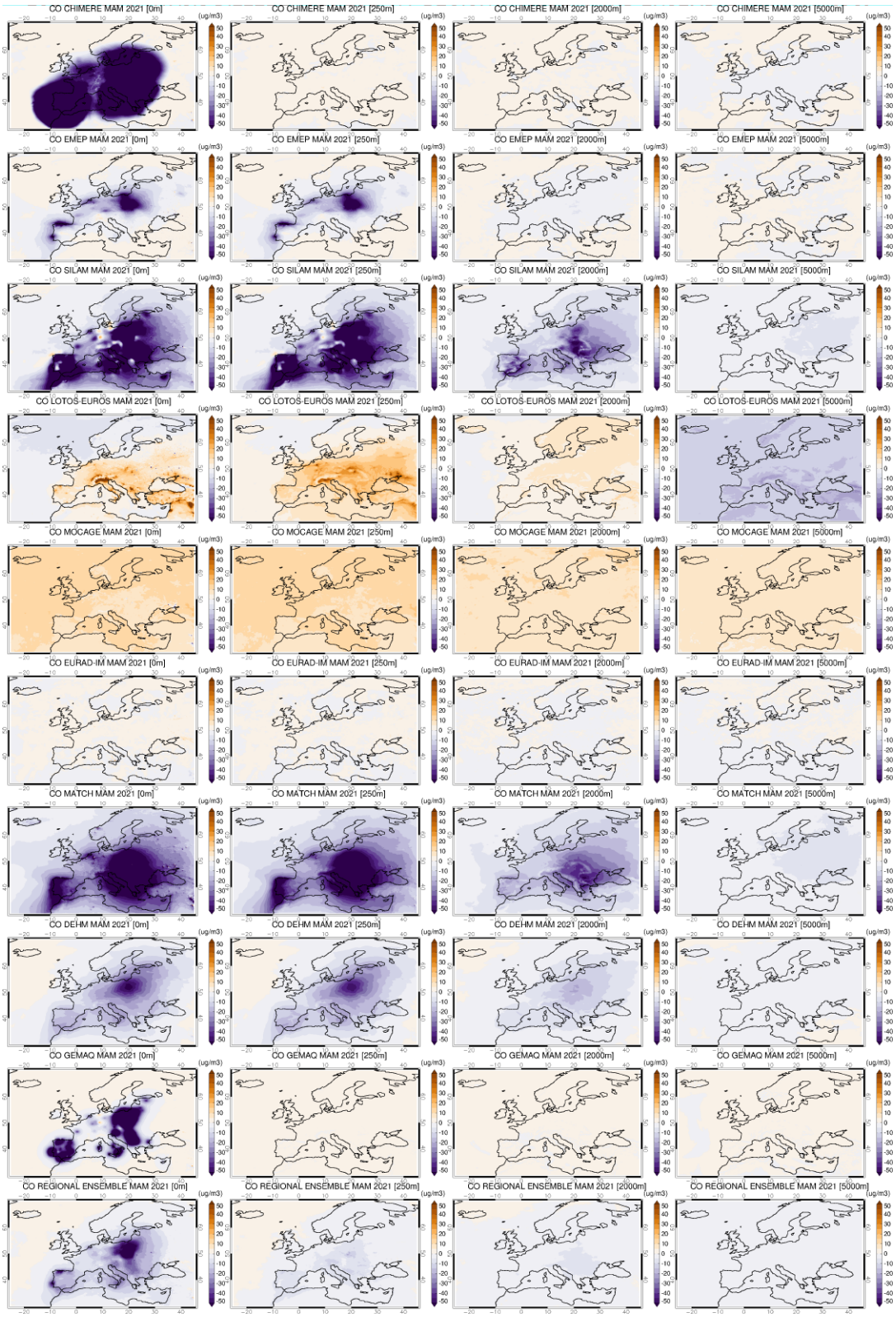

Figure 3.19. Mean regional CO differences between analysis and forecast for MAM2021 for four different vertical layers (0, 250, 2000, 5000 m) from regional ENSEMBLE and individual ensemble members (top to bottom: CHIMERE, EMEP, SILAM, LOTOS-EUROS, MOCAGE, EURAD-IM, MATCH, DEHM, GEM-AQ and ENSEMBLE).

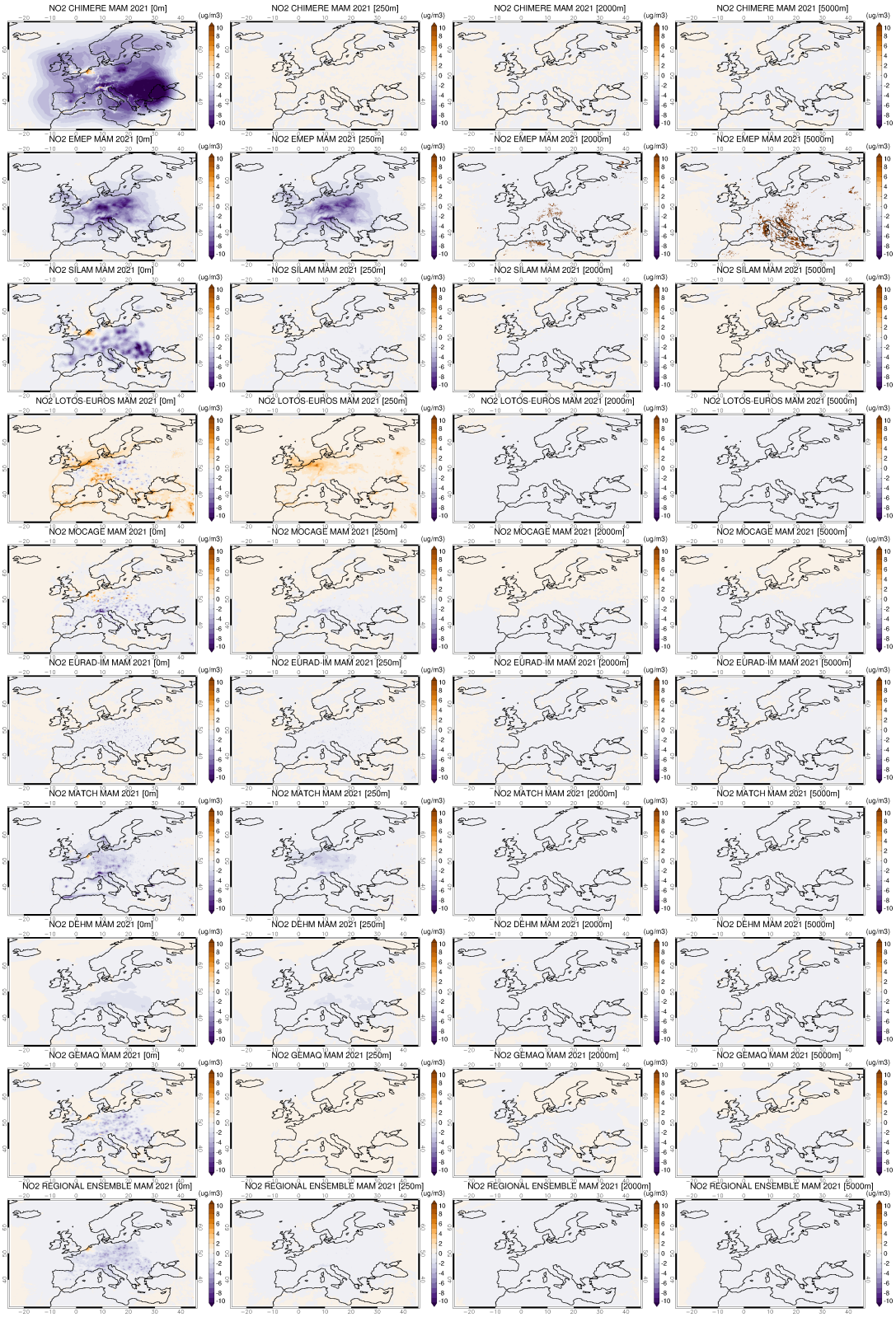

Figure 3.20. Mean regional NO_2 differences between analysis and forecast for MAM2021 for four different vertical layers (0, 250, 2000, 5000 m) from regional ENSEMBLE and individual ensemble members (top to bottom: CHIMERE, EMEP, SILAM, LOTOS-EUROS, MOCAGE, EURAD-IM, MATCH, DEHM, GEM-AQ and ENSEMBLE).

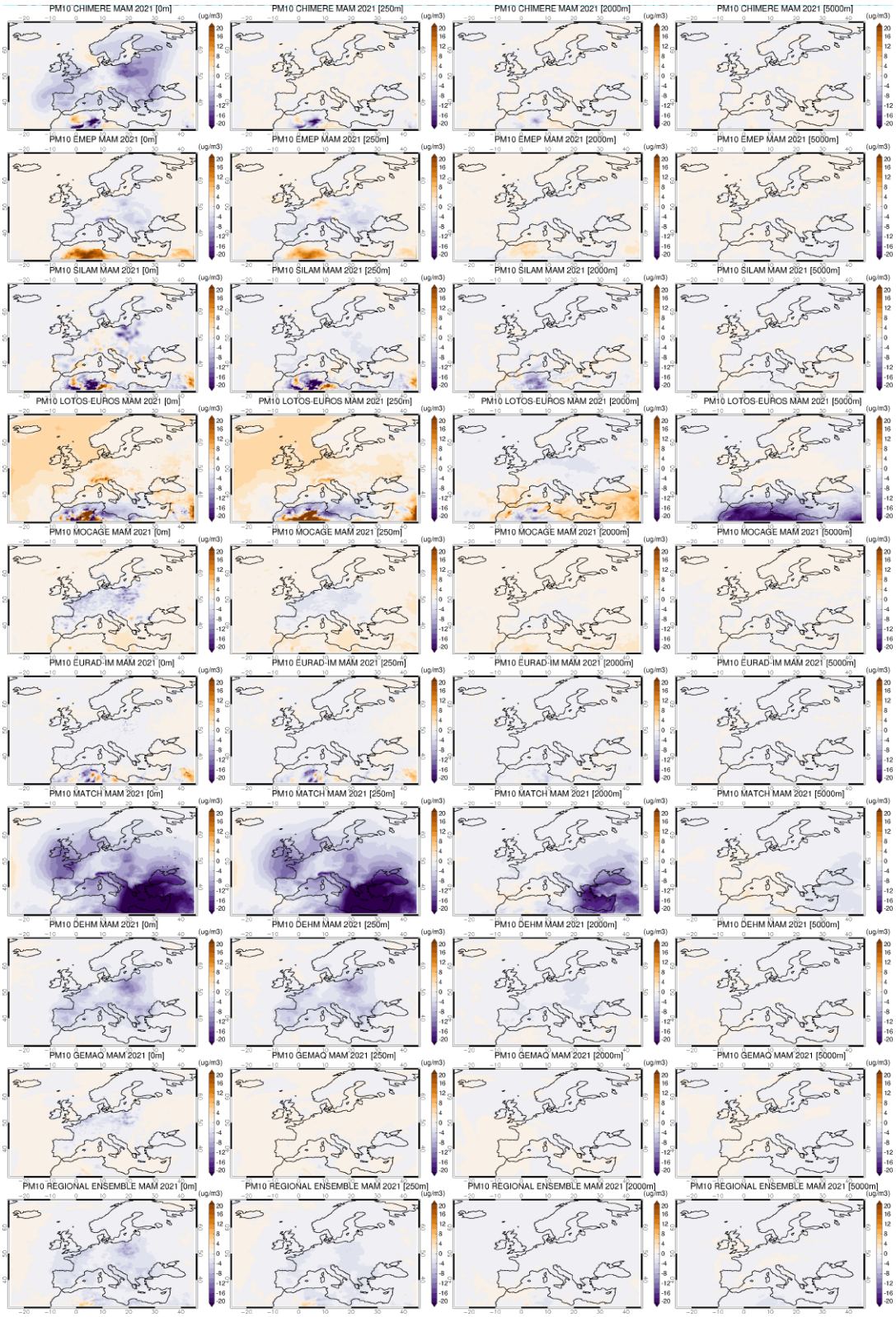

Figure 3.21. Mean regional PM_{10} differences between analysis and forecast for MAM2021 for four different vertical layers (0, 250, 2000, 5000 m) from regional ENSEMBLE and individual ensemble members (top to bottom: CHIMERE, EMEP, SILAM, LOTOS-EUROS, MOCAGE, EURAD-IM, MATCH, DEHM, GEM-AQ and ENSEMBLE).

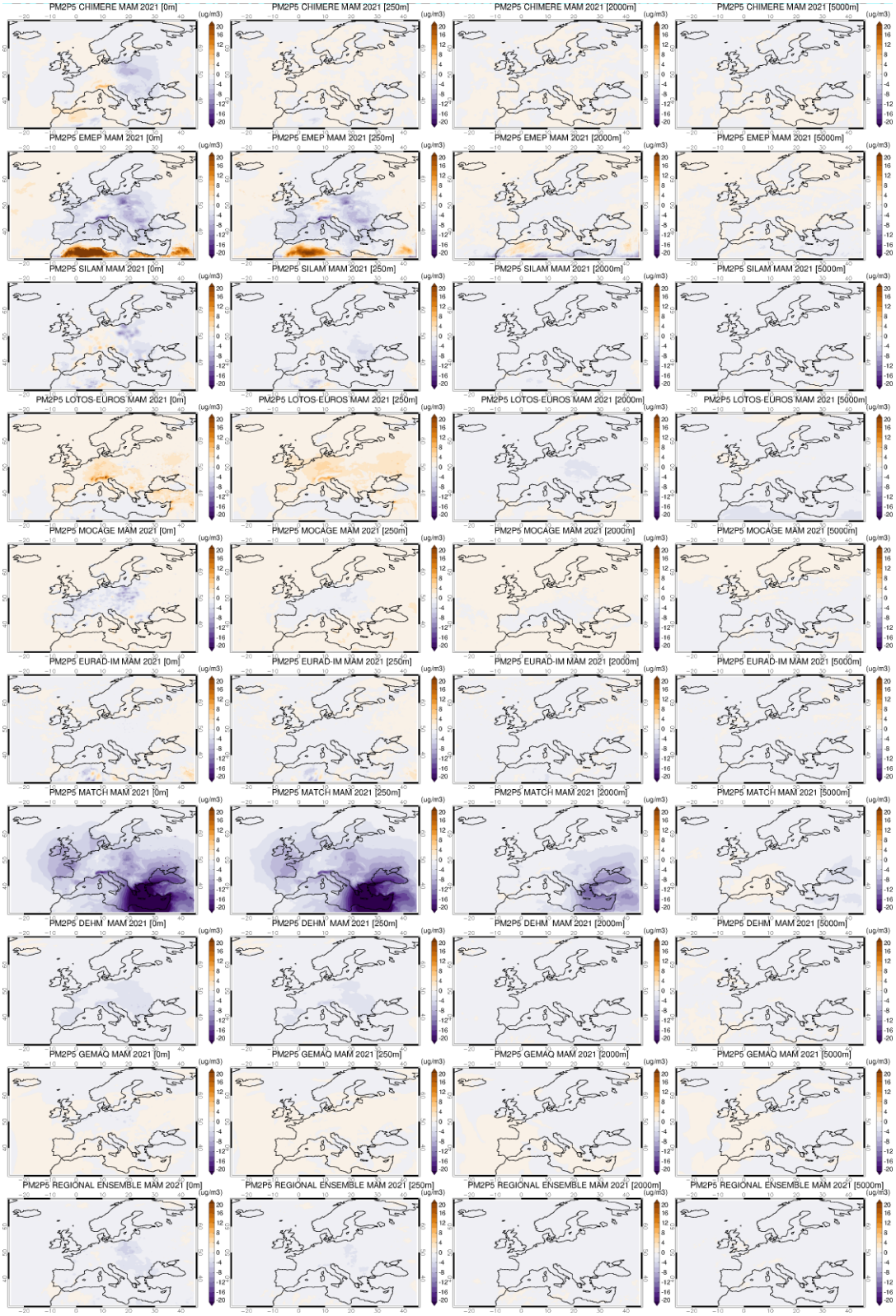

Figure 3.22. Mean regional $PM_{2.5}$ differences of forecast from analysis for MAM2021 for four different vertical layers (0, 250, 2000, 5000 m) from regional ensemble and individual ensemble members (top to bottom: CHIMERE, EMEP, SILAM, LOTOS-EUROS, MOCAGE, EURAD-IM, MATCH, DEHM, GEMAQ and ENSEMBLE).

4 Vertical profile and column aerosol comparisons

4.1 Summary for the EARLINET lidar and Aeronet comparisons

The regional models are compared with climatological lidar profiles for each season (EARLINET/ACTRIS data from 2006-2018). Missing information on composition, size and humidity growth of the aerosol in the models introduces considerable uncertainty to the PM derived extinction, which conservatively spans up to a factor 10 for absolute extinction values. Aeronet data are used to calibrate the conversion from modelled mass to optical property aerosol extinction. This way the order of magnitude in extinction is similar between the models and the lidar profiles, but also significant differences appear at some stations in the lowest layers (Granada, Athens). Relative differences in the form of extinction profiles are more certain. We choose the most representative five stations to compare in retrospective the seasonal average aerosol profiles since 2016. The retrospective of the seasonal comparisons since 2016 shows very similar profiles during this season. The respective overestimation or underestimation of the extinction found in 2016 are usually also found in following years with the ENSEMBLE.

4.2 Introduction

The vertical distribution of aerosol reflects processes like atmospheric mixing, removal, and aerosol transport from outside of the domain or formation of secondary aerosol. The vertical mixing processes determine ground concentrations in polluted areas. Long-range transported aerosol, often carried aloft, may contribute to pollution in clean regions. Evaluation of the simulated aerosol column and vertical profiles are thus valuable for the performance characterisation of air quality models.

The 9 regional models provide mass concentration vertical profiles (PM2.5 and PM10) over Europe and may thus be evaluated for their aerosol vertical distribution. However, only very few aircraft campaigns and mountain sites are available to validate aerosol mass at altitude. In contrast frequent measurements of vertical profiles of aerosol backscatter, extinction or its integral, aerosol optical depth, exist. Deriving aerosol optical properties from the mass concentrations is thus needed, assuming lidar ratios and mass extinction coefficients, at least until the models provide more specific output on aerosol composition and optical properties.

In order to assess mass extinction coefficients chosen, the aerosol optical depth derived from the model mass profiles is first compared to AERONET AOD measurements. Secondly, we document a comparison of the extinction profiles derived from modelled mass concentration with climatological extinction profiles derived from European EARLINET/ACTRIS lidars.

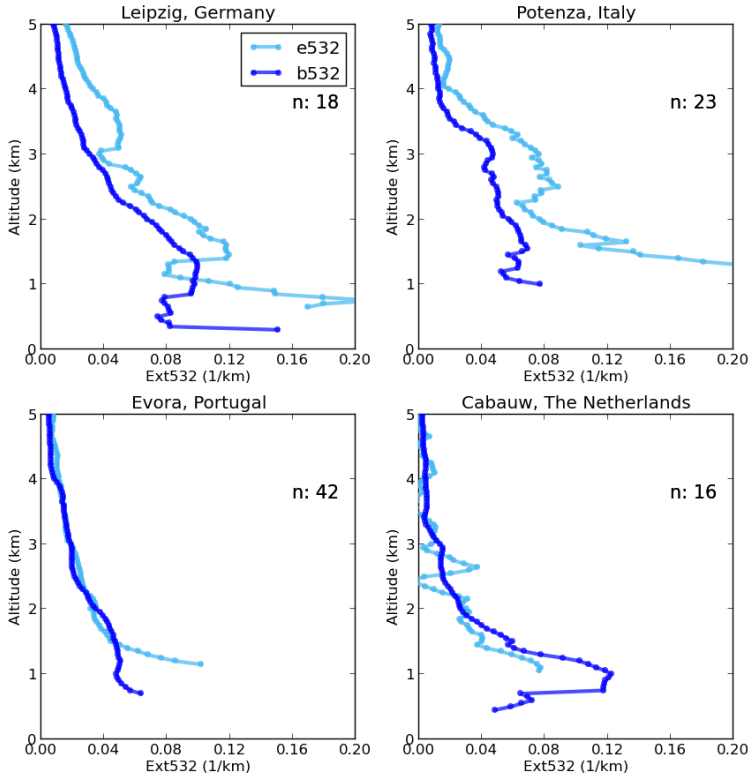

Figure 4.1. Comparison of mean profiles of two aerosol optical properties derived from the same Earlinet Raman lidar at the same time: a) aerosol extinction @532nm (light blue line) and b) extinction @532nm derived from the aerosol backscatter coefficient (dark blue) using a lidar ratio of 50 sr. The profiles use data taken at simultaneous times at each station; number of profiles given as n: x.

4.3 Methodology

AERONET data

The AERONET sun-photometers measure in non-cloudy conditions the aerosol optical depth at several wavelength and in near real time. The spatial distribution of the instruments allows a good coverage of aerosol observation over Europe. The version 3 level 1.5 data has been used in the reporting period presented here. This version and quality level ensures an efficient filtering of the residual clouds (mainly cirrus) for data in near real time. Daily AERONET aerosol optical depth, measured at 550 nm, has been averaged over summer for the European sites available in CAMS model output.

Lidar data

The EARLINET/ACTRIS Lidars are distributed over several locations in Europe and allow comparison across different climates in Europe (Pappalardo et al., 2014). Yet, up to now, there are no near-real-time data available. Regular measurements in EARLINET are sparse and often acquired once per week, with gaps due to maintenance or funding restrictions. A climatology has been computed per station and per season with all measurements available between 2006 and 2018.

The backscatter coefficient and extinction profiles at 532 nm have been extracted from the EARLINET database. The more frequently measured backscatter profiles are considered here with priority. An aerosol extinction coefficient profile is computed from the backscatter coefficient using a range of plausible lidar ratios. This latter parameter depends on the aerosol type and is more likely decreasing with the size of the aerosol. Minimum values are observed for sea salt aerosol (below 30 sr at 550 nm, [Ackermann et al., 1998, Omar et al., 2009]), while larger values are related to urban particles (55 sr in [Muller et al., 2007], 70 sr in [Cattrall et al., 2005]). Desert dust is associated with intermediate lidar ratios, ranging from 30 sr to 60 sr depending on the sources and the transport regime. A climatology of aerosols in West Africa published in Mortier et al. [2016] revealed an average lidar ratio (over 9 years) of about 30±15 sr. Due to the location of the stations involved in this study, both dust and urban aerosols and any a mix of them might occur. In order to represent the uncertainty on the nature of aerosols, we show the range in likely mean extinction using a lidar ratio extending from 30 to 70 sr.

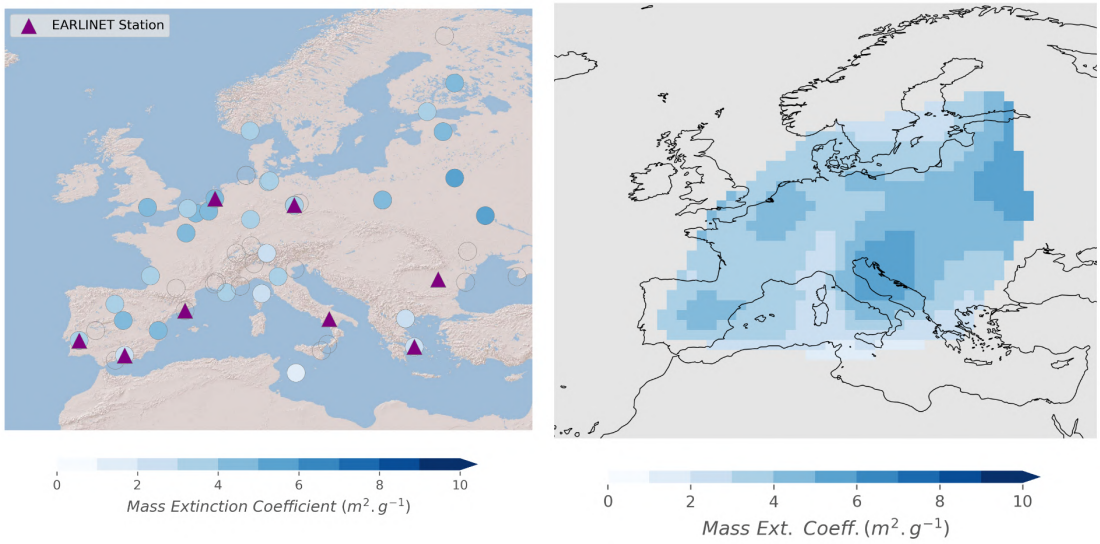

Figure 4.2. Mass extinction coefficient estimated at AERONET location sites (blue dots) and EARLINET stations (triangles) for MAM2021 (left). A European map of the Mass Extinction Coefficient has been constructed with cubic interpolation in the inner part of the region covered by AERONET on the model grid (right), and with the nearest neighbours in the outer part of this region (not shown).

As a test, the conversion of lidar backscatter to extinction coefficient is performed assuming a constant average lidar ratio of 50 sr at locations where both backscatter and extinction coefficients are measured in EARLINET. This allows consistent comparison and visualization of some of the error associated to our simplified constant lidar ratio assumption. We have excluded from this comparison cases where local extinction coefficient was above 0.5 km^{-1} in order to avoid outliers. The profiles shown in figure 4.1 from 4 stations reveal an error in the mean profile of 0-30% in extinction, which is small compared to the model spread documented below. The extinction profiles derived from the backscatter coefficients look vertically smoother. We have excluded from this comparison cases where local extinction coefficient was above 0.5 km^{-1} in order to avoid outliers.

In addition to this aerosol typing uncertainty, a sampling error should be accounted for. The observations are sporadic, while the models predict the aerosol concentration continuously.

Therefore, seasonal averages are not computed with the same coverage in model and observation. Our earlier model-based bootstrap studies revealed, that, depending on the station, a set of ca. 30 daily observations allows reproducing the seasonal average with an error of about 10% [ACTRIS Deliverable WP6/D6.21]. In our case, this error might be larger since the synoptic situation is very different between our EARLINET climatological dataset, covering 2006-2018, and the season covered in this report. An overall uncertainty of about 20% has been chosen to represent the sampling error.

Model data

The ensemble mean and the underlying 9 regional CAMS models are investigated. For each of these models, the hourly PM10 and PM2.5 vertical profiles are extracted at the EARLINET station locations from the first day of each daily forecast at levels 0, 50, 250, 500, 1000, 2000, 3000, 5000 m.

The conversion of PM10 mass concentration to extinction requires a mass extinction coefficient (MEC). MEC depends on the size distribution, refractive index and density of the particles. This information is not yet available from the models. For different kind of aerosols, MEC values can vary from about 0.5 m^2g^{-1} in the case of desert dust aerosols up to 8 m^2g^{-1} for urban particles [Chin et al., 2002]. No variation with height or aerosol type is taken into account, mainly because the models provide no further info on aerosol speciation. We derive the MEC value to convert the model profile data to extinction profiles from a combination of the modelled mass column load and consistent Aeronet AOD data.

For the Aeronet based computation of the MEC, the model data are picked at the location and on the day when sun photometer observations were available. The CAMS-regional mass concentrations have been averaged for coincident days (with the measurements) and averages are converted, with a seasonal and site dependent mass extinction coefficient estimated with AERONET retrievals, into extinction profiles. A seasonal and site dependent mass extinction coefficient is obtained when combining it with AERONET AOD retrievals. Values of MEC are ranging from 1 m^2g^{-1} in South-West of Europe to more than 10 m^2g^{-1} in the North-East. Since some of the EARLINET stations are not co-located with Sun photometers, a European map of MEC has been constructed, for each season, by interpolating (cubic interpolation) and extrapolating (nearest neighbour) the available AERONET based MEC calculations on the grid of the model (figure 4.2). One can notice a gradient with the longitude with lower values found in the Western part while the highest values are observed in the Eastern part of Europe. Also, the values are generally lower as compared to last year, which might reveal a higher concentration in coarse particles (dust). The seasonal AERONET-based MEC is then used at each EARLINET station to calculate the model extinction from concentration profiles. The uncertainty on the MEC being removed allows more accurate comparisons with the observed vertical profiles than using an average MEC over whole Europe.

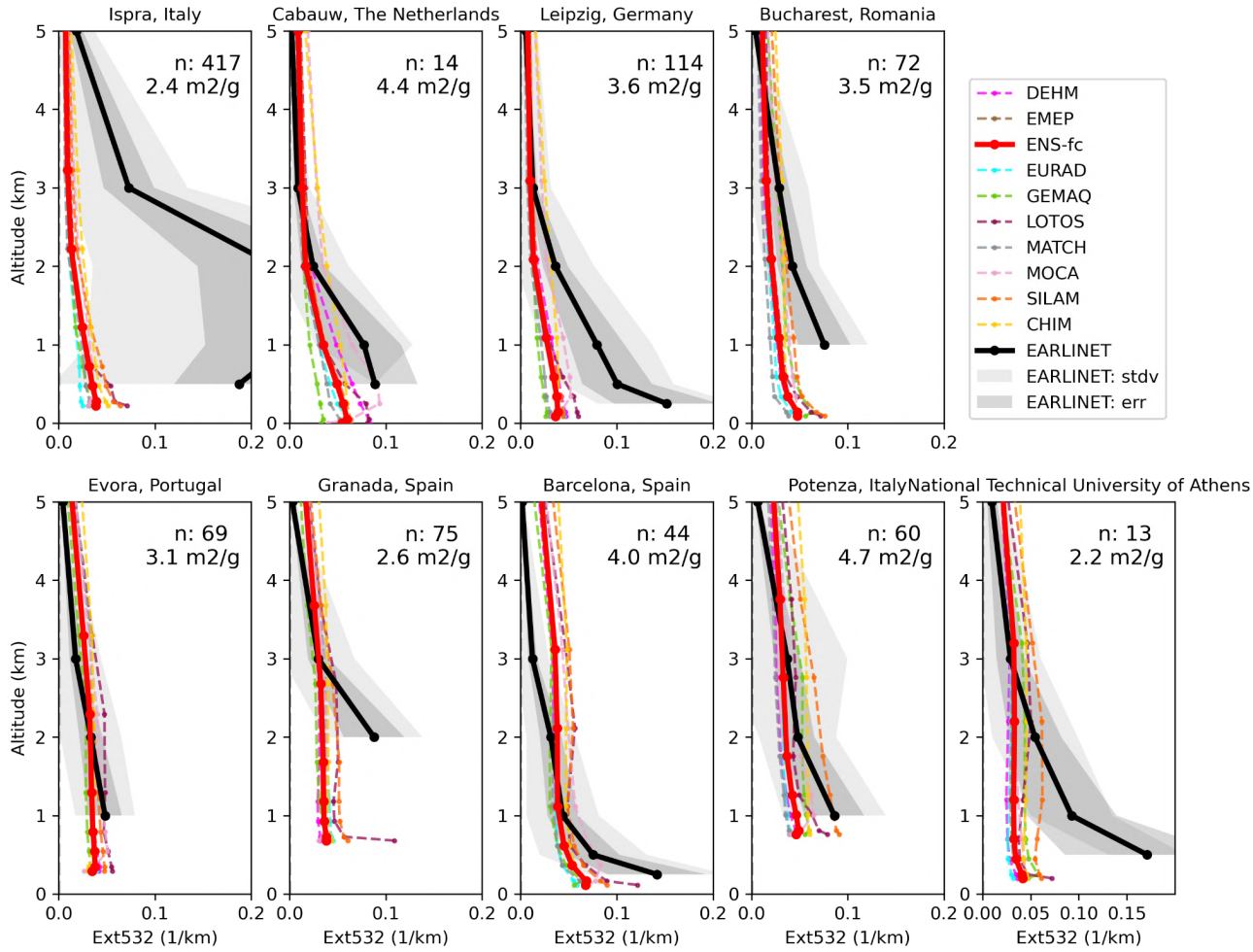

Fig 4.3. Extinction profiles March - May 2021 derived from the ENSEMBLE forecast mass concentration profiles (red envelope) and from EARLINET (climatology) backscatter profiles (grey envelope: lidar ratio uncertainty, light grey: including sampling error). "n: XX means number of individual EARLINET profiles assembled (March - May 2006-2018). The EMC used for the calculation of the extinction from the concentration profiles is indicated for each station below the number of EARLINET profiles "n" used for the calculation of the climatology.

4.4 Results

4.4.1 Comparison of extinction profiles

The extinction profiles estimated from the 9 CAMS models and the ENSEMBLE and EARLINET measurements are compared for MAM 2021 (figure 4.3).

With low EMC values obtained this year, one observed generally an understimation of the extinction in the lowest levels. A good agreement is found in EVora and Potenza where observations present low values along the whole vertical profile. In Barcelona, the agreement in the lowest layers is also good, while the models overestimate, as usual, the extinction derived from EARLINET above 2km of altitude.

4.4.2 Seasonal variability

In order to investigate the performance of the model in reproducing the vertical profiles, it is interesting to observe the inter-annual variability for the different seasons. This will be of use for the development of a score providing an assessment of the models skills, and is also useful to investigate the models synoptic variability. The seasonal profiles have been reported since 2016 at 5 stations (Leipzig, Barcelona, Potenza, Evora and Bucharest) in Figure 4.4, using the new EARLINET climatology. Performances of the models in 2021 look similar to the performances observed in spring 2020. With generally lower EMC values, the extinction values are lower in 2021 as compared to 2020. Therefore, in locations where the extinction was underestimated in 2020, the bias tends to increase, whereas the bias is reduced in Barcelona, where the extinction was overestimated in 2020.

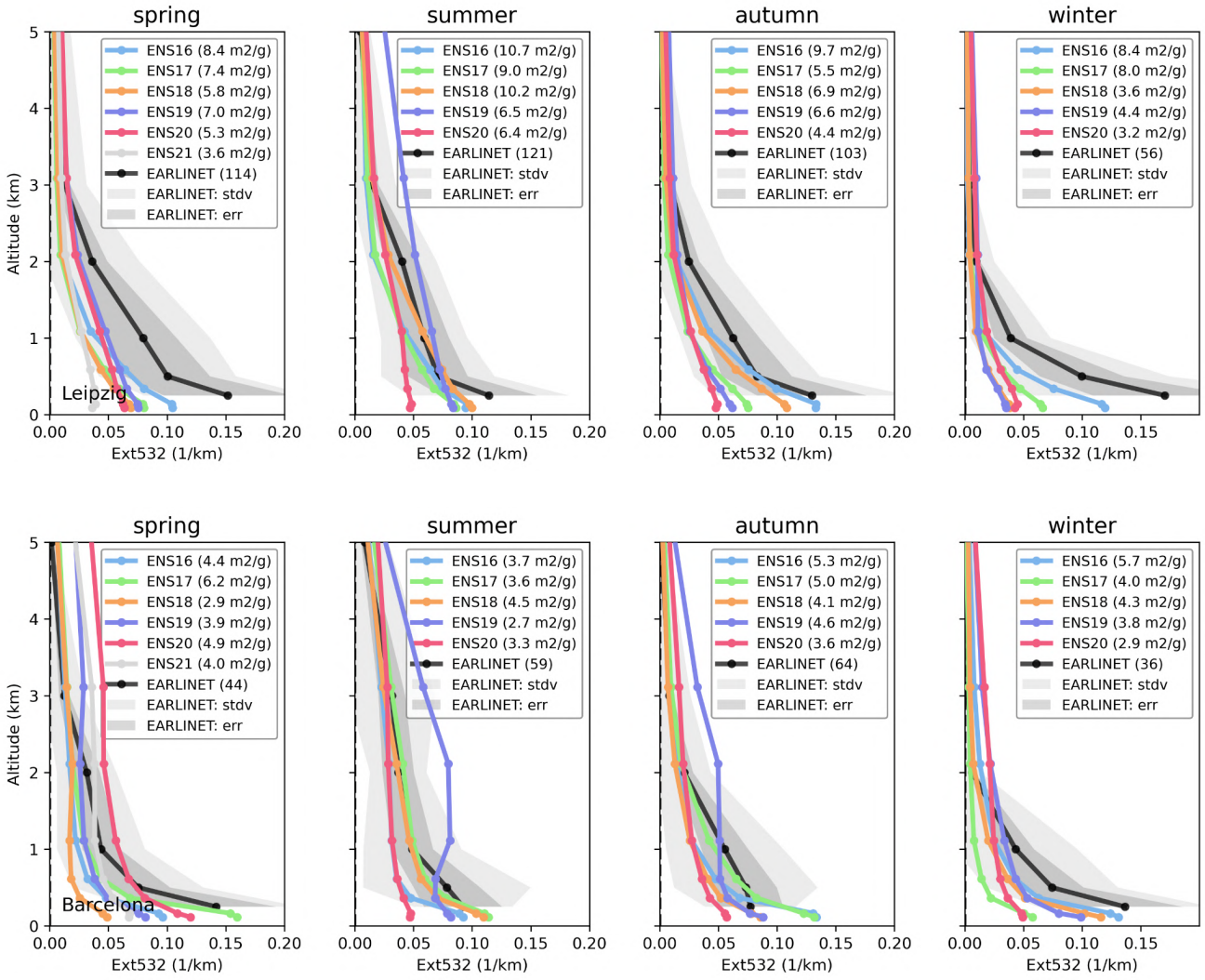

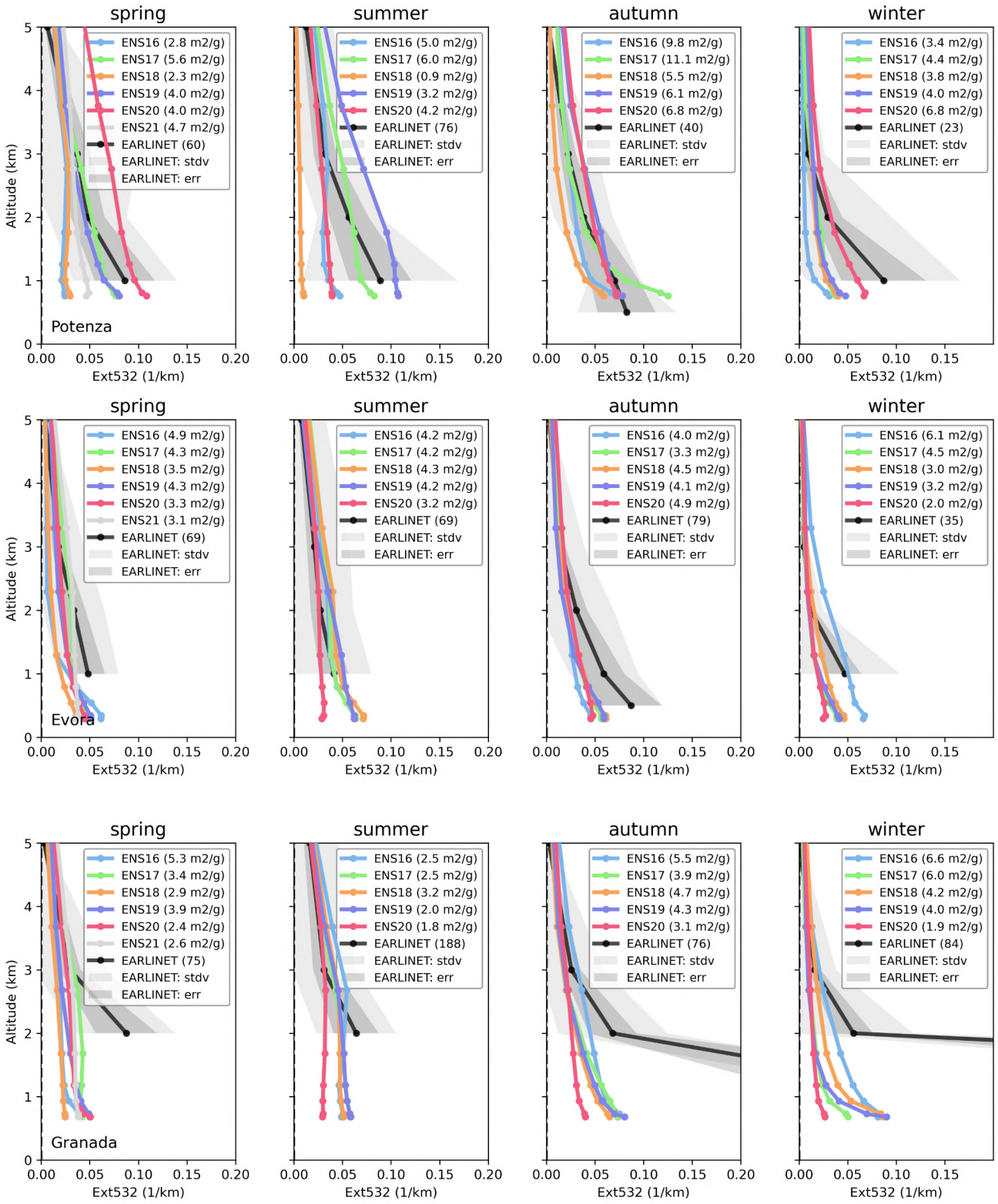

Fig 4.4: Seasonal extinction profiles derived from ENSEMBLE forecast mass concentration profiles for 2016 (ENS16), 2017 (ENS17), 2018 (ENS18), 2019 (ENS19), 2020 (ENS20), 2021 (ENS21) and EARLINET climatology. The parenthesis indicates for the CAMS profiles, the MEC used for the extinction estimation, and for the EARLINET, the number of profiles used for constructing the climatology.

5 IAGOS aircraft CO and O_3 profile comparisons

5.1 Summary

Routine observations of ozone and CO over European airports are available from the IAGOS fleet. Take-off and landing profiles were sampled from the hourly model 3D forecasts along the flight tracks.

Ozone in-situ: In the lowest layers, ozone is well represented by the models with small overestimations and sometimes a better performance from the regional ensemble. The bias in the free troposphere is larger with overestimations from both models.

Carbon monoxide: CO is mostly underestimated in all layers by the regional ENSEMBLE and CAMS global which present similar behaviour in the low troposphere. In the free troposphere the agreement is better for both models and CAMS-global often performs better than the regional ENSEMBLE.

IAGOS Validation Method

Validation is possible at the European airports visited by the IAGOS fleet. For the European-based carriers, there are regular profiles at the home airports. There are two aircraft operated by Lufthansa, one operated by Air France. Thus, when the fleet is fully operational, there are daily profiles Frankfurt and Paris (CDG). IAGOS is also installed on two aircraft operated by the Asian-based carrier China Airlines. Aircraft fly regularly from Taipei to Amsterdam or Vienna and sometimes to Rome. Other airports may be visited depending on the operational schedules of the airlines. Due to persisting restrictions associated to the COVID-19 crisis, IAGOS operations still remain impacted in this period although more observations are available compared to other quarters of 2020. Over Europe only the airport of Frankfurt has been visited as shown in Figure 5.1.

We download the daily latitude-longitude datasets for the 7 regional models and the ENSEMBLE for two species (carbon monoxide and ozone) on 8 vertical levels (surface, 50m, 250m, 500m, 1000m, 2000m, 3000m, 5000m). The aircraft takes about 10 minutes to climb or descend the 5000m vertical extent covered by the regional models. During this time and travelling at up to 166 m s^{-1}, it covers about 120km and therefore traverses many grid-boxes of resolution 10km. We perform a spatial interpolation from the grid of the regional models to the aircraft's trajectory. The IAGOS measurements in ppbv are converted to µg m^{-3} using the temperatures measured by IAGOS. The data are validated by the PI but are not yet calibrated. Calibration takes place after an operational period of about 6 months.

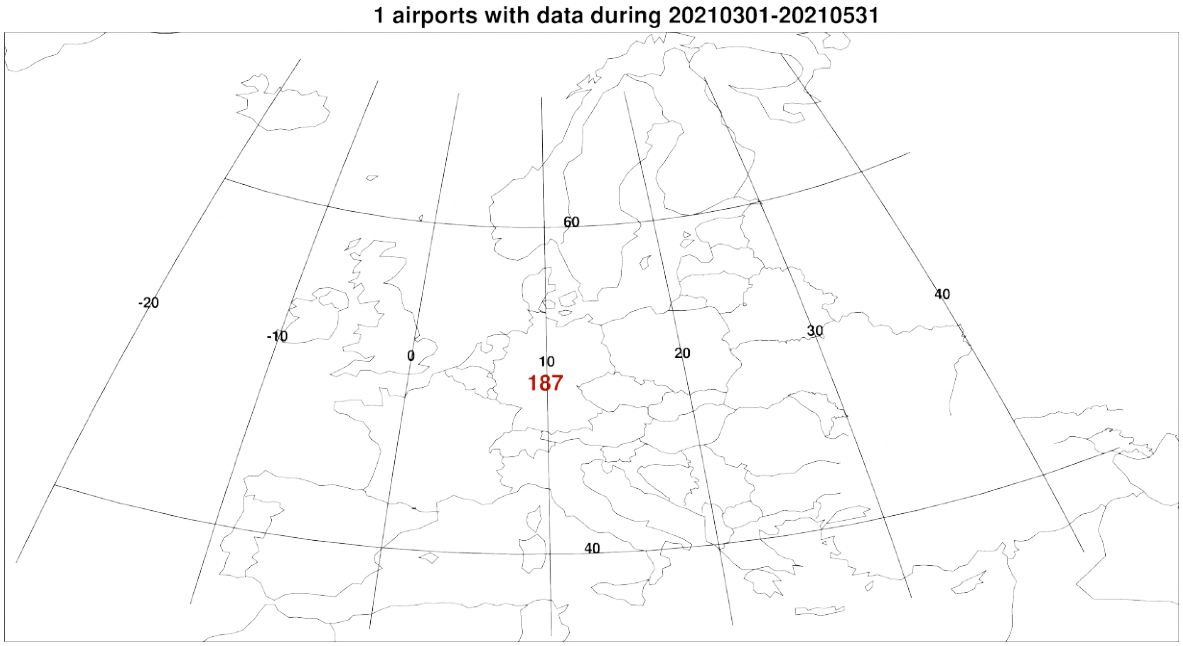

Figure 5.1. Map showing the number of profiles available in the period Mars - May 2021.

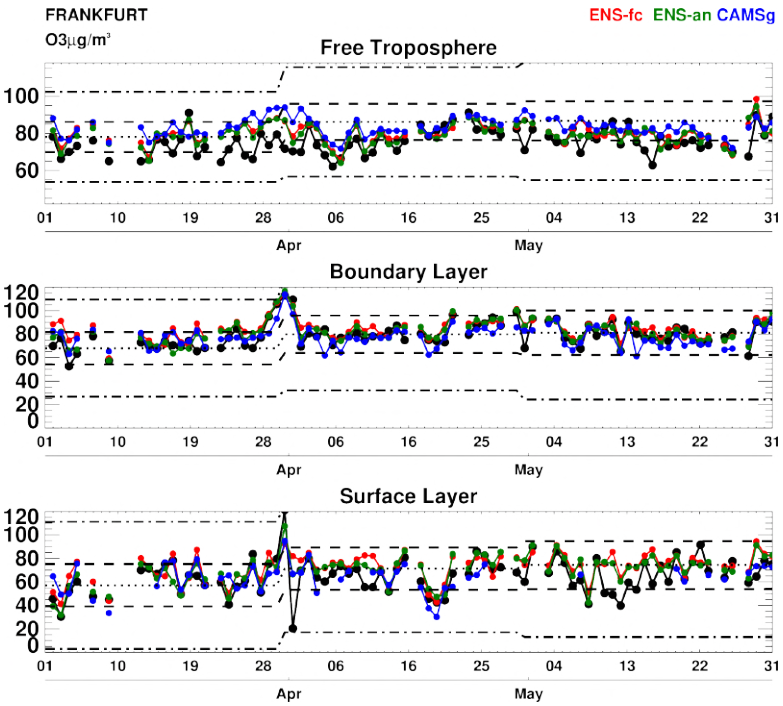

Figure 5.2: Daily time series of ozone at Frankfurt for the period MAM 2021. IAGOS observations are shown in black, the regional ENSEMBLE and associated analysis are shown in red and green respectively, and CAMS-global (o-suite) is shown in blue. The black dotted line is the monthly mean of the observations over the period 2003-2018 (IAGOS/MOZAIC, Level 2 data), the black dashed line shows 1 standard deviation from the monthly mean and the black doted-dashed line shows 3 standard deviations from the monthly mean. (Units: $\mu g.m^{-3}$).

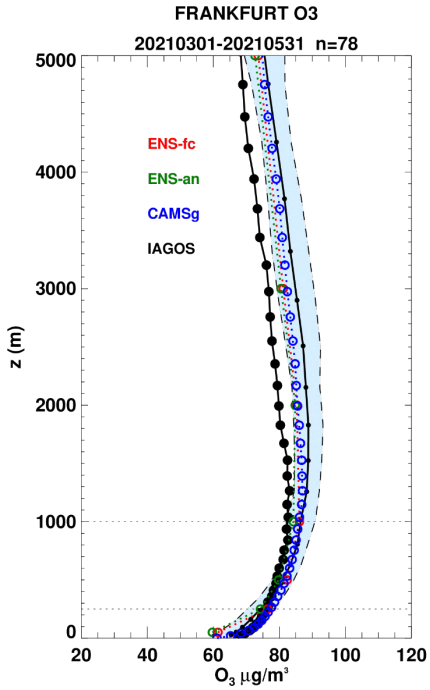

Figure 5.3: Mean profile of ozone at Frankfurt for the period MAM 2021. IAGOS observations are shown in black, the regional ENSEMBLE and associated analysis are shown in red and green respectively, and the global o-suite is shown in blue. The shaded area indicates the range of the mean climatology of the observations plus/minus one standard deviation during the same period for all years between 2003 and 2018 (IAGOS/MOZAIC, level 2 data). (Units: µg.m^{-3}).

5.2 IAGOS Ozone

For the period Mars - May 2021, ozone observations are available only at Frankfurt continuously for the full period. The daily time series are presented in Figure 5.2 and associated averaged profiles over the whole period are presented in Fig. 5.3. In all plots, the forecast and analysis of the regional ENSEMBLE is shown in red and green respectively, and CAMS-global analysis is shown in blue. Fig. 5.3 shows that on average the regional and global models agree well with observations from the surface up to 1 km and perform rather similarly. However, the times series shows that sometimes the ENSEMBLE performs better than CAMS global (Fig. 5.2). In the upper layers, the regional and global models also present similar performance and mostly overestimate (Fig. 5.3).

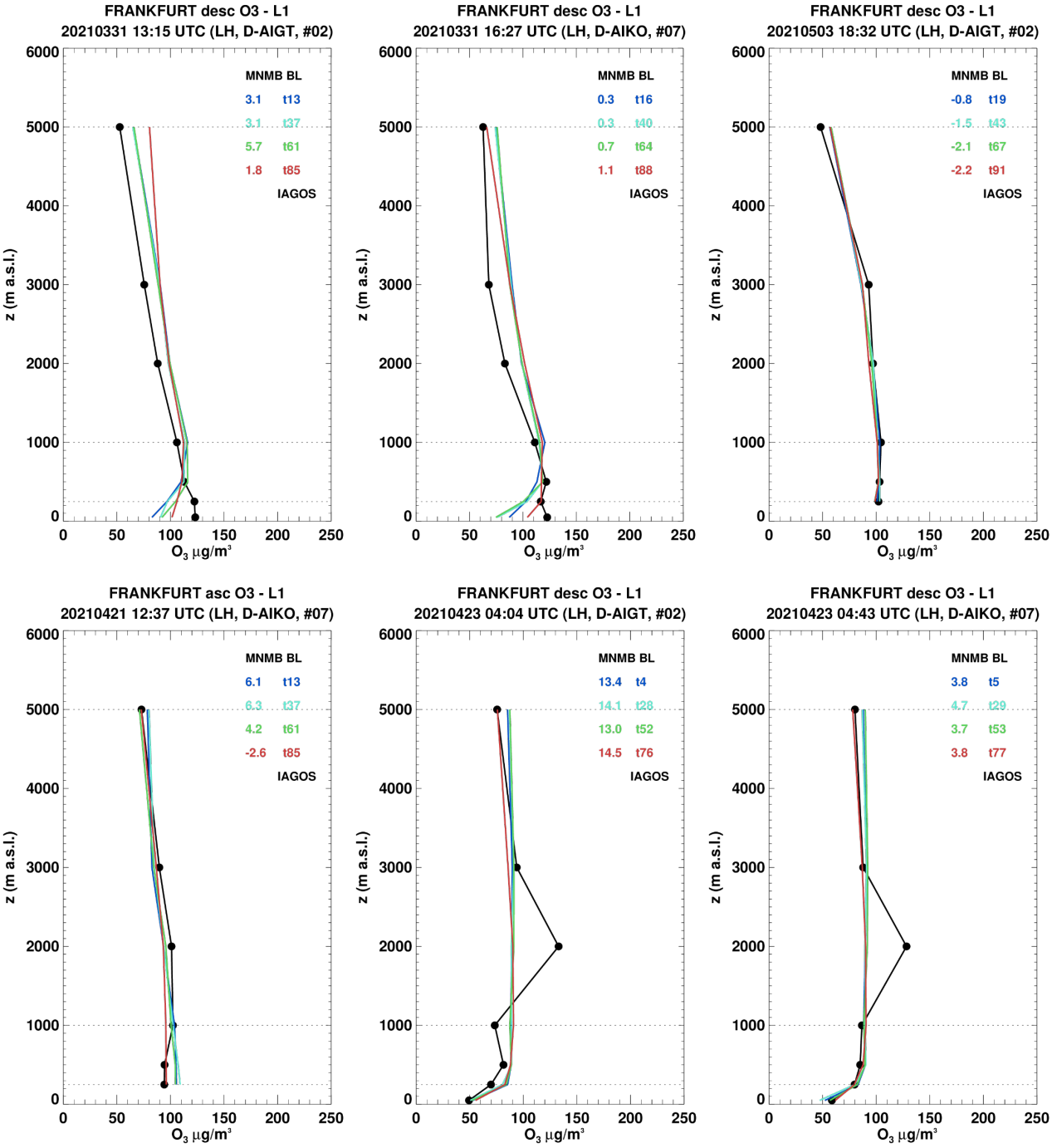

Figure 5.4.a. Selection of ozone profiles at Frankfurt during the period MAM 2021. IAGOS is shown in black and the ENSEMBLE is shown at 4 forecast times (blue: 1-day; cyan: 2-day; green: 3-day; red: 4-day). (Units: µg m^{-3}).

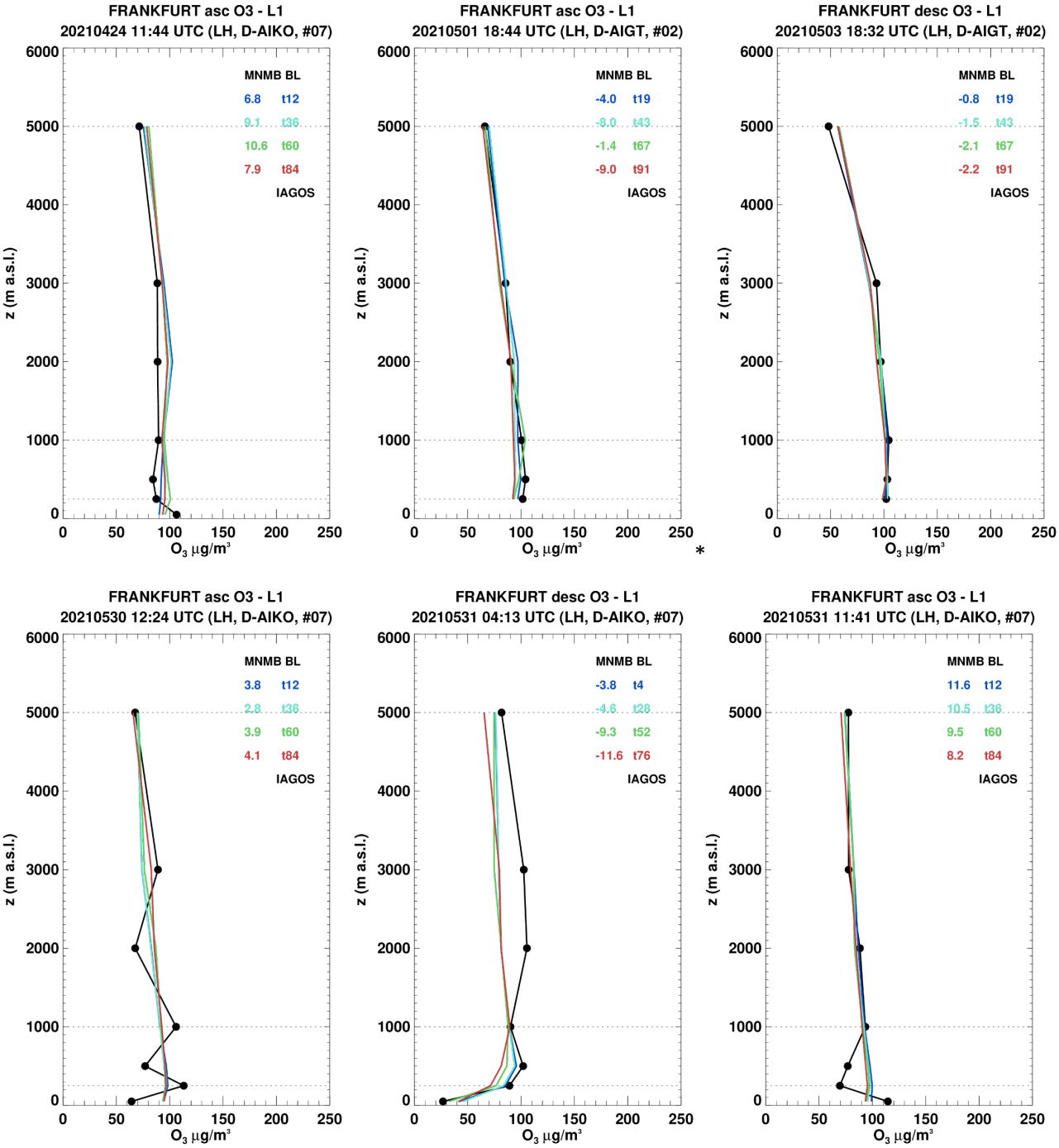

Figure 5.4.b. Selection of ozone profiles at Frankfurt during the period MAM 2021. IAGOS is shown in black and the ENSEMBLE is shown at 4 forecast times (blue: 1-day; cyan: 2-day; green: 3-day; red: 4-day). (Units: µg m^{-3}).

During this MAM period, IAGOS ozone observations in the surface and boundary layer are mostly in the range between plus and minus one standard deviation from the climatological mean with the exception of a major peak at the end of March with values reaching three standard deviations above climatology with about 120 ppbv in the surface and boundary layer on 31 March (Fig. 5.2). Corresponding profiles are also shown in Fig. 5.4.a. This increase in ozone is detected by the models

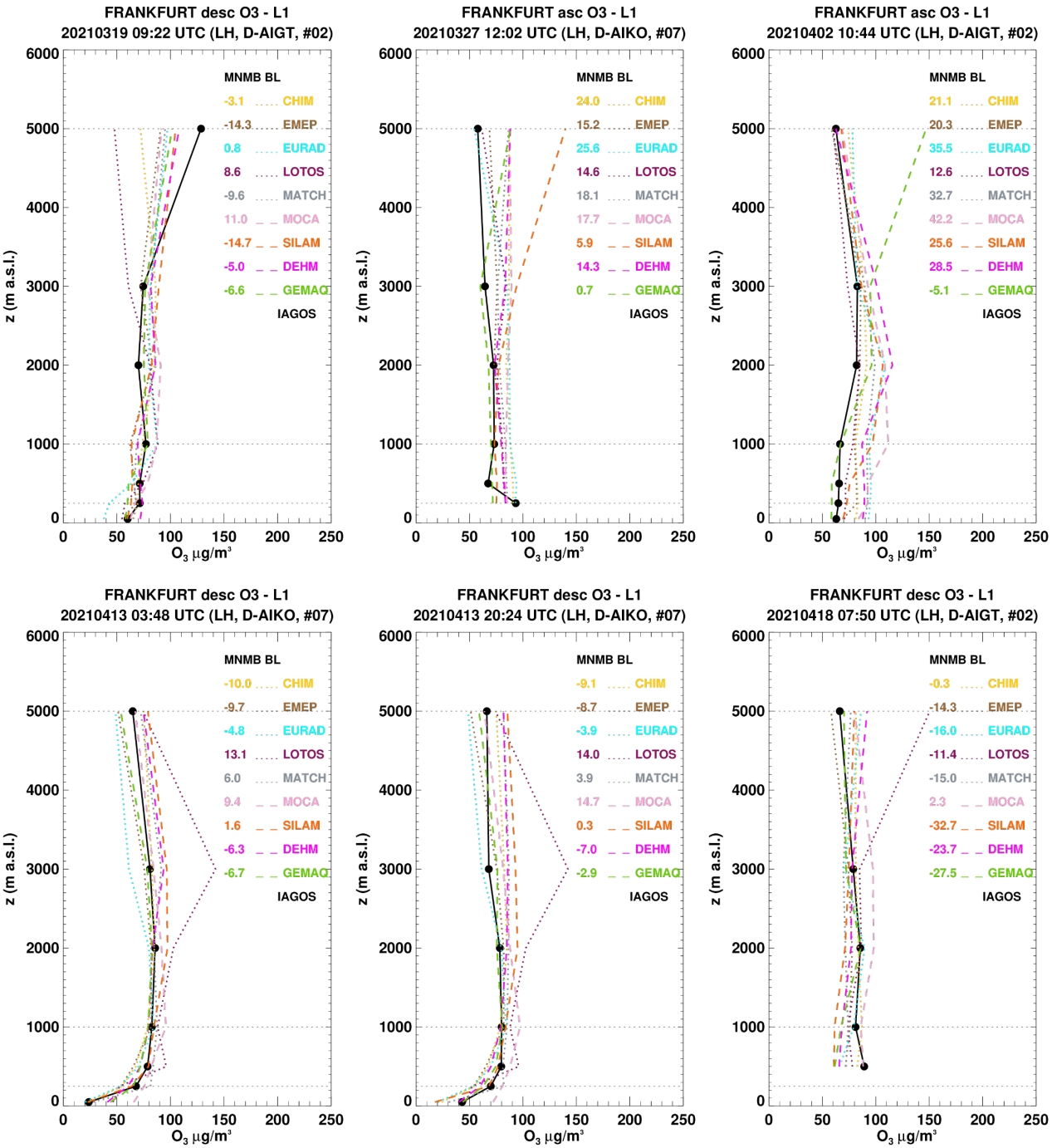

Figure 5.5.a: Ozone profiles at Frankfurt during the period MAM 2021. IAGOS is shown in black and each colour/Line style corresponds to one of the 9 models for the ensemble. In the legend, the models are CHIM=CHIMERE, EMEP=EMEP, SILAM=SILAM, LOTOS=LOTOS-EUROS, MOCA=MOCAGE, EURAD=EURAD, MATCH=MATCH, DEHM=DEHM, GEMAQ=GEM-AQ. (Units: µg m^{-3}).

but underestimated with a value of about 100 ppbv for the regional forecasts on profiles of 31 March (Fig 5.4.a). Several values are also reaching one standard deviation throughout this quarter period, with observation values close to 100 ppbv in the surface and boundary layer as shown on the profiles of 21 and 24 April, 1st, 3 and 31 May (Fig. 5.a-b). These values are in general well

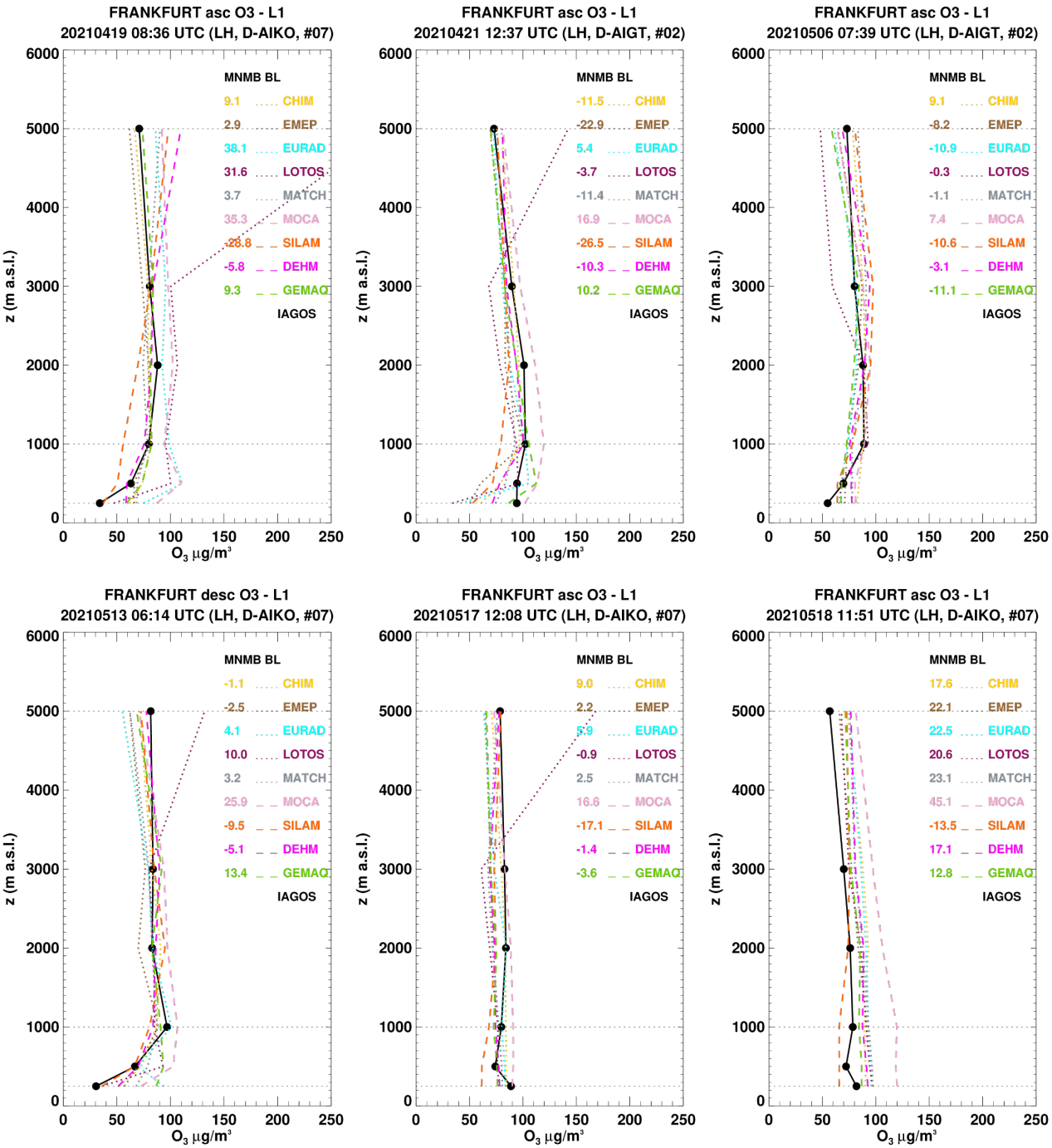

Figure 5.5.b: Ozone profiles at Frankfurt during the period MAM 2021. IAGOS is shown in black and each colour/Line style corresponds to one of the 9 models for the ensemble. In the legend, the models are CHIM=CHIMERE, EMEP=EMEP, SILAM=SILAM, LOTOS=LOTOS-EUROS, MOCA=MOCAGE, EURAD=EURAD, MATCH=MATCH, DEHM=DEHM, GEMAQ=GEM-AQ. (Units: µg m^{-3}).

represented by the models and the results for the different forecast times are similar. On 23 April, a peak of ozone is observed near 2000 m with a value of about 140 ppbv. This peak is not detected by the regional ensemble (Fig 5.4.a).

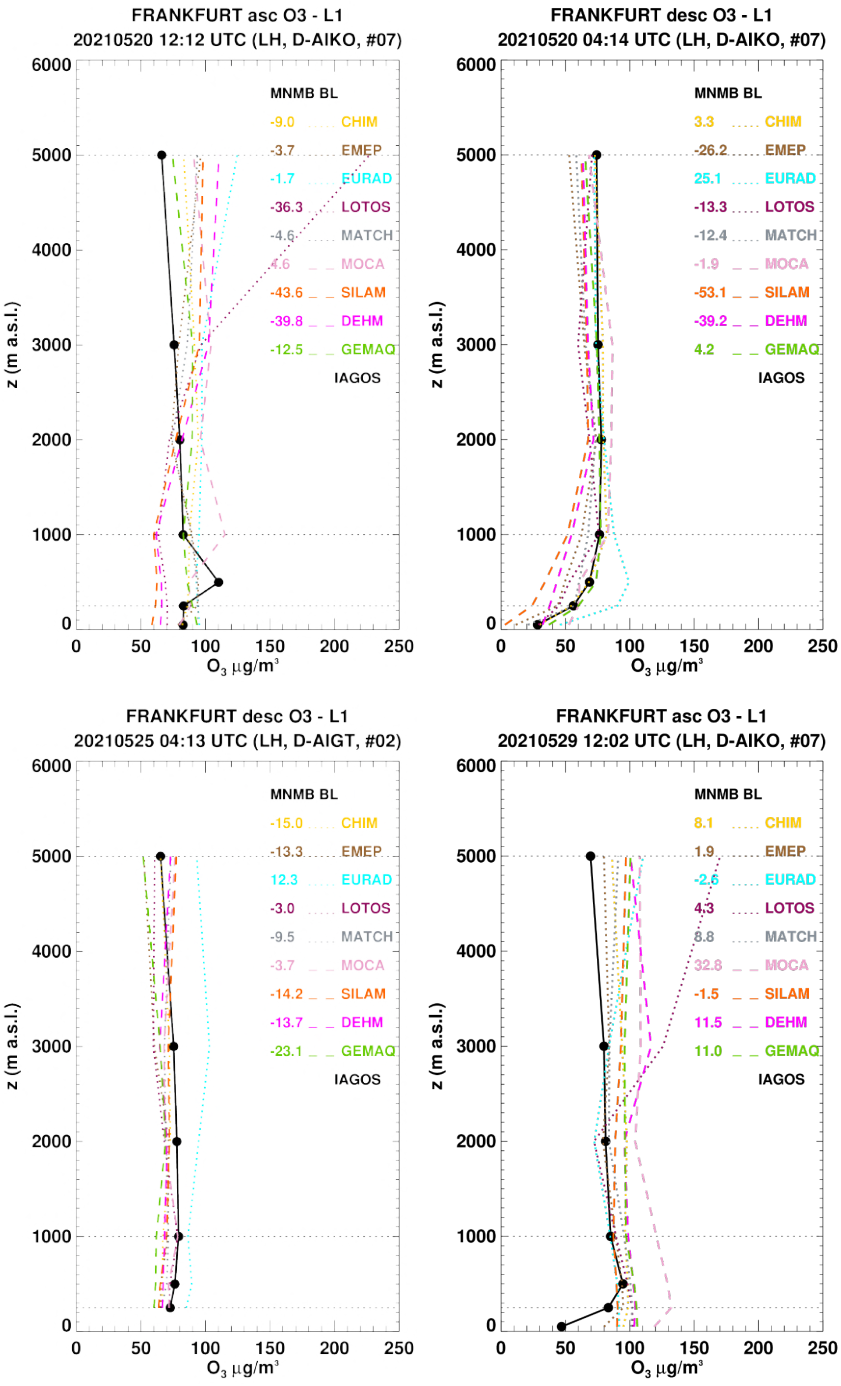

Figure 5.5.c: Ozone profiles at Frankfurt during the period MAM 2021. IAGOS is shown in black and each colour/Line style corresponds to one of the 9 models for the ensemble. In the legend, the models are CHIM=CHIMERE, EMEP=EMEP, SILAM=SILAM, LOTOS=LOTOS-EUROS, MOCA=MOCAGE, EURAD=EURAD, MATCH=MATCH, DEHM=DEHM, GEMAQ=GEM-AQ. (Units: µg m^{-3}).

For most profiles of the period the results from all individual models of the ensemble are similar. The profiles in which the results of the individual models differ are presented in Fig. 5.5.a-c. The LOTOS-EUROS sometimes presents much larger bias than all other models in the free troposphere (in general above 3000 m) with mostly overestimations (0413 03:48, 0413 20:24, 0418 07:50, 0419

08:36, 0421 12:37, 0513 06:14, 0517 12:08, 0520 12:12, 0529 12:02), but also sometimes underestimations (0319 09:22, 0506 07:39). This is also the case sometimes for the EURAD, GEMAQ and SILAM models but very rarely (0525 04:13, 0518 11:51, 0327 12:02). There are also although rarely again, larger overestimations from EURAD and MOCAGE in the low troposphere (0520 04:14, 0529 12:12).

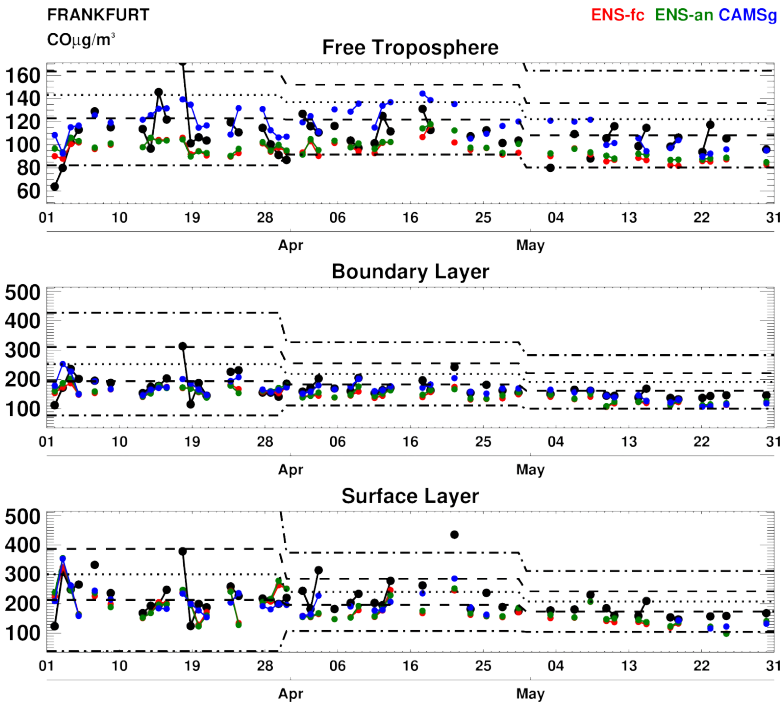

Figure 5.6: Daily time series of CO at Frankfurt for the period MAM 2021. IAGOS observations are shown in black, the regional ENSEMBLE and associated analysis are shown in red and green respectively, and CAMS-global (o-suite) is shown in blue. The black dotted line is the monthly mean of the observations over the period 2003-2018 (IAGOS/MOZAIC, Level 2 data), the black dashed line shows 1 standard deviation from the monthly mean and the black doted-dashed line shows 3 standard deviations from the monthly mean. (Units: $\mu g.m^{-3}$).

5.3 IAGOS Carbon Monoxide

Like for the ozone section, the daily time series of CO and associated averaged profile at Frankfurt are presented in Fig. 5.6 and 5.7. However, time series of CO are discontinuous with frequent but short gaps throughout the period. The forecast and analysis of the regional ENSEMBLE is shown in red and green respectively, and CAMS-global is shown in blue. On the time series, available observations of CO in the lowest layers are mostly below the climatological values and often reaching values below one standard deviation from the mean as it was the case in the previous quarter. However, some values are reaching nearly one standard deviation above the climatology in a few cases on 18 March, 3 and 13 April, and reach more than three standard deviations on 21 of April (Fig. 5.6 and Fig. 5.8).

In the surface and boundary layers CO is always underestimated by both regional and global models (Fig 5.6) with on average a better agreement of the regional model close to the surface and more similar performance for both models above 200 m up to 2000 m presenting smaller underestimations (Fig. 5.7). In the upper layers, from the time series CAMS-global is mostly performing better than the regional ENSEMBLE (Fig. 5.6).

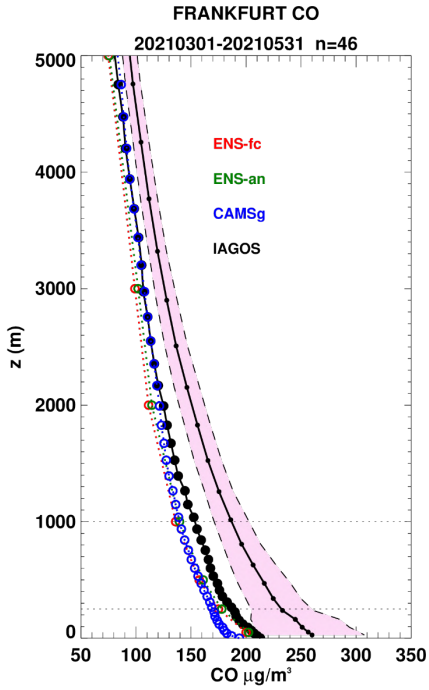

Figure 5.7: Mean profile of CO at Frankfurt for the period MAM 2021. IAGOS observations are shown in black, the regional ENSEMBLE and associated analysis are shown in red and green respectively, and the global o-suite is shown in blue. The shaded area indicates the range of the mean climatology of the observations plus/minus one standard deviation during the same period for all years between 2003 and 2018 (IAGOS/MOZAIC, level 2 data). (Units: $\mu g.m^{-3}$).

Some of the individual profiles at Frankfurt of the ENSEMBLE are presented in Fig. 5.8. These profiles correspond to the highest CO values observed in the low troposphere during this MAM period. The highest daily values of CO in the surface during this period are between 300 and 400 $\mu g.m^{-3}$ (Fig. 5.6). The maximum observed is reached on 18 March at 07:48 with 500 ppbv (Fig. 5.8). As shown on Fig. 5.8, these CO values are in most cases largely underestimated by the regional model in the lowest layers. In general, there is little difference between the different forecast times except in rare cases for example on 13 April (Fig. 5.8).

As regards the results of the individual models (Fig. 5.9), there are in general very similar for all profiles of MAM 2021. Most differences between models are found in the low to mid-troposphere and in particular in the boundary layer, when values of CO are high but not systematically (03/03 09:40, 04/13 07:08, 04/21 08:13).

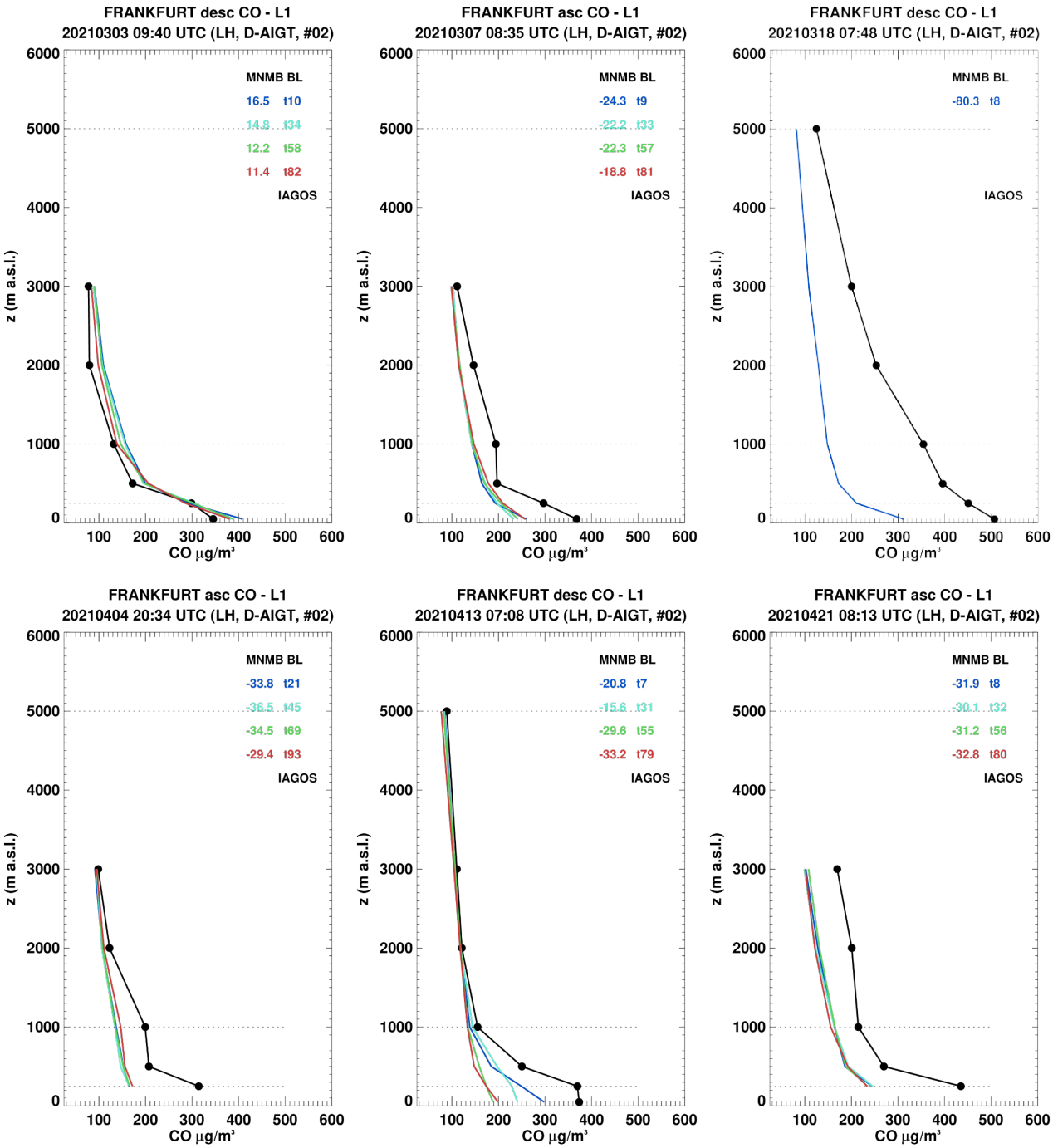

Figure 5.8: Selection of CO profiles at Frankfurt during the period MAM 2021. IAGOS is shown in black, and the ENSEMBLE is shown at 4 forecast times (blue: 1-day; cyan: 2-day; green: 3-day; red: 4-day). (Units: µg.m^3).

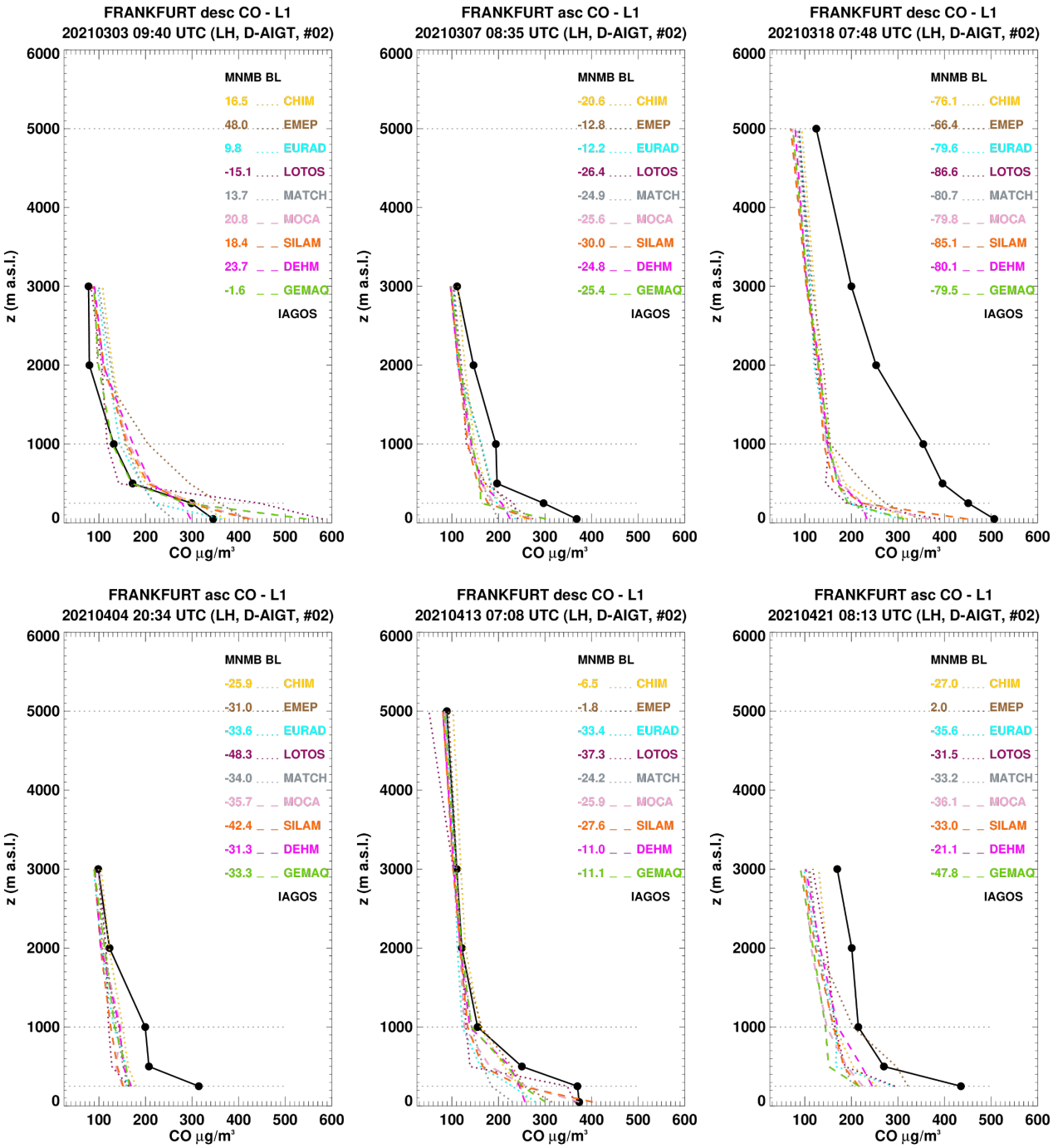

Figure 5.9: CO profiles at Frankfurt during the period MAM 2021. IAGOS is shown in black and each colour/ line style corresponds to one of the 9 models for the ensemble. In the legend, the models are CHIM=CHIMERE, EMEP=EMEP, SILAM=SILAM, LOTOS=LOTOS-EUROS, MOCA=MOCAGE, EURAD=EURAD, MATCH=MATCH, DEHM=DEHM, GEMAQ=GEM-AQ. (Units: µg.m^3).

6 Validation of regional model tropospheric NO_2 using MAX-DOAS

6.1 Summary

MAX-DOAS surface remote sensing observations provide tropospheric columns of NO_2, with the largest sensitivity in the boundary layer. While the magnitude of VCDs derived from the measurements for the urban stations De Bilt and Bremen are reproduced well by the model ENSEMBLE, the ENSEMBLE underestimates the values in Athens (bias ~-2 x 10^{15} molec. cm^{-2}). Large differences can be found between individual models depending on the station. Although many of the model simulated values probably fall within the uncertainty range of MAX-DOAS retrievals, the latter alone cannot explain differences between retrievals and simulations, especially those found for variations in time. For the regional ENSEMBLE, moderate correlations on the order of 30-65 % are found for each station. The regional ENSEMBLE performs significantly better than the global model in terms of correlation at all stations except for De Bilt (where correlations are comparable). However, some of the larger NO_2 values inside individual pollution plumes are underestimated by the models.

6.2 Introduction

MAX-DOAS observations of atmospheric composition are performed by taking measurements of the scattered sunlight at different elevation (and sometimes also azimuthal) angles. Depending on the viewing angle and solar position, the light path through the atmosphere is different, with the observation in the zenith direction usually providing the shortest light path through the lower troposphere. Therefore, using the zenith measurement as intensity of incident radiation and the observations in other angles as intensity of transmitted radiation, the total amount of molecules of a certain species along the light path difference, the so-called slant column densities, can be determined using Lambert Beer's law. Using radiative transfer modelling and Optimal Estimation techniques, this can be inverted to tropospheric columns and even lower altitude tropospheric profiles.

The advantage of MAX-DOAS measurements is their ability to observe several pollution related species at the same time (e.g., NO_2, HCHO, CHOCHO, SO_2, aerosols, potentially also O_3) and to provide data which is virtually free of interferences from other species such as PAN or NO_y for NO_2. Also, the fact that the observations integrate over a comparatively large volume can be an advantage for satellite and model validation as the observed quantity is relatively close to the modelled one. On the other hand, the uncertainty of the retrievals is considerable (on the order of 30% for NO_2 tropospheric columns and larger for individual layers) and depends on cloud occurrence and aerosol loading.

In this report, regional air quality model forecasts of tropospheric NO_2 columns are compared to MAX-DOAS retrievals from 3 urban stations (De Bilt– KNMI, Bremen – IUP-UB, Athens – IUP-UB). The reader is referred to previous reports for comparisons from the rural station OHP (BIRA-IASB) (which showed in general an underestimation by the model ENSEMBLE and an overall better performance for CAMS-global here) as the instrument at this site stopped working in March 2017. The MAX-DOAS instrument for the urban site in Uccle (BIRA-IASB) was dismantled in March 2020, and comparisons for this station are therefore not continued since this time. Since the MAM 2020 report, the MAX-DOAS data used in the comparisons is based on tropospheric column retrievals, meaning that no profile information is

incorporated in the comparisons since this time. A simple block profile is assumed in the MAX-DOAS retrievals and column averaging kernels are estimated based on the box air mass factor for each observation layer. An overview of the station data is given by Table 6.1. The MAX-DOAS instrument in Athens was not working correctly in August and September 2020 leading to gaps in the measurements during these months.

Note that the period investigated starts in June 2020 for consistency, as two new models were recently introduced to the ENSEMBLE.

6.3 Inter-comparison method

Model VCDs (vertical column densities) have been calculated based on regional model data interpolated to MAX-DOAS output altitudes. Column averaging kernels (AVKs) from the measurements were applied to model NO_2 partial columns before summing up NO_2 values in the vertical:

$$VCD_{method2}^{model} = \sum_{i=1}^{Nobs} AVK_i \cdot VCD_i^{model}$$

The averaging kernels are part of the profiling output and represent the sensitivity of the retrieved column to the NO_2 amount at different altitudes. As the sensitivity of MAX-DOAS retrievals is largest in the boundary layer, the application of averaging kernels from the measurements to model simulations can have a crucial influence on validation results.

Only those model values closest to the measurement time are used below. As the model output is given in hourly time steps, the maximum possible time difference between measurements and simulations shown here is 30 minutes.

6.4 Results

Figure 6.1 shows time series of tropospheric NO_2 VCDs derived from MAX-DOAS for the model ENSEMBLE. The magnitude of VCDs from the measurements for De Bilt and Bremen is reproduced by the models, an underestimation is found for Athens. The underestimation for Athens may be related to problems in simulating vertical transport of pollution within the boundary layer, as the instrument is placed on a small hillside above the city centre and the comparisons for Athens are therefore representative for altitudes larger than approximately 500 m absl. The retrievals show a larger variability of values compared to the models. Measurements and simulations don't agree very well for some of the time steps investigated. The models underestimate some of the larger NO_2 values inside individual pollution plumes. Models may fail to reproduce these peaks due to errors in NOx emissions, transport of NO_2 towards the stations and chemistry.

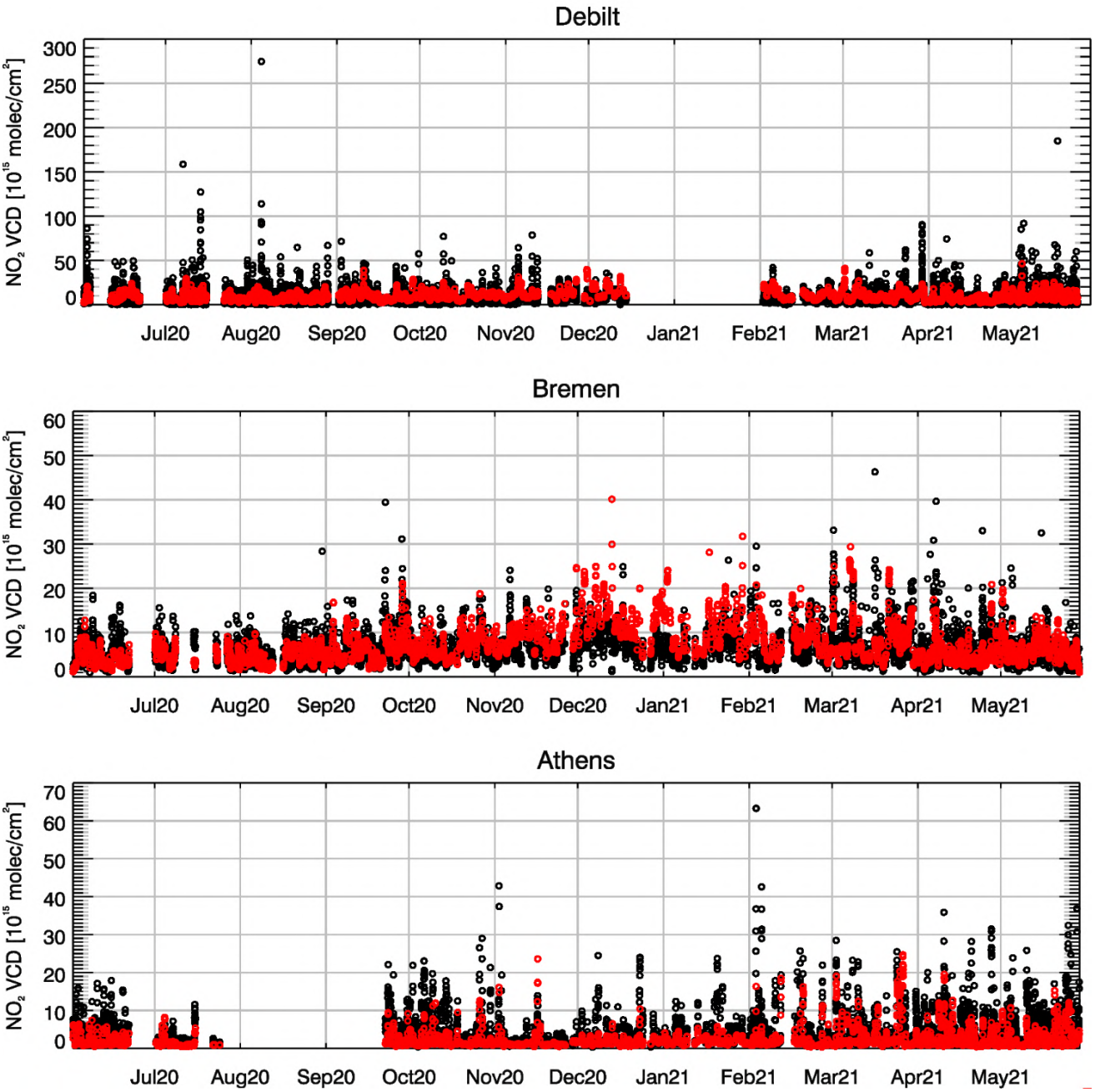

Figure 6.1. . Time series of tropospheric NO_2 VCDs [10^{15} molec. cm^{-2}] from (black circles) MAX-DOAS and (red circles) the ENSEMBLE forecasts for (from top to bottom) De Bilt, Bremen, Athens. Model results were calculated by multiplying NO_2 partial columns with averaging kernels for each observation layer followed by summing up resulting values in the vertical. Model data was interpolated to the averaging kernel layer altitudes prior to calculation of VCDs. Time period: June 2020 - May 2021. The MAX-DOAS instrument in Athens was not working correctly for a period in August and September 2020 leading to gaps in the time series.

Table 6.1. Overview of MAX-DOAS station data used for validation of regional air quality model simulations. The period covered in this report is June 2020 to May 2021.

Station	Latitude, longitude	Altitude above sea level	Institution	Quantity	Character
Bremen (Germany)	53.106°N, 8.86°E	21 m	IUP-UB	column	urban
De Bilt (Netherlands)	52.1° N, 5.18° E	23 m	KNMI	column	urban
Athens (Greece)	38° N,23.7° E	527 m	IUP-UB	column	urban

Figure 6.2 shows comparisons of diurnal cycles. Again, the mean column amounts of the ENSEMBLE are comparable to the observations for Bremen, but overestimated for De Bilt and generally underestimated in Athens. Although larger differences are found depending on the regional model, the model ENSEMBLE performs much better than CAMS-global for all stations, CAMS-global is negatively biased, particularly in Athens. Some regional models show different variations from one hour to another. The afternoon peak observed by MAX-DOAS for De Bilt is not reproduced by all models. This may be related to inadequate photochemistry, scaling of emissions in time or vertical distribution of NO_2 and errors in simulating pollution transport towards the station.

Comparisons of weekly cycles are shown in Figure 6.3. Weekly cycles are underestimated by all regional models, with a stronger decrease of NO_2 columns from workdays towards the weekend retrieved by MAX-DOAS for all urban stations. For Athens, the models do not reproduce the observed weekly cycle at all. The performance of CAMS-global with respect to weekly cycles is comparable to the regional models. Note that some variations of values from one day to another may just be coincidence due to data sampling.

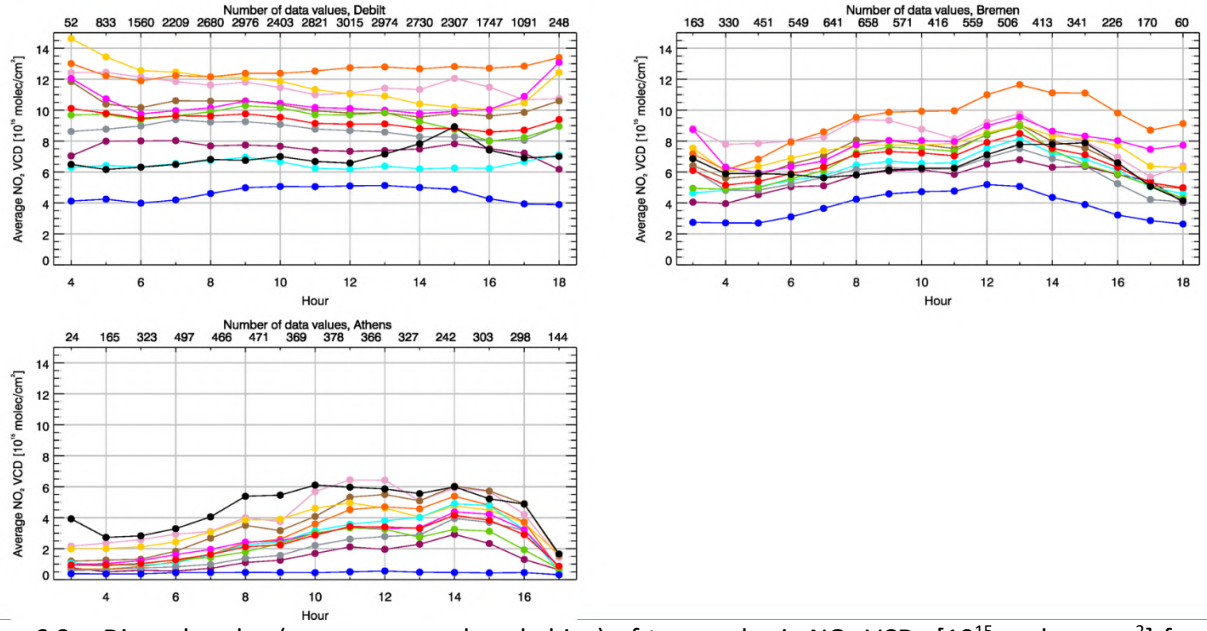

Figure 6.2. . Diurnal cycles (averages over hourly bins) of tropospheric NO_2 VCDs [10^{15} molec. cm^{-2}] for (top left) De Bilt, (top right) Bremen and (lower left) Athens. The black lines show the MAX-DOAS retrievals. All other lines refer to model data: (red) ENSEMBLE, (yellow) CHIMERE, (brown) EMEP, (orange) SILAM, (purple-blue) LOTOS-EUROS, (cyan) EURAD-IM, (pink) MOCAGE, (grey) MATCH, (fuchsia) DEHM, (light green) GEM-AQ and (blue) CAMS-global. Time period: June 2020 – May 2021.

Scatter density plots or heat maps of tropospheric NO_2 VCDs from MAX-DOAS against model ENSEMBLE values corresponding to the time series displayed in Figure 6.1 as well as statistical values (root mean squared error, bias, correlation) are given in Figure 6.4. Corresponding statistical values for all individual models are given in Table 6.2. Correlations on the order of 30-60 % are found for each station for all regional models. The ENSEMBLE reaches the highest correlation of about 60 % at Athens. Models tend to overestimate lower and underestimate higher NO_2 VCDs for the three urban stations. While the spread of values is quite large for individual data points, there is a fair agreement between models and retrievals for the majority of the measurements for urban stations (as shown by the high percentage of values close to the reference line). The ENSEMBLE performs significantly better than CAMS-global in terms of correlation for all stations. CAMS-global has a rather strong negative bias at all stations and the correlation is nearly zero for Athens, where the VCDs appear to be strongly underestimated. This may be related to problems in simulating vertical transport within the boundary layer, as the instrument is placed on a small hillside above the city centre and the comparisons are therefore representative for altitudes larger than approximately 500m asl. All regional models are negatively biased in Athens.

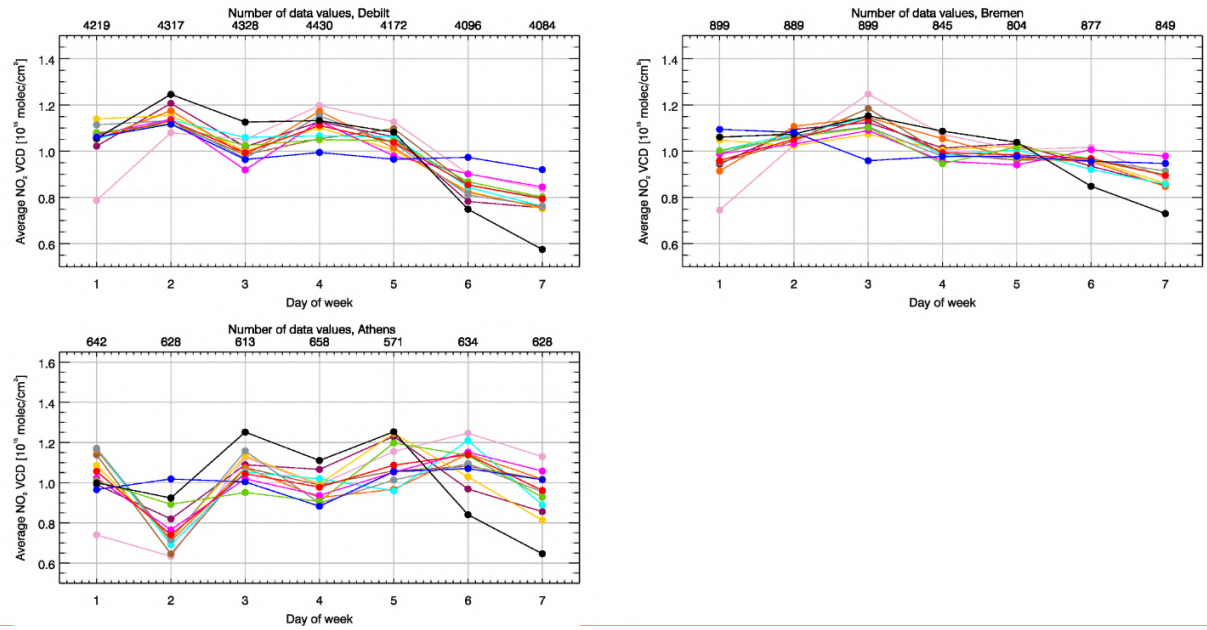

Figure 6.3. Weekly cycles (averages over daily bins divided by mean over whole week) of tropospheric NO_2 VCDs [10^{15} molec cm^{-2}] for (top left) De Bilt, (top right) Bremen and (lower left) Athens. The black lines show the MAX-DOAS retrievals. All other lines refer to model data: (red) ENSEMBLE, (yellow) CHIMERE, (brown) EMEP, (orange) SILAM, (purple) LOTOS-EUROS, (cyan) EURAD-IM, (pink) MOCAGE, (grey) MATCH, (fuchsia) DEHM, (light green) GEM-AQ and (blue) CAMS-global. Time period: June 2020 - May 2021.

	De Bilt	Bremen	Athens
ENS	6.727/2.201/0.391	3.869/0.507/0.503	4.636/-2.415/0.565
CHIMERE	8.389/4.353/0.365	3.988/1.276/0.502	4.064/-1.155/0.606
EMEP	7.299/3.047/0.390	4.524/1.063/0.490	4.825/-1.134/0.565
SILAM	10.397/5.474/0.321	6.460/3.236/0.446	4.715/-1.899/0.537
LOTOS-EUROS	6.729/0.559/0.316	4.312/-0.623/0.441	5.764/-3.452/0.311
EURAD-IM	8.715/4.476/0.336	6.003/2.118/0.415	6.783/-0.451/0.444
MOCAGE	5.990/-0.587/0.371	3.716/0.041/0.529	4.926/-2.183/0.506
MATCH	7.151/1.721/0.358	3.980/-0.351/0.430	5.050/-2.913/0.510
DEHM	7.934/3.134/0.317	4.762/1.407/0.423	4.553/-2.217/0.562
GEMAQ	7.821/2.491/0.299	4.593/0.538/0.421	5.143/-2.647/0.398
OSUITE	6.355/-2.280/0.328	4.412/-2.291/0.312	6.524/-4.426/0.041

Table 6.2: Statistics on how tropospheric NO_2 VCDs [10^{15} molec. cm^{-2}] from models compare to MAX-DOAS retrievals at the three stations. Each column entry shows from left to right: root mean squared error [10^{15} molec. cm^{-2}], bias [10^{15} molec. cm^{-2}] and correlation coefficient (cor). Time period: June 2020 - May 2021.

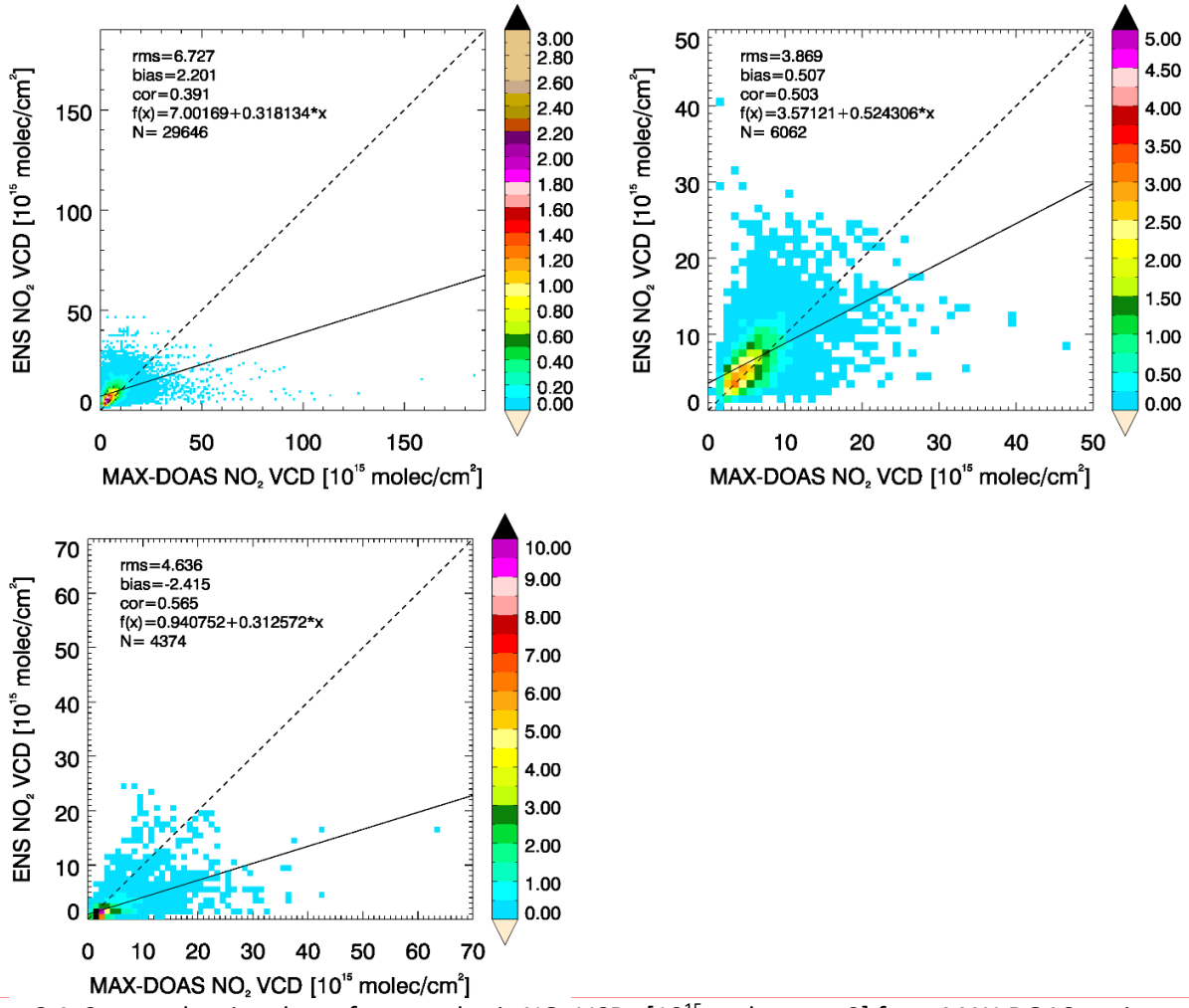

Figure 6.4. Scatter density plots of tropospheric NO_2 VCDs [10^{15} molec. cm−2] from MAX-DOAS against model ENSEMBLE hourly data for (top left) De Bilt, (top right) Bremen and (lower left) Athens. The data is shown with a bin size of 1 x 10^{15} molec. cm^{-2} and colour according to the number of data points per bin [%]. The dashed line is the reference line (f (x)=x). The solid line is the regression line (see top left of each plot for f(x) of this line). The root mean squared error (rms) [10^{15} molec. cm^{-2}], bias [10^{15} molec. cm^{-2}], Pearson correlation coefficient (cor) as well as the number of data points N are given at the top left of each plot. Time period: June 2020 - May 2021.

7 Validation of tropospheric NO_2 columns against satellite retrievals

7.1 Summary

Regional air quality model columns of tropospheric NO_2, derived from the output provided on 8 levels with a top at 5km, are compared to 9:30 local time GOME-2/MetOp-C NO_2 satellite retrievals (IUP-UB v1.0 product). The overall spatial distribution of tropospheric NO_2 is reproduced by the ENSEMBLE, but values over central European emission hotspots are overestimated by the majority of the models, which results in a positive bias of ~1-2 x 10^{15} molec/cm^2 for the regional ensemble analysis for values averaged over the region of Europe, while the also positive bias for CAMS-global is < 0.5 x 10^{15} molec/cm^2. There are stronger shipping signals in the model than in the satellite data. As a result of a major regional model upgrade in June (2019), which includes the use of an updated European emissions inventory with improved estimates for North African and Middle Eastern anthropogenic emissions, enhanced tropospheric columns of NO_2 are reproduced over these regions by all models.

7.2 Comparison with GOME-2 NO_2

In this section, regional air quality model columns of tropospheric NO_2 are compared to GOME-2/MetOp-C NO_2 satellite retrievals (IUP-UB v1.0) [Richter et al., 2011] for January – May 2021 (see former reports for comparisons to the older GOME-2A instrument for September 2016 – February 2021). This GOME-2C product uses the CAMS global forecasts as NO_2 a priori and corrects for the stratospheric contribution using a variant of the STREAM method (Beirle et al., 2016). This satellite data provides excellent coverage in space and time and very good statistics. However, only integrated tropospheric columns are available, and the satellite data is always taken at 09:30 LT for GOME-2C and at clear sky only. Therefore, model data are vertically integrated, interpolated in time and then sampled to match the satellite data. Uncertainties in NO_2 satellite retrievals are large and depend on the region and season. Winter values in mid and high latitudes are usually associated with larger error margins. As a rough estimate, systematic uncertainties in regions with significant pollution are on the order of 20% – 30%. Conclusions may differ for comparisons to other satellite NO_2 products (e.g., TEMIS GOME-2C, http://www.temis.nl shows lower retrieved NO_2 values for January). It should be noted here that model data is only available for altitudes up to 5000 m, meaning that (depending on tropopause height) tropospheric model columns may not be representative of the total amount of NO_2 in the troposphere. Note that since 05 May 2020 GOME-2C observations are assimilated by the CAMS global system. This is, however, a different retrieval product than what is used in the validation reported here (University of Bremen retrieval).

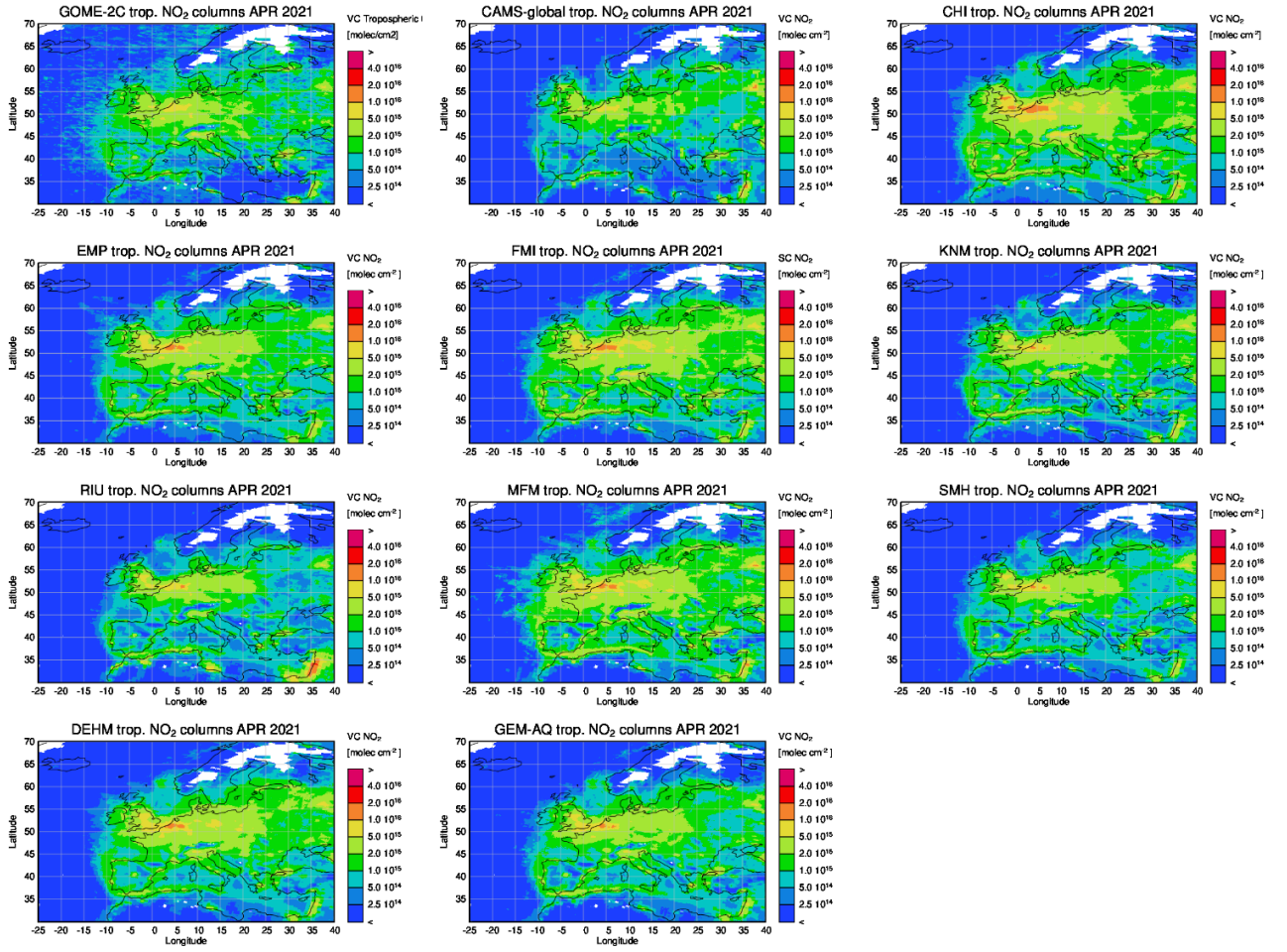

Figure 7.1. Maps of satellite-retrieved and model-simulated tropospheric NO_2 columns [molec cm^{-2}] for April 2021. From left to right: (first row) GOME-2C, CAMS-global and CHIMERE; (second row) EMEP, SILAM and LOTOS-EUROS; (third row) EURAD-IM, MOCAGE and MATCH; (fourth row) DEHM and GEM-AQ. GOME-2C data were gridded to regional model resolution (i.e. 0.1° x 0.1°). Both measurements and model data were treated with a reference sector (25°W - 20°E) subtraction approach to account for the lack in free tropospheric signal. Model data were linearly interpolated to the satellite overpass time (9:30 LT).

Figure 7.1 shows maps of monthly mean tropospheric NO_2 columns from GOME-2C, regional models and CAMS-global for April 2021. The overall spatial distribution and magnitude of tropospheric NO_2 is reproduced by the regional models in principle. There are generally stronger shipping signals in the models compared to the satellite data, which may result from errors in anthropogenic emissions or from chemical processing inside the ship exhaust plumes (see e.g., Vinken et al., 2014).

Compared to CAMS-global, regional models perform better for some emission hotspots like Moscow, but show an overestimation over emission hotspots in Central Europe. As a result of a major regional model upgrade in June 2019, which includes the use of an updated European emissions inventory with improved estimates for North African and Middle Eastern anthropogenic emissions, enhanced tropospheric columns of NO_2 are now reproduced over these regions (e.g., Lebanon, Israel) by all models.

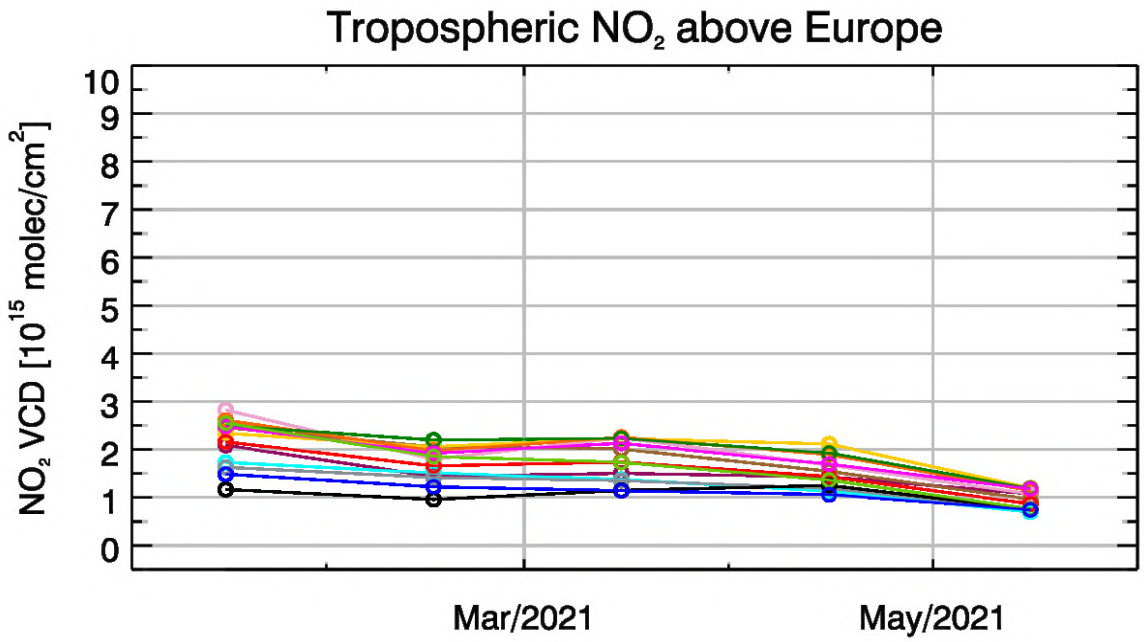

Figure 7.2. Time series of monthly averaged tropospheric NO_2 columns [10^{15} molec cm^{-2}] retrieved by (black) GOME-2C and simulated by (red) ENSEMBLE forecast, (green) ENSEMBLE analyses, (yellow) CHIMERE, (brown) EMEP, (orange) SILAM, (purple) LOTOS-EUROS, (cyan) EURAD-IM, (pink) MOCAGE, (grey) MATCH, (fuchsia) DEHM, (light green) GEM-AQ and (blue) CAMS-global. GOME-2C data were gridded to regional model resolution (i.e., 0.1° x 0.1°). Both measurements and model data were treated with a reference sector (25°W - 20°E) subtraction approach. Model data are linearly interpolated to the satellite overpass time (9:30 LT). Time period: January 2021 - May 2021 (see former reports for comparisons to GOME-2A for September 2016 – February 2021).

Figure 7.2 shows time series of monthly mean tropospheric NO_2 columns for GOME-2C and the models. All model simulations are positively biased compared to GOME-2C for the time period investigated (Jan 2021 - May 2021), probably because of the overestimation of values over Central European emission hotspots. The bias is comparatively large for the regional ensemble analysis (~1-2 x 10^{15} molec/cm^2) and comparatively small for CAMS-global (< 0.5 x 10^{15} molec/cm^2).

8 Comparison with high-altitude EEA Air Quality e-reporting surface stations

8.1 Summary

European ozone EA Air Quality e-reporting measurements from high-altitude stations (above 1km) have been used to evaluate the regional models. Differences between the regional model orography and the true altitude of the station were used to select the model altitude level to compare with. The ensemble median mostly overestimates ozone levels during the period March – March 2021. More specific, depending on the station the observed ozone levels are reproduced to within -5% and 30% by the ensemble median D+0 forecast (1h-24h). Correlations observed were between 0.60 and 0.80 and the ensemble median D+0 forecast has a performance better than any of the individual nine models. CHIMERE, MOCAGE models were deviating significantly from the ensemble median in terms of MNMBs and LOTOS EUROS, MOCAGE and EURAD is deviating significantly from the ensemble median in terms of correlations with observations. Validation metrics are also given for the ENS analysis. The ENS analysis has almost equivalent performance with ENS D+0 forecast in terms of MNMBs but performs better than ENS D+0 forecast in terms of correlations (significantly higher correlations).

8.2 Introduction

The seven models and their ENSEMBLE median (D+0 forecast as well as the analysis) have been compared against Background-Rural EA Air Quality e-reporting measurements for surface stations at elevation greater than 1000 m above mean sea level (http://www.eea.europa.eu/data-and-maps/data/airbase-the-european-air-quality-database-7). Elevated stations were selected to fall within classes 1-2 in the O_3 Joly-Peuch (2012) classification for EA Air Quality e-reporting NRT stations. Table 8.1 shows the stations altitude above mean sea level together with the LOTOS-EUROS model altitude (i.e., from model's topography) pertaining to the nearest to the station grid point. Modelled gas mixing ratios were extracted at the model level, which is closest to the stations altitude as defined from the orography (see column 7 in Table 8.1).

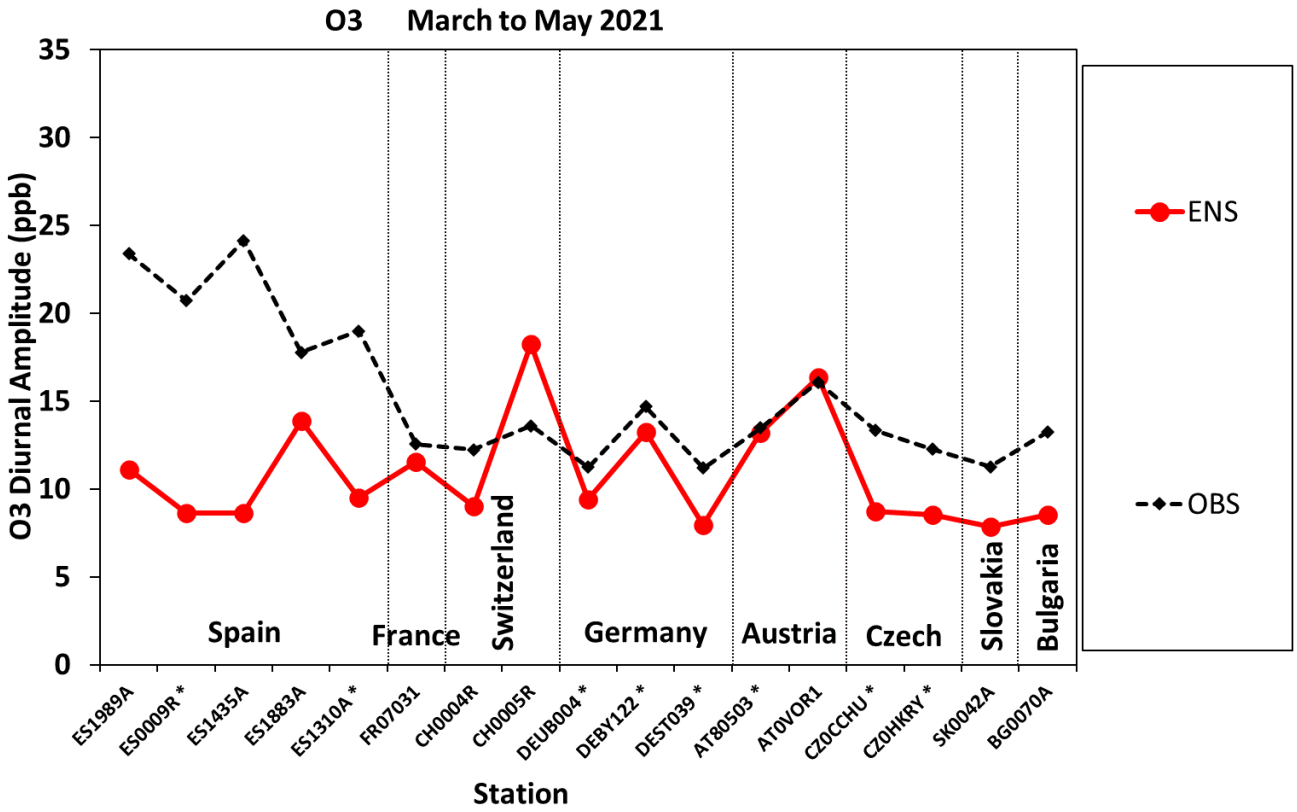

Figure 8.1. Amplitude of the diurnal cycle as measured (ppb) from stations observations (black diamonds) and as calculated from the ENSEMBLE forecast D+0 (red circles). With asterisks are denoted stations used in the assimilation process.

Table.8.1: Background-Rural EEA Air Quality e-reporting Stations (with NRT data) with elevation higher than 1000 m.

Station Name	Stat_id	Longitude	Latitude	real Altitude	model Altitude	nearest Level	use in CAMS50
Lario	ES1989A	-5.09	43.04	1140	1199	0	validation
Capmisabalos	ES0009R	-3.14	41.27	1360	1124	2	assimilation
Vilafranca	ES1435A	-0.25	40.42	1125	907	2	validation
Torrelisa	ES1883A	0.18	42.46	1005	1282	0	validation
Ak- Pardines	ES1310A	2.21	42.31	1226	1117	1	assimilation
Chaumont	CH0004R	6.98	47.05	1136	727	3	-
Schauinsland	DEUB004	7.91	47.91	1205	554	3	assimilation
Rigi-Seebodenalp	CH0005R	8.46	47.07	1031	997	1	validation
Sulzberg im Bregenzerwald	AT80503	9.93	47.53	1020	961	1	assimilation
Bad Hindelang/Oberjoch	DEBY122	10.40	47.52	1169	1150	0	assimilation
Brocken	DEST039	10.62	51.80	1130	302	4	assimilation
Vorhegg bei Kötschach-Mauthen	AT0VOR1	12.97	46.68	1020	1427	0	validation
Churanov	CZ0CCHU	13.62	49.07	1118	739	4	assimilation
Krkonose-Rychory	CZ0HKRY	15.85	50.66	1001	530	4	assimilation
Bratislava - Jeséniova	SK0042A	20.99	48.78	1244	445	5	validation
Vitosha mountain	BG0070A	23.24	42.64	1321	863	4	-

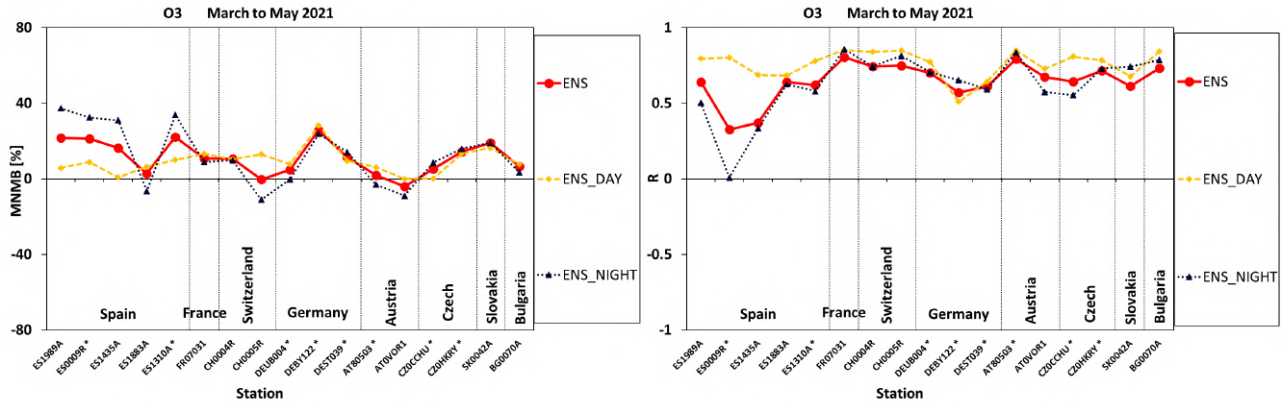

Figure 8.2. MNMBs [%] (left) and temporal correlations (right) calculated for the ENSEMBLE model for during daytime (orange) night-time (dark blue) as well as for the whole day (red) for the MAM 2021 period. With asterisks are denoted stations used in the assimilation process.

For the validation, hourly O_3 concentration values (μg/m^3) are extracted from the nine models as well as for the regional ENSEMBLE. It should be noted that, in the EEA Air Quality e-reporting network the O_3 measurements that were made by the instrument in ppb were converted from ppb to μg/m^3, following the EU directive 2008/50, i.e., by multiplying by 2. This conversion is approximately correct for low altitude stations. However, at high altitude stations pressure and temperature should be considered when converting from ppb to μg/m^3 and vice versa. As hourly pressure and temperature data were not available for all EEA Air Quality stations the comparison between observed and modelled ozone was done by re-converting both modelled and observed hourly O_3 concentration in ppb. For modelled ozone values the conversion was done by applying the following ideal gas equation with the model's estimates of temperature (T) and pressure (P) (from CAMS- global):

$$O3\ (\text{in ppb}) = O3\ (\text{in mg/m3}) * \left(\frac{R * T}{p_m * M_{o3}}\right)$$

8.3 Regional ENSEMBLE results

In the previous report it was shown that comparing the observed and modelled amplitude of the diurnal variation of ozone at each high-altitude station could provide a criterion concerning the exposure suitability of the stations. We found out in this report that an additional criterion is needed to differentiate stations as to their suitability in exposure. The additional criterion is the correlation coefficients between the amplitude of the diurnal cycle as observed and modelled to be statistically significant roughly higher than 0.3. Figure 8.1 shows the observed and modelled diurnal amplitude of ozone at each station, moving from Spain to Bulgaria. Figure 8.2 shows the MNMBs and the correlation coefficients calculated for the ENSEMBLE model during daytime, at night-time as well as for the whole day. We can see that the 2 criteria of diurnal amplitude and day and night MNMBs and correlation coefficients differentiate the 3 stations in Spain from all other stations. For the above-mentioned findings these 3 high altitude stations will be excluded from our analysis. It should also be noted that daytime correlations have very small variations from stations to station and are higher than those calculated for night-time as well as for the 24-h daily means.

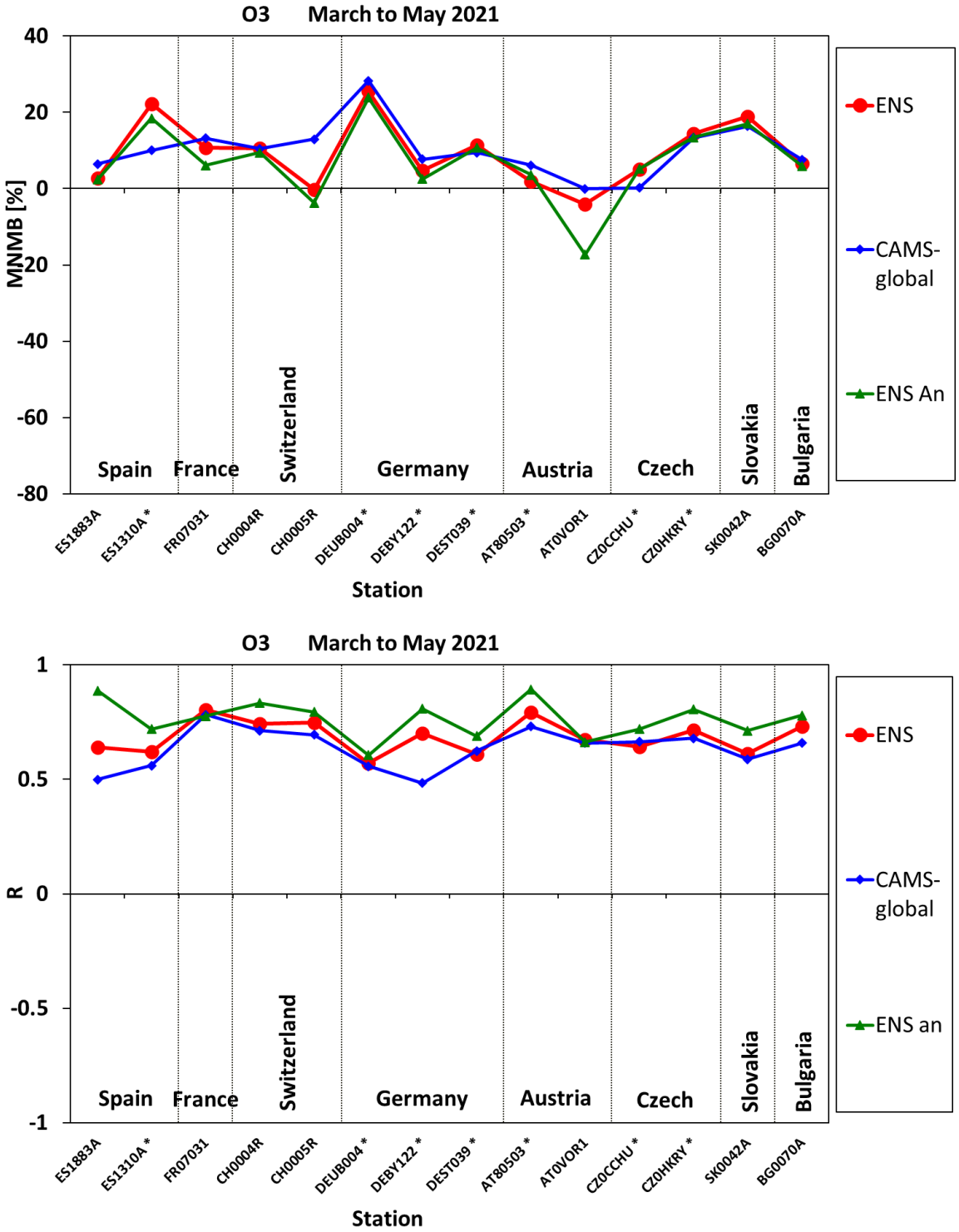

Figure 8.3. O_3 MNMBs [%] (top) and correlation coefficient (bottom) for the regional ENSEMBLE (forecast D+0; red circles and analysis; green triangles) as well as for CAMS-global (forecast D+0; blue diamonds) for the period MAM 2021. With asterisks are denoted stations used in the assimilation process.

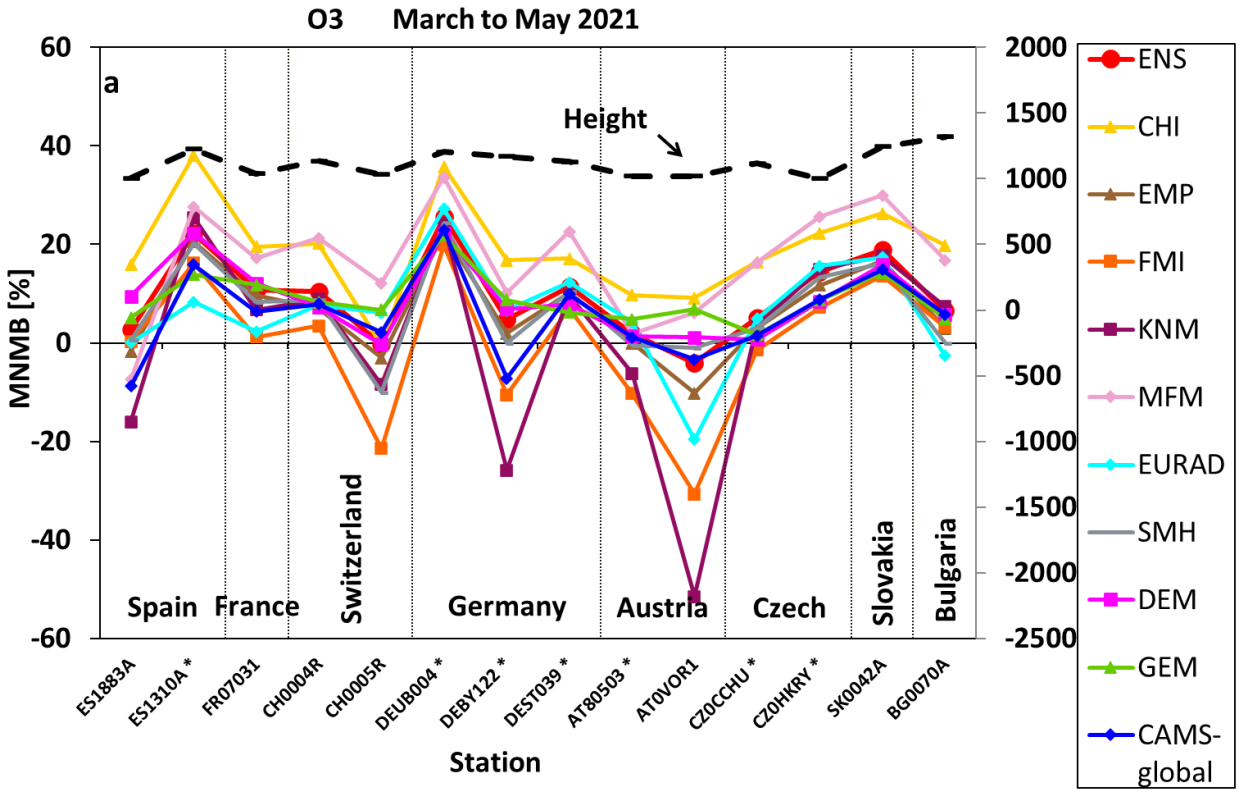

Fig. 8.4. Ozone MNMBs [%] for each of the 9 models forecasts (D+0), the ENSEMBLE forecast and CAMS-global (March to May 2021) for stations above 1000m altitude.

Figure 8.3 shows the Modified Normalized Mean biases (top) and correlation coefficients (bottom) at each of the remaining stations, moving from Spain to Bulgaria (i.e., from West to East) pertaining to the median of the ENSEMBLE forecast (D+0) and analysis (D+0) as well as CAMS-global (D+0). The ensemble median mostly overestimates ozone levels during the period March – March 2021. Depending on the station the range of MNMB for the ENSEMBLE D+0 forecast was found to be between -5% and 30%. From Figure 8.3 (bottom panel) it is obvious that the Ensemble Mean reproduces well the ozone variability. As it appears from Figs 8.3 (bottom panel) the correlation coefficients are highly significant (0.6<r<0.8). It should be noted performed almost equal in terms of both MNMBs and correlations.

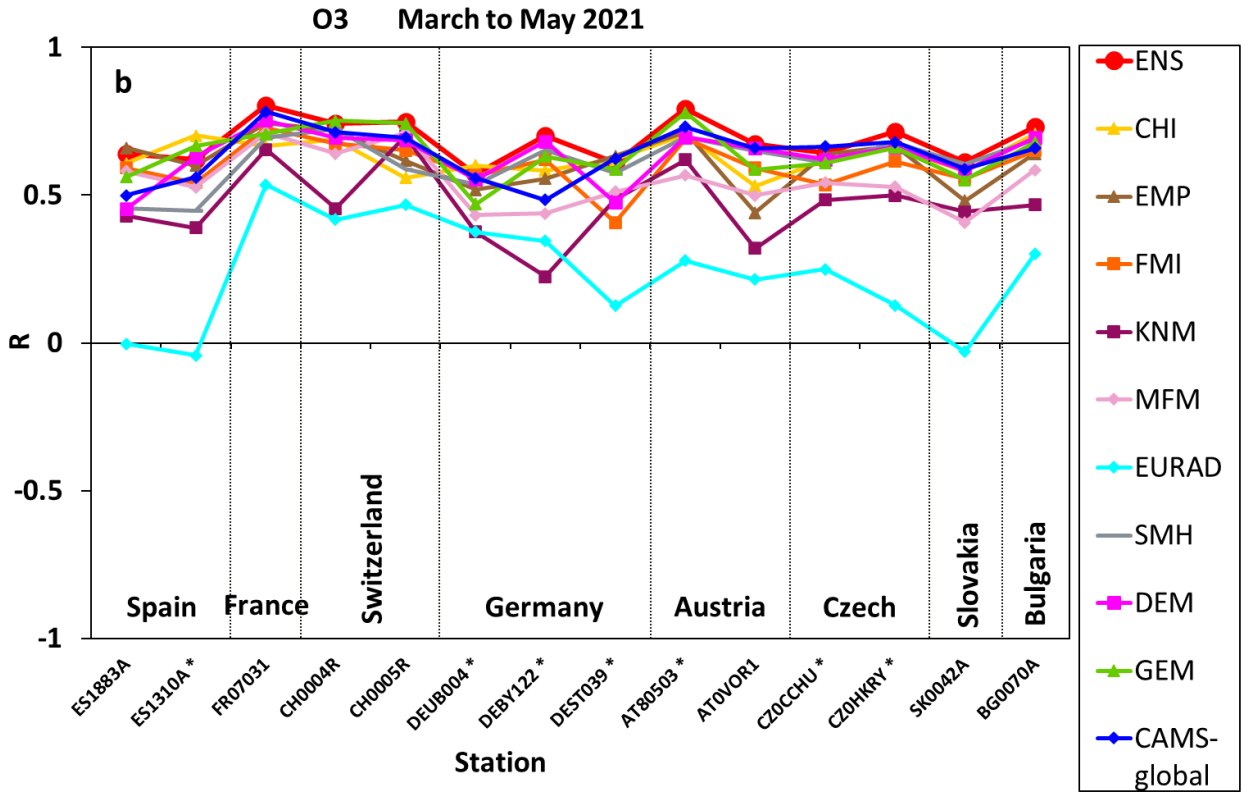

Fig. 8.5: Correlation coefficients (from hourly values) between observed and modelled ozone for the D+0 forecasts of all 9 models, the ENSEMBLE and CAMS-global (o-suite) for March to May 2021.

8.4 Results for the nine regional models

Figure 8.4 shows Modified Normalized Mean biases at each station with elevation greater than 1000 m above mean sea level, moving from Spain to Bulgaria (from West to East) pertaining to each one of the 9 model forecast calculations, the ENSEMBLE forecast as well as CAMS-global (o-suite). On top of the graph shown is the elevation of the station. Depending on the station the observed ozone levels are reproduced to within -5% and 30% from the ENSEMBLE. CHIMERE and MOCAGE models deviate notably from the ENSEMBLE in several stations (significant higher MNMBs), while the remaining models show scores closer to the ENSEMBLE. The plot for the analysis (fig. 8.6) reveals that for most individual models the analysis performs almost equal with the forecast D+0 in terms of bias (exceptions are LOTOS-EUROS and MOCAGE models for which the analysis provides an improvement compering to the forecast D+0).

Figure 8.5 shows the correlations between observations and each model for the forecasts. The ENSEMBLE reproduces well the ozone variability and has a better score than any of the individual models. LOTOS EUROS, MOCAGE, and most prominently EURAD, exhibit a lower correlation while the remaining models show scores closer to the ENSEMBLE. The respective correlations for the analysis are shown in Figure 8.7. EURAD exhibits again significantly lower correlation, while the remaining models show scores closer to the ENSEMBLE. It should be noted that for all individual models except GEM the analysis provides significantly higher correlation than the forecast D+0.

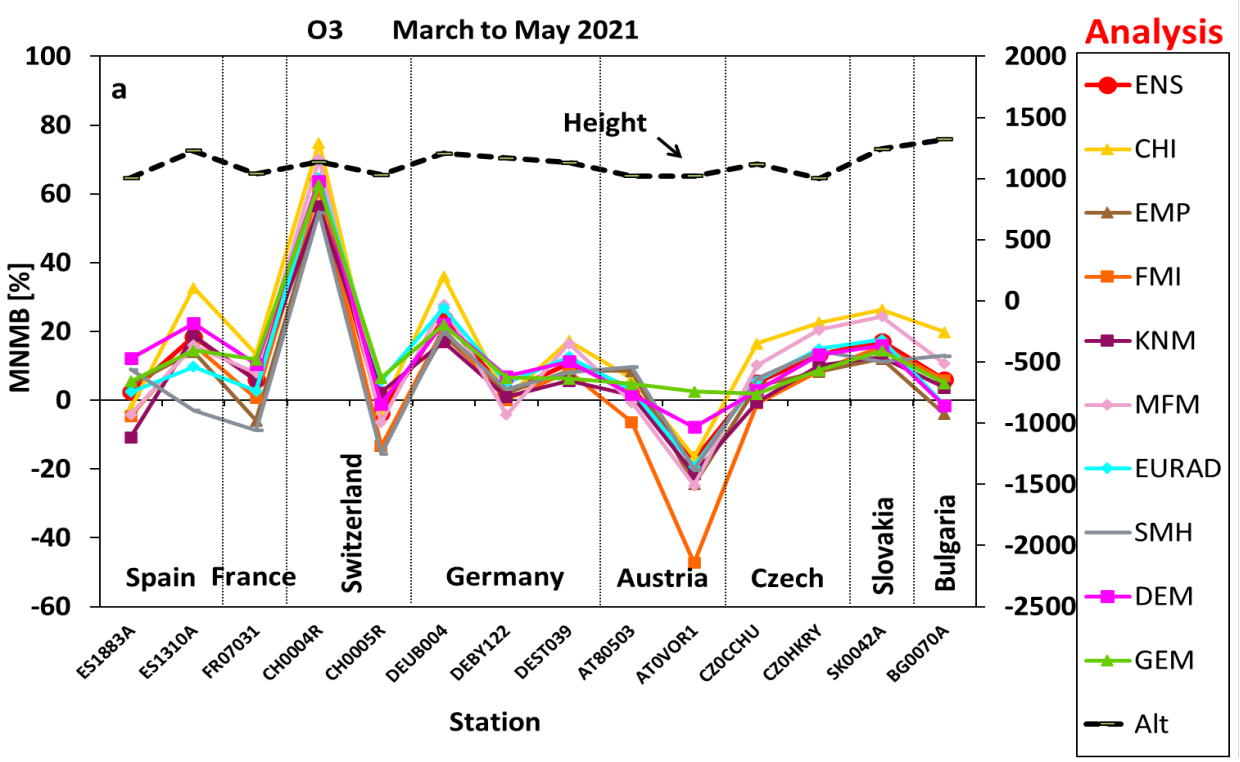

Fig. 8.6. Ozone MNMBs [%] for each of the 9 models' analysis and the ENSEMBLE analysis (March to May 2021) for stations above 1000m altitude. With asterisks are denoted stations used in the assimilation process.

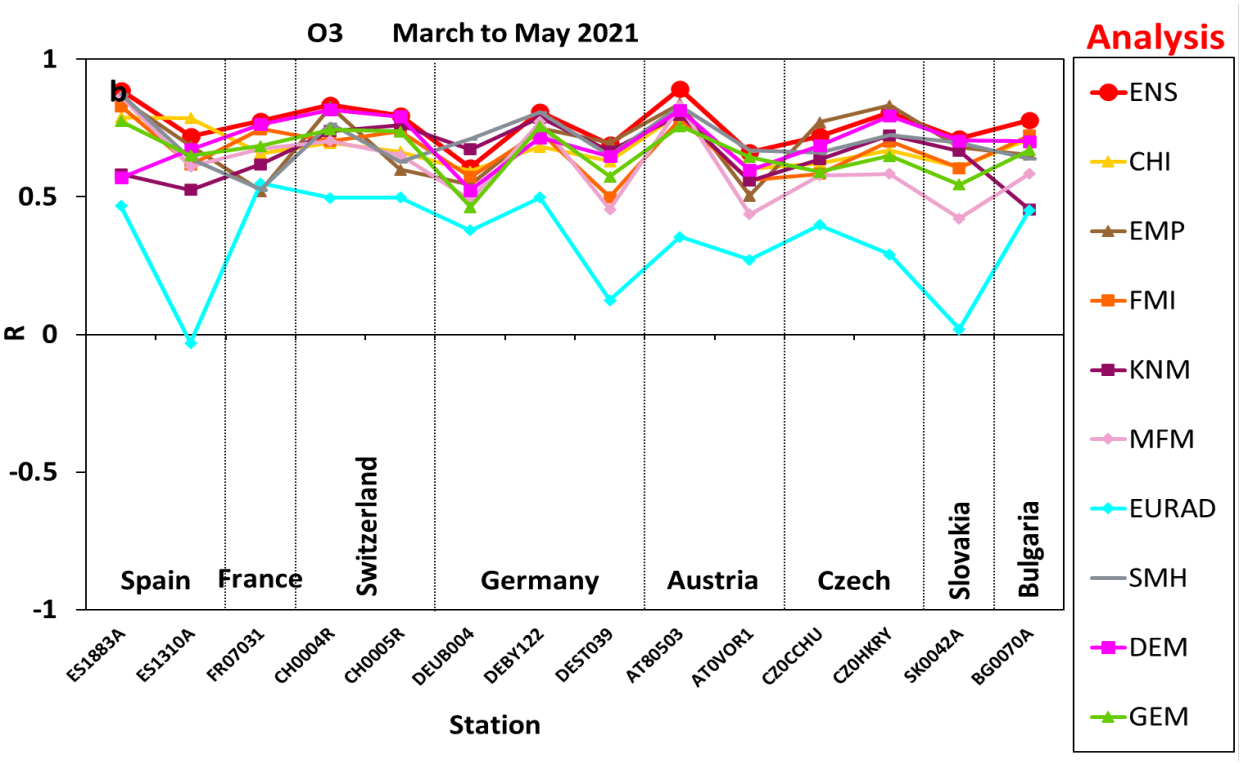

Fig. 8.7. Correlation coefficients (from hourly values) between observed and modelled ozone for the analysis of all 9 models and the ENSEMBLE for March to May 2021. With asterisks are denoted stations used in the assimilation process.

9 Comparison with ozone sonde observations

9.1 Summary

Free tropospheric ozone (<850 hPa) could be reproduced by the ENSEMBLE forecast and analysis with MNMBs between -16.3% and 15% during MAM 2021. The other models show MNMBs between -15% and 15% (forecasts and analysis) (Fig 9.2).

9.2 Comparison approach

For the validation, the sonde profiles are compared to the model data closest in time. The model data is provided at the geographical coordinates of the sonde stations, the horizontal drift during the ascend of the sonde is considered negligible.

The model concentrations at the different height levels (0, 50, 250, 500, 1000, 2000, and 5000m above the ground) are matched to the respective sonde observations and are converted to mass mixing ratios. Pressure and temperature values needed for the conversion are taken from the sonde observations. For each station and all individual launches, the differences between observation and model are calculated. In order to be able to compare the profiles of different stations, this is done for fixed altitude levels between 0 and 6000m (interval for the surface 50m, above 100m, interval 100m). The sonde and model values are then aggregated to monthly means for each station and altitude level. For each month mean modified normalized biases (MNMB) are then calculated over all European stations for the free troposphere (<850 hPa).

9.3 Results for the ENSEMBLE

For the period May 2020 to May 2021, the ENSEMBLE forecast shows MNMBs between -4.9% and 10%. The ENSEMBLE analysis shows a slightly poorer behaviour, with MNMBs between -16.3% and 15%, see Fig. 9.1. driven by outliners of single models in certain months.

Table 9.1: Sonde stations used in the validation for MAM2021

Station/location	Lat	lon	alt [m]
De Bilt	52.1	5.2	4
Hohenpeissenberg	47.8	11.2	976
Jokioinen	60.8	23.5	103
Legionow	52.4	20.97	96
Lerwik	60.14	-1.19	84
Madrid Spain	40.5	-3.8	631
Prag	50	14.4	302
Sodankyla	67	27	180
Uccle Belgium	51	4	100

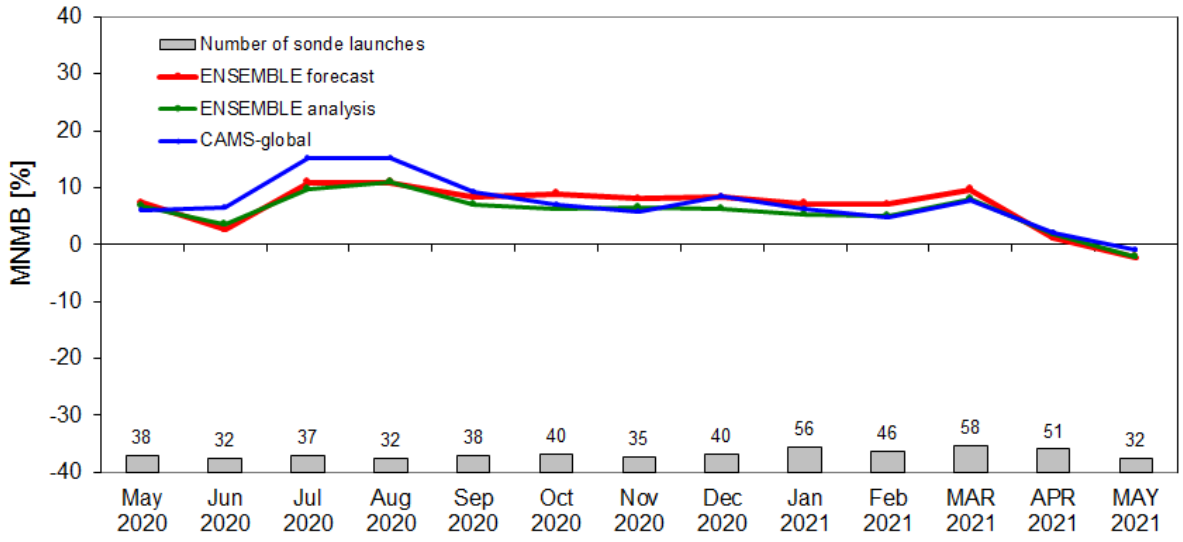

Figure 9.1 - MNMBs for the regional ENSEMBLE and CAMS-global between May 2020 and May 2021 for the free troposphere region (<850 hPa).

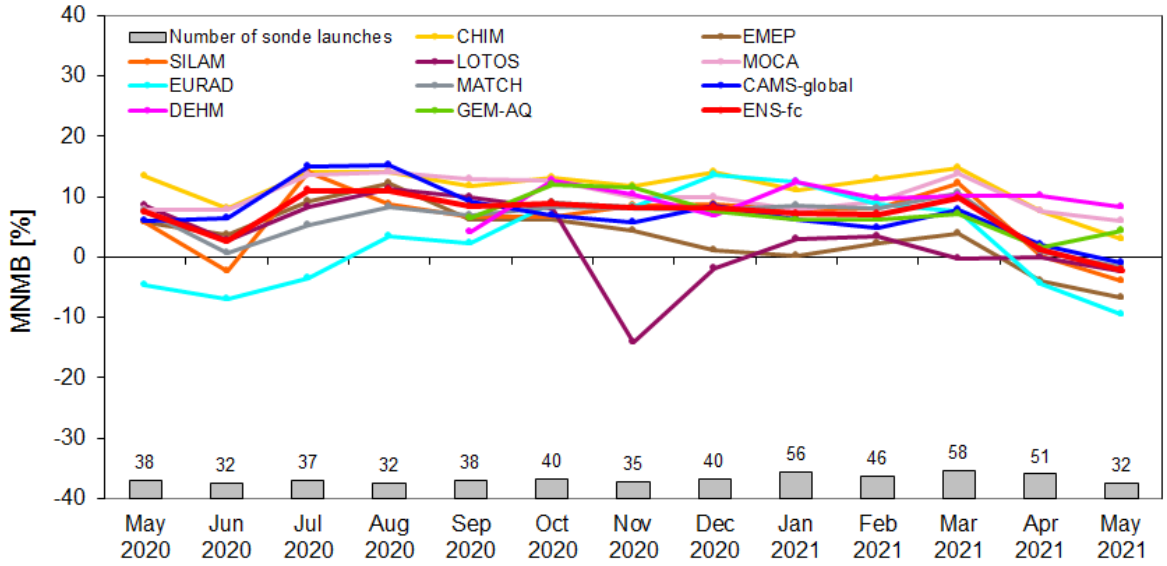

Figure 9.2. MNMBs for the individual regional models between May 2020 and May 2021 for the free troposphere region (pressure < 850 hPa).

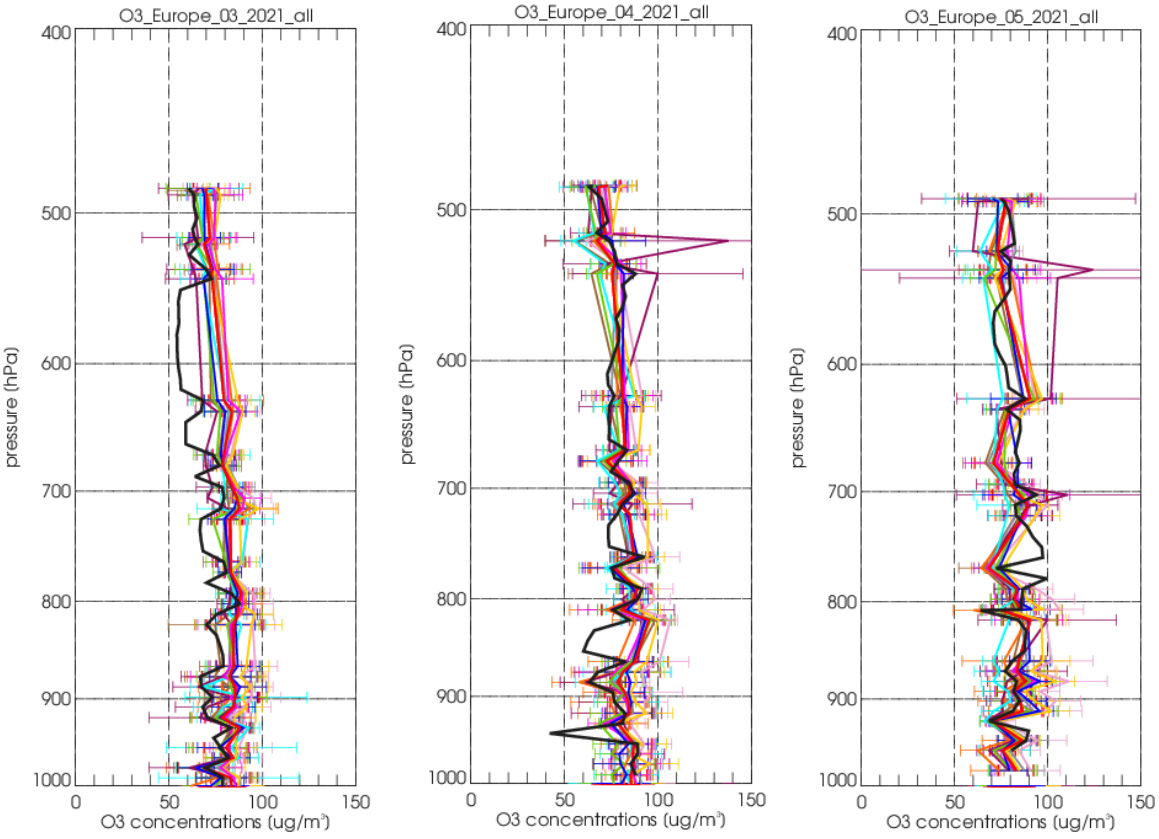

Figure 9.3. Averaged monthly profiles from the model forecast and sonde comparisons over European sonde stations for December 2020 until May 2021 (red: ENSEMBLE, blue: CAMS-global, yellow: CHIMERE, brown: EMEP, orange: SILAM, purple: LOTOS-EUROS, cyan: EURAD-IM, pink: MOCAGE, grey: MATCH, fuchsia: DEHM, light green: GEM-AQ).

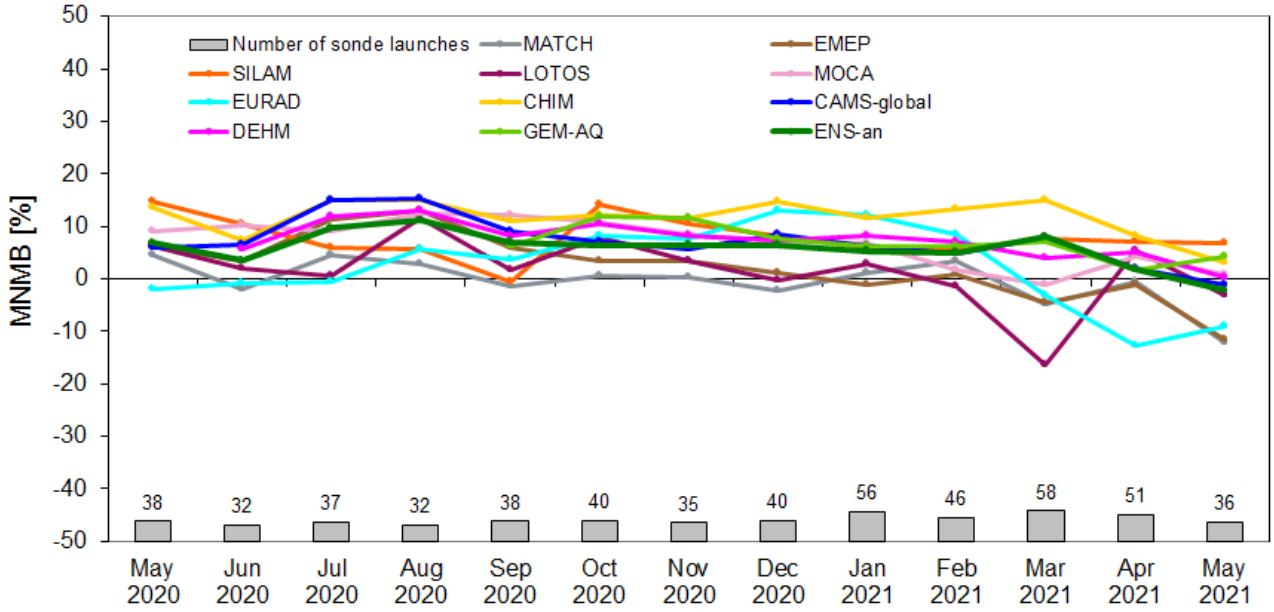

Figure 9.4. MNMBs for the regional models between May 2020 and May 2021 for the free troposphere region (pressure < 850 hPa).

9.4 Results for individual regional models

Between May 2020 and May 2021 regional model forecasts show MNMBs in the range of -9.4 % and 14.8%, see Fig. 9.2.

Results for the regional model analyses

Similar to the results of the individual models' forecasts, the analyses show MNMBs between -12.6% and 14.9% (Fig. 9.4). Only the LOTOS model shows larger negative MNMBs in 2021 up to -16.1%.

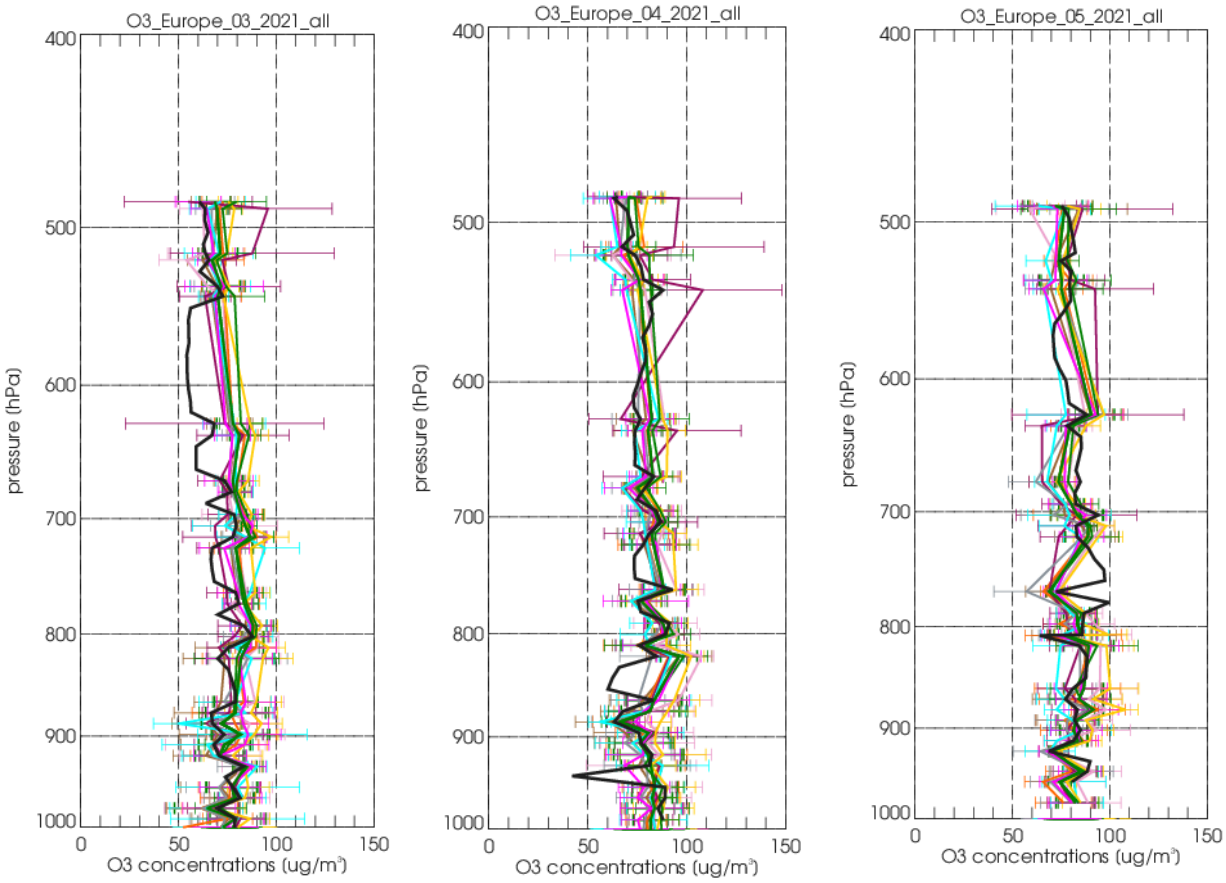

Figure 9.5. Averaged monthly profiles from the model analysis and sonde comparisons over European sonde stations for March, April and May 2021 (green: ENSEMBLE, blue: CAMS-global, yellow: CHIMERE, brown: EMEP, orange: SILAM, purple: LOTOS-EUROS, cyan: EURAD-IM, pink: MOCAGE, grey: MATCH, fuchsia: DEHM, light green: GEM-AQ).

10 Comparison with GAW stations

10.1 Summary

The model concentrations of O_3 and CO at higher model levels were compared with five GAW high-altitude stations in mountainous terrain. As for the EEA air quality e-reporting stations, differences between the regional model orography and the true altitude of the station were used for this model level selection. Good results were obtained for the ENSEMBLE for ozone with small biases and good correlations. The EURAD-IM model shows significant lower MNMBs in both the analysis and the forecast. For CO, also the EURAD-IM shows significant lower correlation, however, maintaining good MNMB. The time series and correlation coefficients for CO and O_3 show that the ENSEMBLE reproduces for a large part the variability observed.

10.2 Comparison method

Hourly O_3 and CO concentration values in µg/m^3 are extracted from the seven models and are compared to the GAW measurements, which were converted from volume mixing ratios (ppb) into concentrations by using pressure and temperature values at the respective pressure levels from the CAMS-global model.

The altitude of the stations Hohenpeissenberg (HPB), Jungfraujoch (JFJ), Monte Cimone (CMN), Sonnblick (SNB) and Zugspitze (ZUG) in the model has been extracted from the orography as used in the LOTOS-EUROS model, see Table 10.1. For the level choice, the GAW stations' altitudes together with the best correlation of the corresponding levels were taken into account. Uncertainties due to the choice of level (calculated as mean differences between the chosen level and one up/down for the period MAM 2021 for HPB) are up to ±27.73 µg/m^3 for CO and up to ±10.00 µg/m^3 for O_3.

Table 10.1 - Validation set-up for March – May 2021.

station	altitude station [m]	altitude model [m]	level choice (range 0-7)	altitude at level [m]
HPB	985	813	2	1063
JFJ	3580	1837	5	3837
CMN	2165	602	4	1602
SNB	3105	1687	3	2187
ZUG	2670	1348	4	2348

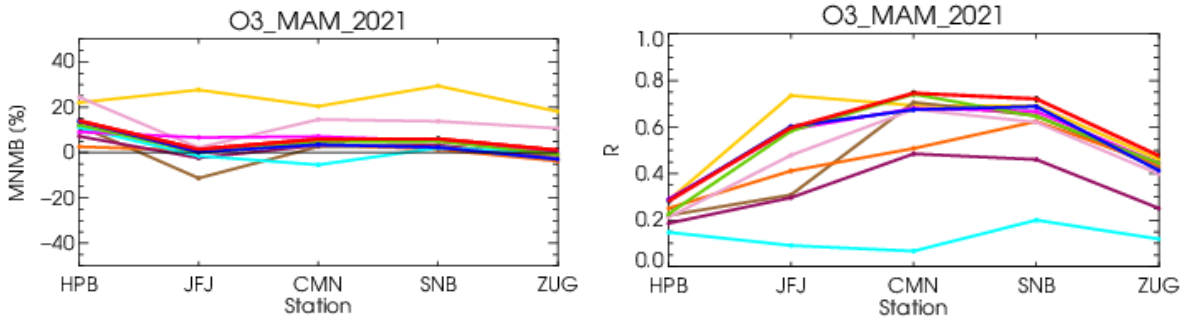

Figure 10.1. MNMBs [%] (left) and correlation coefficients (right) for all model forecasts for ozone (red: ENSEMBLE, blue: CAMS-global, yellow: CHIMERE, brown: EMEP, orange: SILAM, purple: LOTOS-EUROS, cyan: EURAD-IM, pink: MOCAGE, grey: MATCH, fuchsia: DEHM, light green: GEM-AQ). Altitudes are listed in Table 10.1.

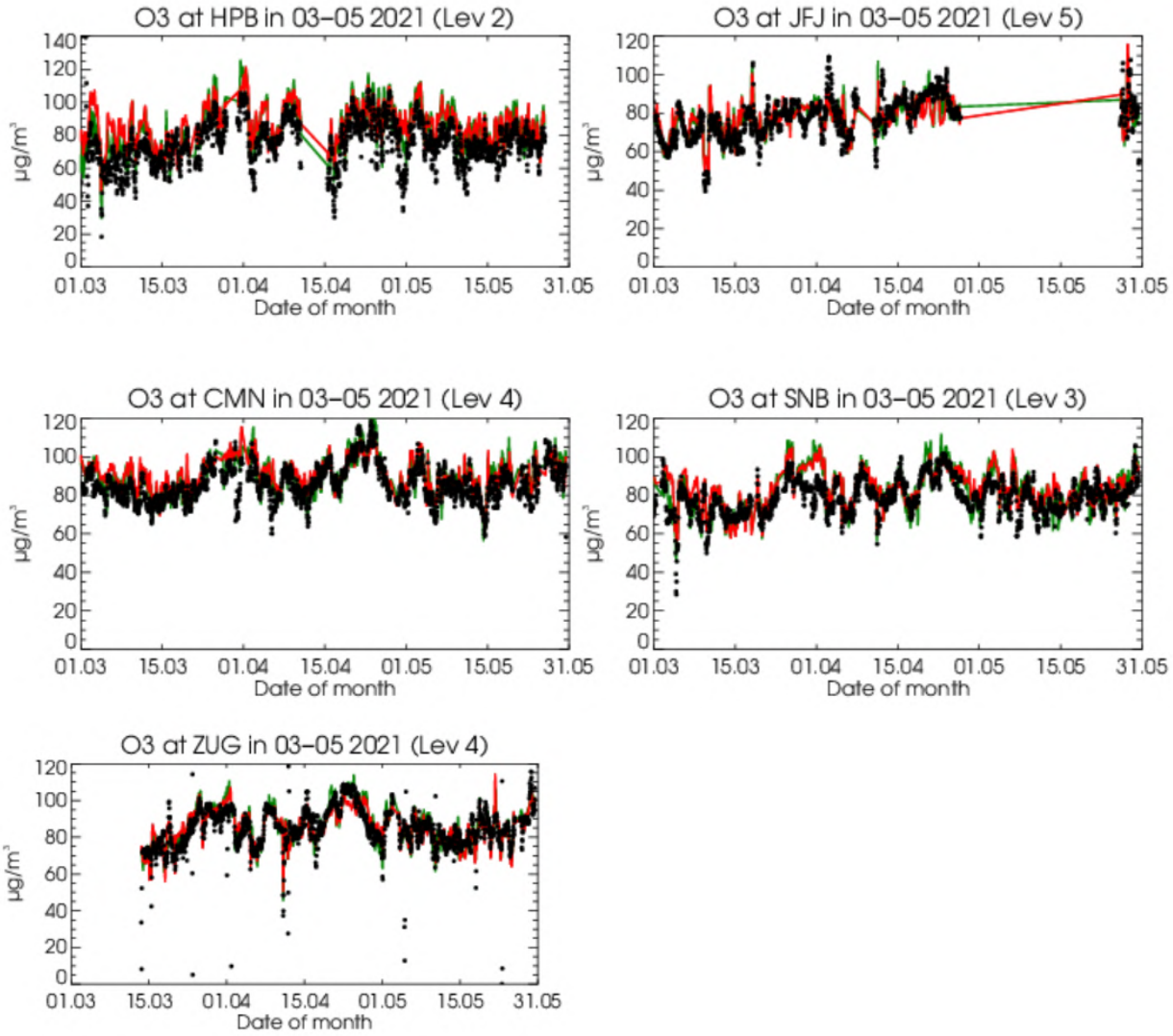

Figure 10.2. Time series plots for the ENSEMBLE forecast (red) and ENSEMBLE analysis (green) for surface O_3 in comparison with high altitude stations for the period March 2021 to May 2021.

10.3 Ozone

The ENSEMBLE forecast shows MNMBs between -16% and 15% and correlation coefficients ranging between 0.2 and 0.8 for the period March 2021 to May 2021 (Figure S2). The ENSEMBLE analysis shows almost the same MNMBs (between -9% and 15%) and slightly lower correlation coefficients ranging from 0.2 and 0.77 (see Fig. 10.1), except for the EURAD-IM Model which significantly outlines.

The time series plots show a good correspondence between model and observations (Fig. 10.2).

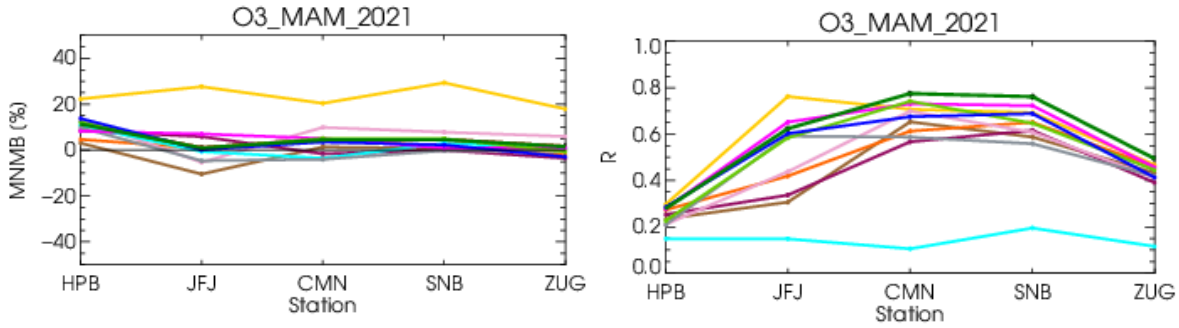

Figure 10.3. MNMBs [%] (left) and correlation coefficients (right) for all models analyses for ozone (green: ENSEMBLE, blue: CAMS-global, yellow: CHIMERE, brown: EMEP, orange: SILAM, purple: LOTOS-EUROS, cyan: EURAD-IM, pink: MOCAGE, grey: MATCH, fuchsia: DEHM, light green: GEM-AQ). Altitudes are listed in Table 10.1.

Results for individual model forecasts:

The models show MNMBs in the range of -9% and 18% for the period March to May 2021 (Fig. 10.1). The CHIMERE model shows larger positive MNMBs than the other models. During MMA 2021, correlation coefficients vary between 0.3 and 0.8. An exception is the EURAD model with general low correlation coefficients down to 0.3.

Results for the individual model analyses:

For the individual model analyses (Fig. 10.23), MNMBs range between 18% and -5% and are very similar to the forecast. Same as for the forecast, correlation coefficients range between 0.3 and 0.80, except for the EURAD model, which shows lower correlation.

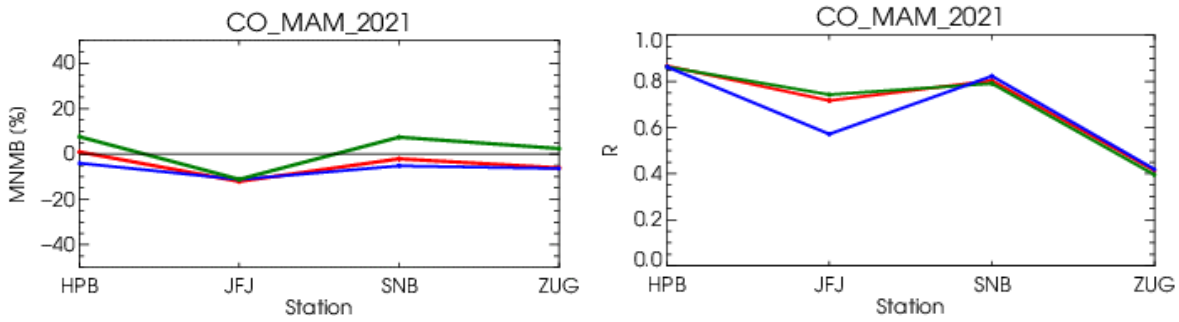

Figure 10.6. MNMBs [%] (left) and correlation coefficients (right) for the ENSEMBLE for CO (red: ENSEMBLE forecast, green: ENSEMBLE analysis, blue: CAMS-global).

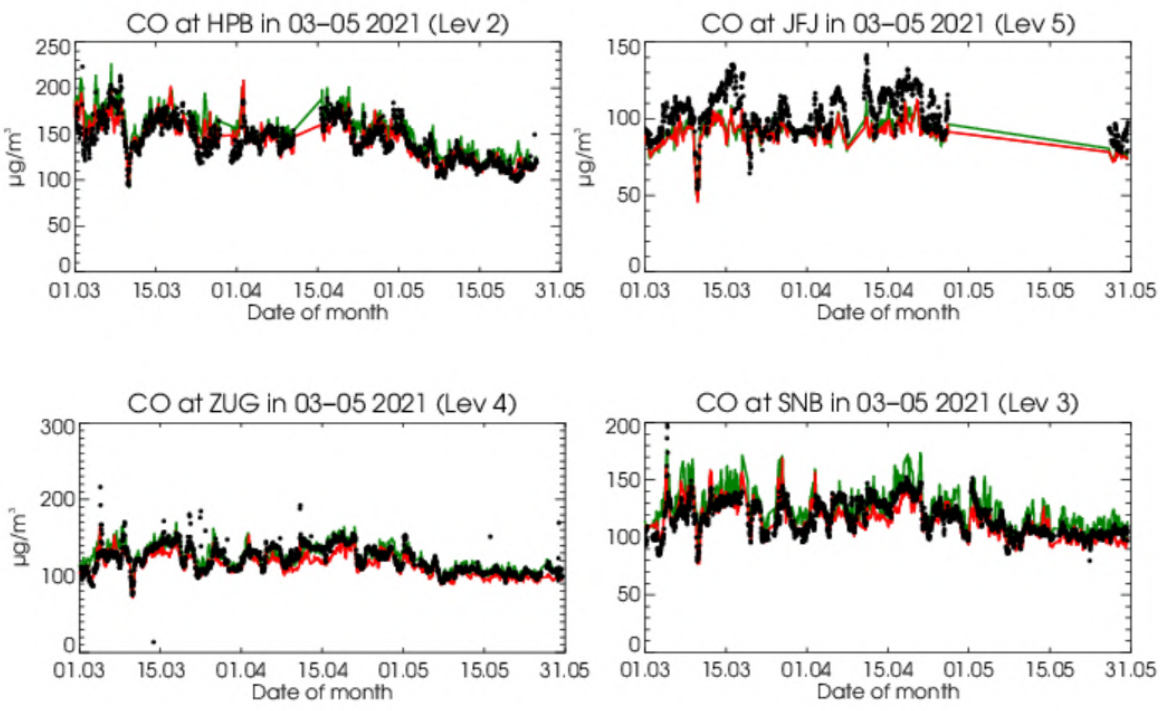

Figure 10.4. Time series plots for the ENSEMBLE forecast (red) and ENSEMBLE analysis (green) for surface CO in comparison with high altitude stations.

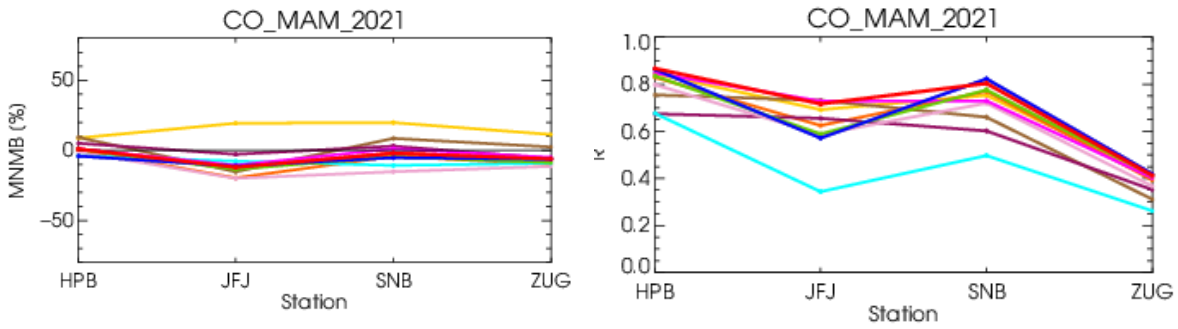

Figure 10.5. CO MNMBs [%] (left) and correlation coefficients (right) for all regional model forecasts, the ENSEMBLE and CAMS-global (red: ENSEMBLE forecast, blue: CAMS-global, yellow: CHIMERE, brown: EMEP, orange: SILAM, purple: LOTOS-EUROS, cyan: EURAD-IM, pink: MOCAGE, grey: MATCH, fuchsia: DEHM, light green: GEM-AQ). Altitude ranges are listed in Table 10.1.

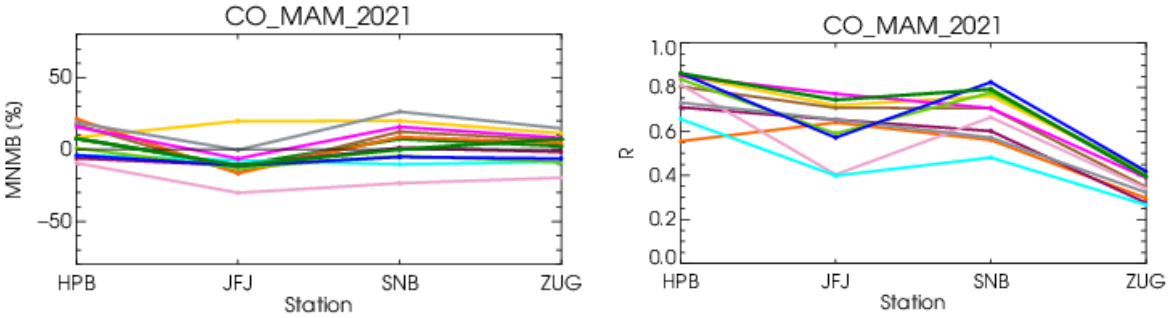

Figure 10.6. CO MNMBs [%] (left) and correlation coefficients (right) for all regional model analyses, the ENSEMBLE and CAMS-global (green: ENSEMBLE analysis, blue: CAMS-global, yellow: CHIMERE, brown: EMEP, orange: SILAM, purple: LOTOS-EUROS, cyan: EURAD-IM, pink: MOCAGE, grey: MATCH, fuchsia: DEHM, light green: GEM-AQ). Altitude ranges are listed in Table 10.1.

10.4 Carbon monoxide

For CO, the ENSEMBLE forecast and analysis MNMBs range between between -15% and -15% for both forecast and analysis during March 2021 - May 2021. The analysis shows higher CO concentrations and thus slightly more positive MNMBs. Correlation coefficients are between 0.4 and 0.85 for the analysis and forecast (Fig. 10.6). The time series plots (Fig. 10.7) show mostly a very good agreement between model and observations, except for a small vertical offset for some stations.

CO results for individual model forecasts:

CO show MNMBs between -15% and 15% (Fig. 10.5). The CAMS-global model shows the largest positive MNMBs of all models, see Fig. 10.9. Correlation coefficients are between 0.3 and 0.85 for the forecasts, with EURAD-IM at a significantly lower overall correlation.

Results for the individual model analyses:

CO mixing ratios range between -5% and 25%, except for the MOCAGE model, which shows larger negativ MNMBs (up to -30%) (Fig. 10.6). Correlation coefficients between the models vary

significantly and range between 0.3 and 0.85. The MOCAGE behave differently in analysis and forecast, with larger negative biases in the analysis.

11 Comparisons with MOPITT CO

11.1 Summary

MOPITT shows relatively high CO values over the large terrestrial part of domain in March and April, except Scandinavia, Spain, France and Germany, where the values are relatively low. The ENSEMBLE forecast data show good agreement with the satellite observations with slight underestimation. The bias is within 20%. The analysis data are very similar to the forecast data. The analysis data shows slightly better agreement with the observations reflecting in the smaller negative bias.

11.2 Method

CO total column forecasts over Europe from seven regional models and the model ensemble are compared with CO total column retrievals from MOPITT Version 7 (thermal infrared radiances) (Emmons et. al., 2009). Modelled CO data were converted from µg/m³ to VMR by using temperature obtained from CAMS-global (o-suite) model. Pressure at the middle of the layers was also interpolated from the global model. Regional model data are available from the surface up to altitude of 5 km. For the comparison with satellite retrievals, the averaging kernels were applied to the modelled data.

Regional model data up to 5 km were merged with CAMS-global data above 5 km in order to minimize uncertainty error. We performed several confidence tests to establish the method. To check the error due to coarse sampling of the profiles up to 5 km as provided by the regional models, CAMS-global data were sampled at the height levels of the regional models up to 5 km and merged with the CAMS-global original levels above 5 km. Comparison of this results with the original CAMS-global data showed that the errors due to coarse sampling of the profiles up to 5 km were very small. Both results showed slight underestimation of the MOPITT data. CAMS-global values up to 5 km sampled at the height levels as the regional models and ENSEMBLE data without merging with the levels above 5km show overestimation of the satellite data over almost entire region. From this we concluded that error due to missing values above 5 km is significant and merging the regional data with CAMS-global values above 5 km is necessary for the proper comparison.

MOPITT shows relatively high CO values over the large terrestrial part of domain in March and April, except Scandinavia, Spain, France and Germany, where the values are relatively low. In May, the satellite data are relatively low. The ENSEMBLE forecast data show good agreement with the satellite observations with slight underestimation. The bias is within 20% and slightly bigger underestimation in April. All the models have very similar patterns to ENSEMBLE. CHIMERE shows slightly better agreement with the satellite data. The analysis data are very similar to the forecast data. MOCAGE shows slightly higher negative bias compared to other models.

MOPITT

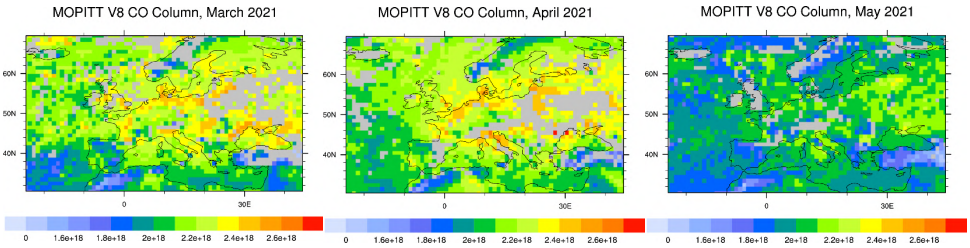

ENSEMBLE-MOPITT
Forecast (0H-24H)

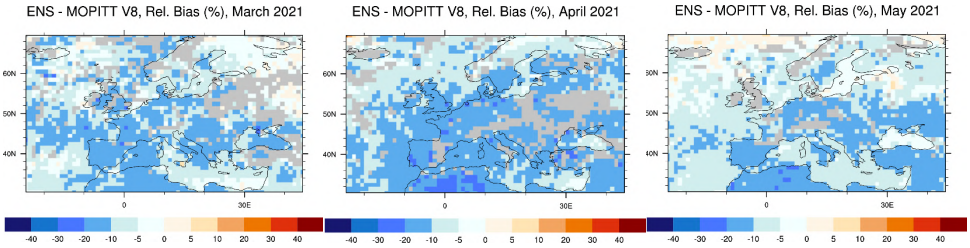

EMEP-MOPITT
Forecast (0H-24H)

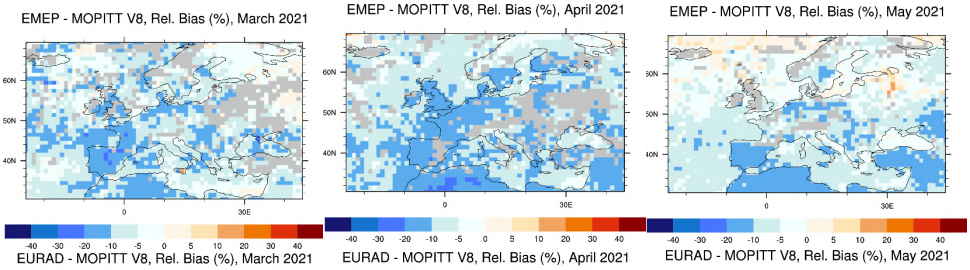

EURAD-MOPITT
Forecast (0H-24H)

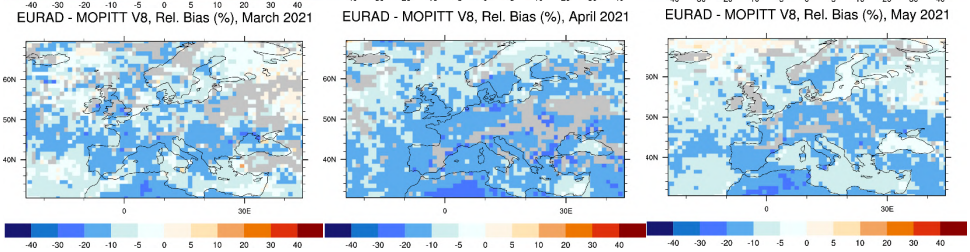

CHIMERE-MOPITT
Forecast (0H-24H)

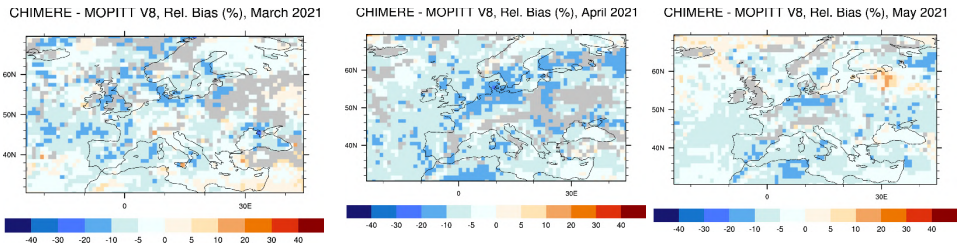

LOTOS-EUROS-MOPITT
Forecast (0H-24H)

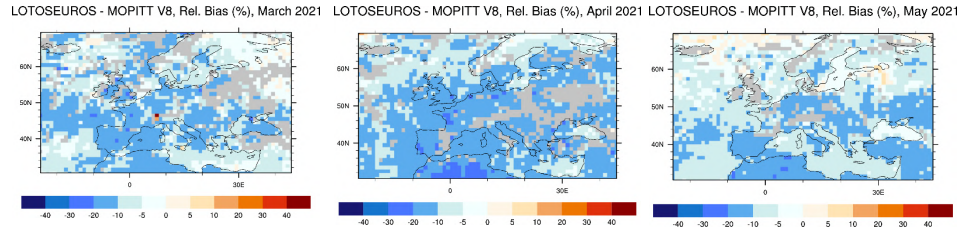

SILAM-MOPITT Forecast (0H-24H)

MATCH-MOPITT Forecast (0H-24H)

MOCAGE-MOPITT Forecast (0H-24H)

GEMAQ-MOPITT Forecast (0H-24H)

DEHM-MOPITT Forecast (0H-24H)

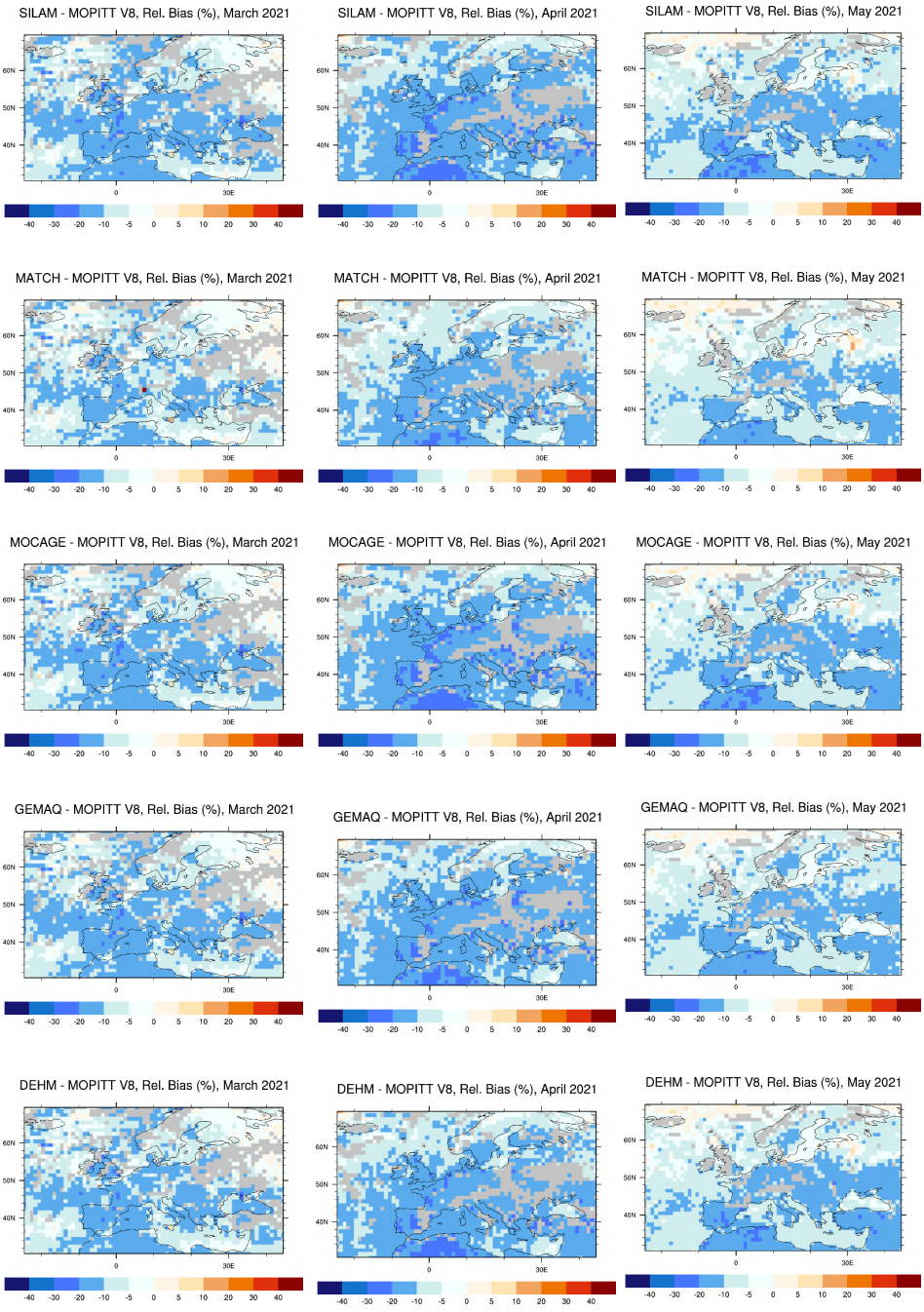

Figure 11.1. CO total column for MOPITT V8 satellite retrievals (top row, in molecules/cm^2), relative difference between the regional forecasts of the nine models and the ENSEMBLE and MOPITT (other rows) for March (left column), April (middle column) and May 2021 (right column). Grey colour indicates missing values.

MOPITT

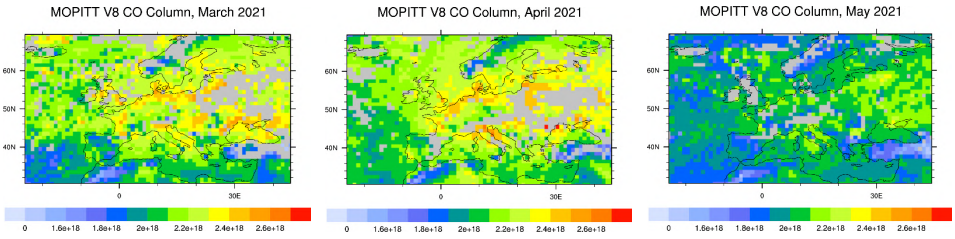

ENS-MOPITT
Analysis (-24H-1H)

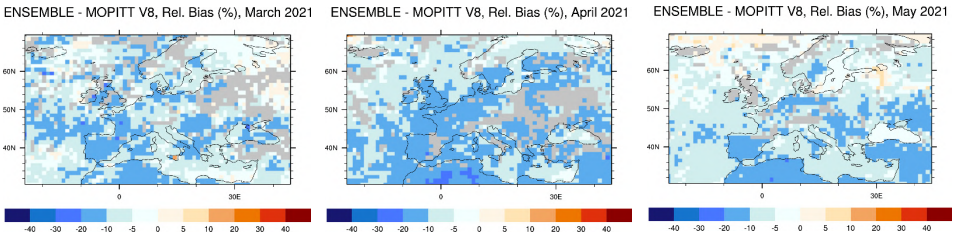

EMEP-MOPITT
Analysis (-24H-1H)

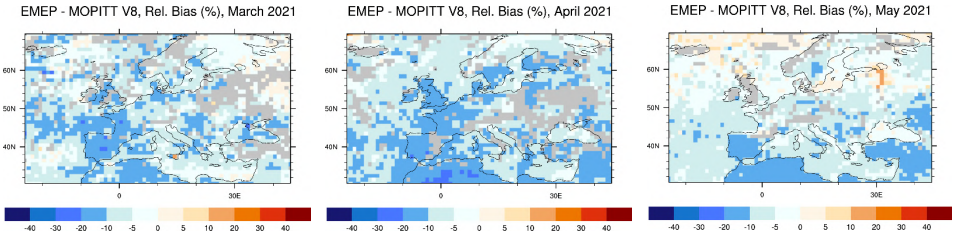

EURAD-MOPITT
Analysis (-24H-1H)

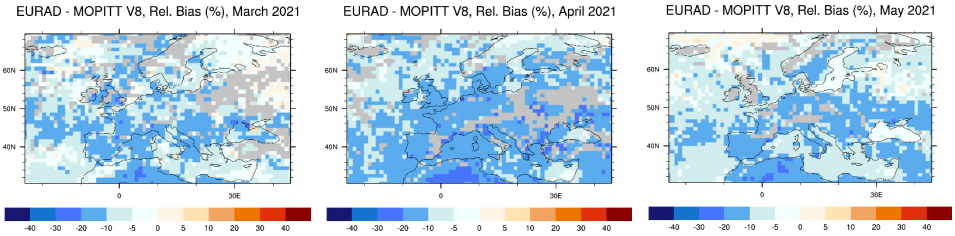

CHIMERE-MOPITT
Analysis (-24H-1H)

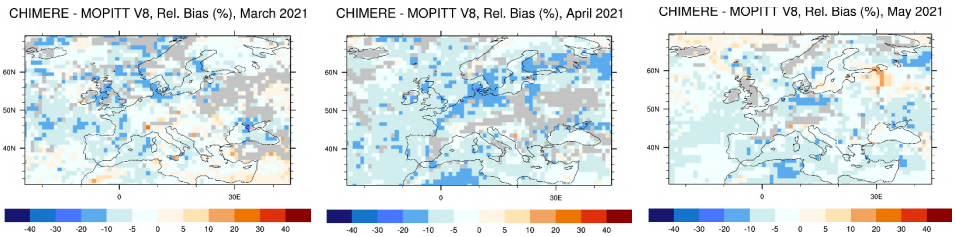

LOTOS-EUROS-MOPITT
Analysis (-24H-1H)

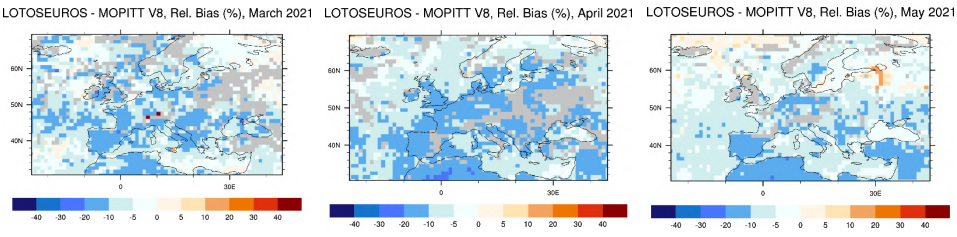

SILAM-MOPITT Analysis (-24H-1H)

MATCH-MOPITT Analysis (-24H-1H)

MOCAGE-MOPITT Analysis (-24H-1H)

GEMAQ-MOPITT Analysis (-24H-1H)

DEHM-MOPITT Analysis (-24H-1H)

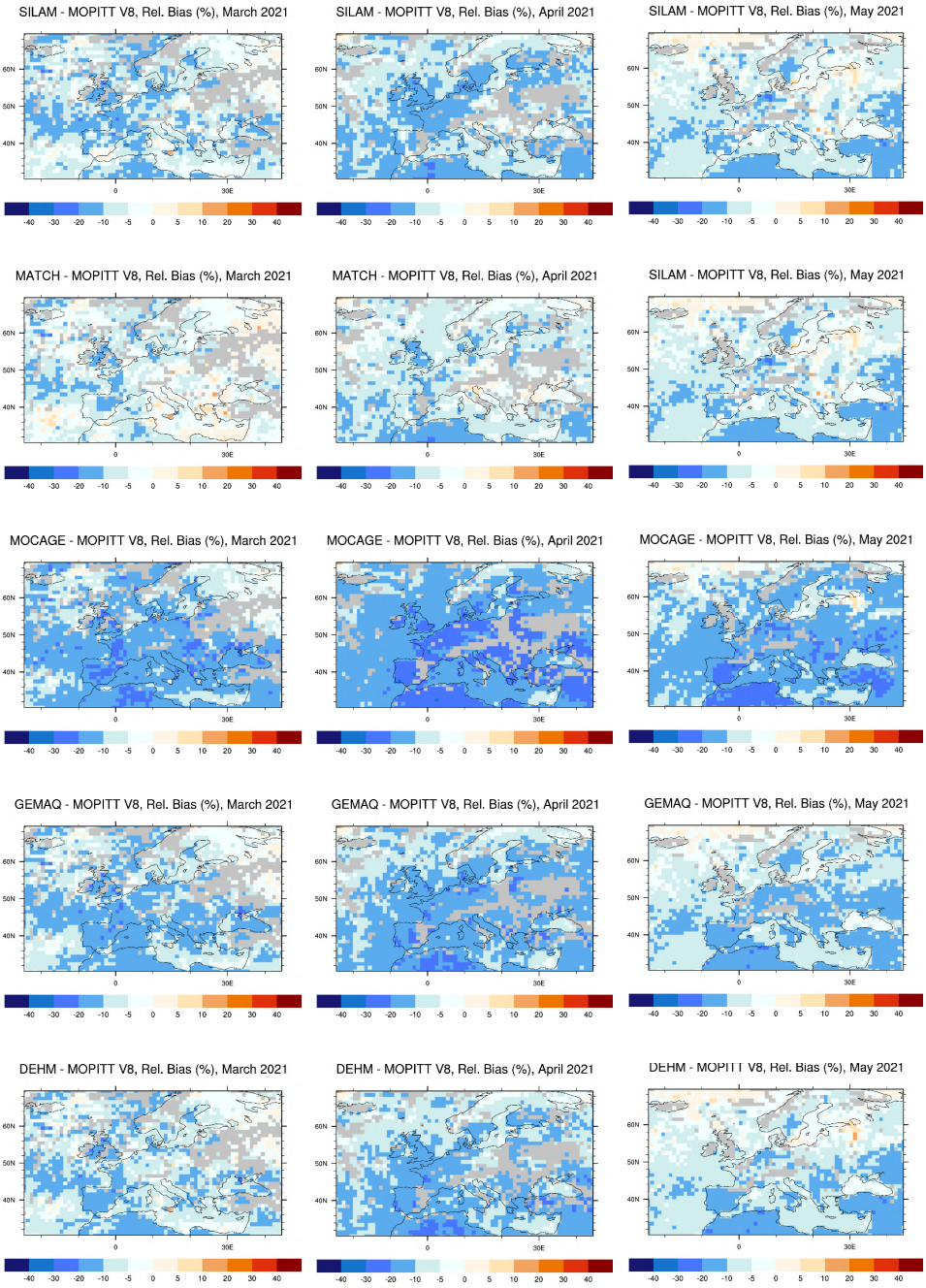

Figure 11.1. CO total column for MOPITT V8 satellite retrievals (top row, in molecules/cm^2), relative difference between the regional analyses of the seven models and the ENSEMBLE and MOPITT (other rows) for March (left column), April (middle column) and May 2021 (right column). Grey colour indicates missing values.

12 Summary of issues identified in individual models

This section provides a short overview of the main, model specific issues of this report.

CHIMERE

Ozone ,CO and PM10 cross sections at the lateral boundaries show features that are not in line with what is seen in CAMS-global or the other models (figs 3.13 and 3.14). This indicates a possible issue with the CAMS-global boundary conditions implementation. Comparison with the GAW stations also indicates relatively high MNMBs for ozone for both the forecasts and the analyses (figs 10.3 and 10.4) and CO for the forecasts (fig 10.7).

EURAD

Ozone correlation coefficients at high altitude and GAW stations are much lower than for CAMS-global and the other models in both forecasts and analyses (figs 8.5, 10.3 and 10.4). Similar results are found in the correlation coefficients for CO based on comparisons at the GAW stations for the forecasts (fig 10.7).

LOTOS-EUROS

Differences between forecasts and analyses for ozone seem to be large compared most other models above 3000m (fig 3.18). Moreover, based on IAGOS ozone observations, the model often presents higher biases than the other models, especially above 3000m (fig. 5.5). Ozone MNMBs and correlation coefficients at high altitude stations deviate considerably from the ENSEMBLE (figs 8.4 and 8.5). To some extent, these findings can be attributed to the increase, at the upgrade in November 2020, of the vertical resolution of the model for the forecasts.

MOCAGE

High PM10 concentrations are spotted over the Atlantic, up to 250m above the surface (fig 3.9). The western boundary for PM10 is also quite high, while the southern boundary is low (fig 3.13), indicating possible issues with the implementation of the CAMS-global boundary conditions.

13 Acknowledgements

The authors acknowledge all EARLINET and European ACTRIS/Aeronet data providers for providing aerosol lidar profiles and sun photometer data available from the ACTRIS data portal (http://actris.nilu.no), and the Aeronet NRT data dissemination system respectively (https://aeronet.gsfc.nasa.gov). The ACTRIS 2 project (http://www.actris.eu) has received funding from the European Union's Horizon 2020 research and innovation program under grant agreement No 654109.

We wish to acknowledge the provision of GAW hourly NRT station data by: the National Air Pollution Monitoring Network (NABEL) (Federal Office for the Environment FOEN and Swiss Federal Laboratories for Materials Testing and Research EMPA) for Jungfraujoch station, the Umweltbundesamt (UBA, Germany) for Zugspitze (Schneefernerhaus) station, the Umweltbundesamt (Austria) for Sonnblick station, the Observatory Hohenpeissenberg (Deutscher Wetter Dienst, DWD) for Hohenpeissenberg station, and the Institute of Atmospheric Sciences and Climate (ISAC) of the Italian National Research Council (CNR) for Monte Cimone station.

We wish to acknowledge the provision of ozone sonde data by the World Ozone and Ultraviolet Radiation Data Centre established at EC in Toronto (http://woudc.org), by the Data Host Facility of the Network for the Detection of Atmospheric Composition Change established at NOAA (http://ndacc.org), and by the Norwegian Institute for Air Research (http://nilu.no).

We acknowledge the EEA Air quality e-reporting Network (https://www.eea.europa.eu/data-and-maps/data/aqereporting-8) for the provision of hourly NRT station observations.

We wish to acknowledge the Department of Labour Inspection - Ministry of Labour and Social Insurance, of Cyprus (http://www.airquality.dli.mlsi.gov.cy/) for the provision of hourly NRT ozone data from Mountain Troodos station.

The programmes MOZAIC and CARIBIC, and the current Research Infrastructure IAGOS are operated with support from the European Commission, national agencies in Germany (BMBF), France (MESR), and the UK (NERC), and the IAGOS member institutions (http://www.iagos.org/partners). The participating airlines (Lufthansa, Air France, Austrian, China Airlines, Iberia, Cathay Pacific, Air Namibia, Sabena) supported IAGOS by carrying the measurement equipment free of charge since 1994. The data are available at http://www.iagos.fr thanks to additional support from AERIS (CNRS and CNES).

GOME2 lv1 radiances and irradiances were provided by EUMETSAT.

We acknowledge the NASA Langley Research Center Atmospheric Science Data Center for providing the MOPITT data.

AUTH acknowledges the AUTH Scientific Computing Centre (https://it.auth.gr/en/services) for providing technical and infrastructure support for data analysis performed in this WP.

14 References

*Richter, A., Begoin, M., Hilboll, A., and Burrows, J. P.: An improved NO2 retrieval for the GOME-2 satellite instrument, Atmos. Meas. Tech. , **4**, 1147-1159, doi:10.5194/amt-4-1147-2011, 2011.*

Ackermann, J. (1998). The extinction-to-backscatter ratio of tropospheric aerosol: A numerical study. Journal of atmospheric and oceanic technology, 15(4), 1043-1050.

ACTRIS Deliverable WP6/D6.21,
http://www.actris.net/Portals/97/deliverables/PU/WP6_D6.21_M45v2.pdf

Cattrall, C., Reagan, J., Thome, K., & Dubovik, O. (2005). Variability of aerosol and spectral lidar and backscatter and extinction ratios of key aerosol types derived from selected Aerosol Robotic Network locations. Journal of Geophysical Research: Atmospheres, 110(D10).

Chin, M., Ginoux, P., Kinne, S., Torres, O., Holben, B. N., Duncan, B. N., ... & Nakajima, T. (2002). Tropospheric aerosol optical thickness from the GOCART model and comparisons with satellite and Sun photometer measurements. Journal of the atmospheric sciences, 59(3), 461-483.

Eskes, H. J., S. Basart, A. Benedictow, Y. Bennouna, A.-M. Blechschmidt, Q. Errera, K. M. Hansen, J. Kapsomenakis, B. Langerock, A. Richter, N. Sudarchikova, M. Schulz, C. Zerefos, Upgrade verification note for the CAMS real-time global atmospheric composition service: Evaluation of the e-suite for the CAMS 47R2 upgrade of 18 May 2021, Copernicus Atmosphere Monitoring Service (CAMS) report, CAMS84_2018SC3_D3.2.1-202105_esuite.pdf, May 2021, doi: 10.24380/1ef3-gq26.

Eskes, H.J., S. Basart, A. Benedictow, Y. Bennouna, A.-M. Blechschmidt, S. Chabrillat, Y. Christophe, E. Cuevas, H. Flentje, K. M. Hansen, J. Kapsomenakis, B. Langerock, M. Ramonet, A. Richter, M. Schulz, N. Sudarchikova, A. Wagner, T. Warneke, C. Zerefos, Observation characterisation and validation methods document, Copernicus Atmosphere Monitoring Service (CAMS) report, CAMS84_2018SC2_D6.1.1-2020_observations_v5.pdf, January 2021. Available from: http://atmosphere.copernicus.eu/user-support/validation/verification-global-services

Eskes, H., Huijnen, V., Arola, A., Benedictow, A., Blechschmidt, A.-M., Botek, E., Boucher, O., Bouarar, I., Chabrillat, S., Cuevas, E., Engelen, R., Flentje, H., Gaudel, A., Griesfeller, J., Jones, L., Kapsomenakis, J., Katragkou, E., Kinne, S., Langerock, B., Razinger, M., Richter, A., Schultz, M., Schulz, M., Sudarchikova, N., Thouret, V., Vrekoussis, M., Wagner, A., and Zerefos, C.: Validation of reactive gases and aerosols in the MACC global analysis and forecast system, Geosci. Model Dev., 8, 3523-3543, doi:10.5194/gmd-8-3523-2015, 2015.

Flemming, J., Huijnen, V., Arteta, J., Bechtold, P., Beljaars, A., Blechschmidt, A.-M., Diamantakis, M., Engelen, R. J., Gaudel, A., Inness, A., Jones, L., Josse, B., Katragkou, E., Marecal, V., Peuch, V.-H., Richter, A., Schultz, M. G., Stein, O., and Tsikerdekis, A.: Tropospheric chemistry in the Integrated Forecasting System of ECMWF, Geosci. Model Dev., 8, 975-1003, doi:10.5194/gmd-8-975-2015, 2015.

Joly, Mathieu, and Vincent-Henri Peuch, Objective classification of air quality monitoring sites over Europe, Atmospheric Environment 47, 111-123, 2012.

Katragkou, E., Zanis, P., Tsikerdekis, A., Kapsomenakis, J., Melas, D., Eskes, H., Flemming, J., Huijnen, V., xsxcInness, A., Schultz, M. G., Stein, O., and Zerefos, C. S.: Evaluation of near-surface ozone over Europe from the MACC reanalysis, Geosci. Model Dev., 8, 2299-2314, doi:10.5194/gmd-8-2299-2015, 2015.

Marécal, V., Peuch, V.-H., Andersson, C., Andersson, S., Arteta, J., Beekmann, M., Benedictow, A., Bergström, R., Bessagnet, B., Cansado, A., Chéroux, F., Colette, A., Coman, A., Curier, R. L., Denier van der Gon, H. A. C., Drouin, A., Elbern, H., Emili, E., Engelen, R. J., Eskes, H. J., Foret, G., Friese, E., Gauss, M., Giannaros, C., Guth, J., Joly, M., Jaumouillé, E., Josse, B., Kadygrov, N., Kaiser, J. W., Krajsek, K., Kuenen, J., Kumar, U., Liora, N., Lopez, E., Malherbe, L., Martinez, I., Melas, D., Meleux, F., Menut, L., Moinat, P., Morales, T., Parmentier, J., Piacentini, A., Plu, M., Poupkou, A., Queguiner, S., Robertson, L., Rouïl, L., Schaap, M., Segers, A., Sofiev, M., Tarasson, L., Thomas, M., Timmermans, R., Valdebenito, Á., van Velthoven, P., van Versendaal, R., Vira, J., and Ung, A.: A regional air quality forecasting system over Europe: the MACC-II daily ensemble production, Geosci. Model Dev., 8, 2777-2813, doi:10.5194/gmd-8-2777-2015, 2015.

Morcrette, J.-J., O. Boucher, L. Jones, D. Salmond, P. Bechtold, A. Beljaars, A. Benedetti, A. Bonet, J. W. Kaiser, M. Razinger, M. Schulz, S. Serrar, A. J. Simmons, M. Sofiev, M. Suttie, A. M. Tompkins, and A. Untch: Aerosol analysis and forecast in the ECMWF Integrated Forecast System. Part I: Forward modelling, J. Geophys. Res., 114, D06206, doi:10.1029/2008JD011235, 2009.

Mortier, A., Goloub, P., Derimian, Y., Tanré, D., Podvin, T., Blarel, L., ... & Ndiaye, T. (2016). Climatology of aerosol properties and clear‐sky shortwave radiative effects using Lidar and Sun photometer observations in the Dakar site. Journal of Geophysical Research: Atmospheres.

Müller, D., Ansmann, A., Mattis, I., Tesche, M., Wandinger, U., Althausen, D., & Pisani, G. (2007). Aerosol‐type‐dependent lidar ratios observed with Raman lidar. Journal of Geophysical Research: Atmospheres, 112(D16).

Omar, A. H., Winker, D. M., Vaughan, M. A., Hu, Y., Trepte, C. R., Ferrare, R. A., ... & Kuehn, R. E. (2009). The CALIPSO automated aerosol classification and lidar ratio selection algorithm. Journal of Atmospheric and Oceanic Technology, 26(10), 1994-2014.

Pappalardo, G., A. Amodeo, A. Apituley, A. Comeron, V. Freudenthaler, H. Linne, A. Ansmann, J. Bösenberg, G. D'Amico, I. Mattis, L. Mona, U. Wandinger, V. Amiridis, L. Alados-Arboledas, D. Nicolae, and Wiegner, M.: EARLINET: towards an advanced sustainable European aerosol lidar network, Atmos. Meas. Tech., 7, 2389–2409, www.atmos-meas-tech.net/7/2389/2014/, doi:10.5194/amt-7-2389-2014, 2014.

*Richter, A., Begoin, M., Hilboll, A., and Burrows, J. P.: An improved NO2 retrieval for the GOME-2 satellite instrument, Atmos. Meas. Tech. , **4**, 1147-1159, doi:10.5194/amt-4-1147-2011, 2011.*

Vinken, G. C. M., Boersma, K. F., van Donkelaar, A., and Zhang, L.: Constraints on ship NOx emissions in Europe using GEOS-Chem and OMI satellite NO2 observations, Atmos. Chem. Phys., 14, 1353-1369, doi:10.5194/acp-14-1353-2014, 2014.

Wagner, A., M. Schulz, Y. Christophe, M. Ramonet, H. J. Eskes, S. Basart, A. Benedictow, Y. Bennouna, A.-M. Blechschmidt, S. Chabrillat, E. Cuevas, A. El- Yazidi, H. Flentje, K.M. Hansen, U. Im, J. Kapsomenakis, B. Langerock, A. Richter, N. Sudarchikova, V. Thouret, T. Warneke, C. Zerefos, Validation report of the CAMS near-real-time global atmospheric composition service: Period September - November 2019, Copernicus Atmosphere Monitoring Service (CAMS) report, CAMS84_2018SC2_D1.1.1_SON2019_v1.pdf, February 2020, doi:10.24380/xzkk-bz05.

Copernicus Atmosphere Monitoring Service

ECMWF - Shinfield Park, Reading RG2 9AX, UK

Contact: info@copernicus-atmosphere.eu

atmosphere.copernicus.eu copernicus.eu ecmwf.int